INFORMATION TO USERS

This manuscript has been reproduced from the microfilm master. UMI films the text directly from the original or copy submitted. Thus, some thesis and dissertation copies are in typewriter face, while others may be from any type of computer printer.

The quality of this reproduction is dependent upon the quality of the copy submitted. Broken or indistinct print, colored or poor quality illustrations and photographs, print bleedthrough, substandard margins, and improper alignment can adversely affect reproduction.

In the unlikely event that the author did not send UMI a complete manuscript and there are missing pages, these will be noted. Also, if unauthorized copyright material had to be removed, a note will indicate the deletion.

Oversize materials (e.g., maps, drawings, charts) are reproduced by sectioning the original, beginning at the upper left-hand corner and continuing from left to right in equal sections with small overlaps. Each original is also photographed in one exposure and is included in reduced form at the back of the book.

Photographs included in the original manuscript have been reproduced xerographically in this copy. Higher quality 6" x 9" black and white photographic prints are available for any photographs or illustrations appearing in this copy for an additional charge. Contact UMI directly to order.

U·M·I

University Microfilms International
A Bell & Howell Information Company
300 North Zeeb Road, Ann Arbor, MI 48106-1346 USA
313/761-4700 800/521-0600

Order Number 9207063

The metal-insulator transition in boron-doped silicon: Transport properties

Dai, Peihua, Ph.D.

City University of New York, 1991

U·M·I
300 N. Zeeb Rd.
Ann Arbor, MI 48106

H

THE METAL-INSULATOR TRANSITION IN BORON-DOPED SILICON: TRANSPORT PROPERTIES

by

PEIHUA DAI

A dissertation submitted to the Graduate Faculty in Physics in partial fulfillment of the requirements for the degree of Doctor of Philosophy, The City University of New York.

1991

This manuscript has been read and accepted for the Graduate Faculty in Physics in satisfaction of the dissertation requirement for the degree of Doctor of Philosophy.

9/11/91
Date

Professor Myriam P. Sarachik
Chair Of Examining Committee

9/12/91
Date

Professor Joseph Krieger
Executive Officer

Professor Joseph Birman

Professor Azriel Genack

Professor Russell Giannetta

Doctor Stephan von Molnar
Supervisory Committee

The City University of New York

Abstract

THE METAL-INSULATOR TRANSITION IN BORON-DOPED SILICON: TRANSPORT PROPERTIES

by

Peihua Dai

Advisor: Professor Myriam P. Sarachik

The conductivity has been studied for a series of uncompensated *p*-type boron-doped silicon samples with dopant concentrations near the metal-insulator transition. For ten metallic samples, data were taken at temperatures down to 55 mK, and in magnetic fields up to 9 Tesla in a dilution refrigerator. Some data were also taken at dilution refrigerator temperatures, for barely insulating samples.

Our study in zero magnetic field shows the interesting result that the critical conductivity exponent for Si:B is $0.65^{+0.05}_{-0.14}$, which is close to the anomalous value of 1/2 found for other *n*-type uncompensated silicon systems, and different from the value near 1 found in most other materials. This indicates that spin-orbit scattering, which is important in Si:B, does not determine the critical exponent as the theory predicts. Our results also indicate that the critical exponent is shifted to a value near 1 by the application of a strong magnetic field. This is consistent with the prediction of the theory and is the first observation of such a clear shift.

Our study also shows that the correction to the zero-temperature conductivity arising from electron-electron interactions is comparable in size for n- and p-type silicons. Further, the temperature dependence of the conductivity in various fixed magnetic fields is similar for Si:P and Si:B. This is surprising, given the differences between the conduction and valence bands of silicon, such as anisotropy and the nature of the scattering.

The single important difference between n- and p-type silicons is the sign and size of the magnetoresistance. Our systematic study of the Si:B samples shows that the magnetoresistance of Si:B is always positive, unlike Si:P which has both positive and negative components. We attribute this to the strong spin-orbit scattering in p-type silicon associated with the degenerate valence bands.

ACKNOWLEDGMENTS

I would first of all like to thank my thesis advisor, professor Myriam P. Sarachik for her enormous input, guidance and encouragement.

I would also like to thank other members of the group, Dr. Youzhu Zhang and Dr. Miguel Levy, for their help and many useful discussions.

I am especially grateful to Dr. Alice White of AT&T Bell Laboratories, who contributed generously to this research by carrying out the ion implants needed to make electrical contact to our samples.

I thank Prof. David Schmeltzer for many useful discussions. I thank Prof. H. Cummins for his advice on error analysis and Prof. O. Martin for his help on numerical calculations.

I thank Mr. J. Altmann and others in the machine shop for their help and patience.

Finally, I thank my family for their understanding and support.

Table of Contents

List of Tables....x

List of Figures....xi

1. Introduction....1

2. Background....6

2.1 Mott Transition....6

2.1.a Screening and Mott Transition....6

2.1.b Hubbard Bands....7

2.1.c Minimum Metallic Conductivity....8

2.2 Anderson Transition....10

2.2.a Localization....10

2.2.b Anderson Transition....11

2.3 Scaling Theory and Critical Conductivity Exponent....12

2.3.a Scaling Theory for Non - Interacting Electrons....12

2.3.b Scaling Theory for Interacting Electrons....14

2.3.c Experimental Findings....15

2.4 Weak Localization....15

2.4.a Correction to Conductivity due to Weak Localization....17

2.4.b Magnetoresistance due to Weak Localization....18

2.4.c Weak Anti-Localization....19

2.5 Electron-Electron Interactions....20

2.5.a Correction to Conductivity from Interactions....21

2.5.b Magnetoconductivity due to Interactions....21

2.5.c Correction to Hall Coefficient due to Interactions....22

3. Experimental........24
3.1 Samples........24
3.1.a Obtaining Samples........24
3.1.b Cutting and Cleaning Samples........25
3.1.c Attaching Leads........25
3.2 Room T Resistivity and Resistivity Ratio Measurements........26
3.2.a Introduction........26
3.2.b Three Kinds of Samples........28
3.2.c Van der Pauw Geometry and Resistivity Measurements........28
3.2.d Short Bar Shaped Samples........31
3.2.e Long Bar Shaped Sample........32
3.3 Measurements above 1.5 K........32
3.3.a Glass Dewar........32
3.3.b Small Magnet........33
3.3.c Sample Holder and Electrical Wiring........33
3.3.d Mounting of Samples and Effect of Stress........34
3.3.e Temperature Control........35
3.4 Measurements below 1 K........35
3.4.a General........35
3.4.b Designing the Right Sample Holder........36
3.4.c Glass Mixing Chamber........39
3.4.d Feed-Through........39
3.4.e The Sample Holder and Electrical Wiring........40
3.4.f Temperature Gradient of the Glass Mixing Chamber........42
3.4.g The Magnet........42
3.4.h Electrical Contacts........43

3.4.i Thermometery....44
3.4.j AC Measurements....44

4. Results and Discussion....46
4.1 Introduction....46
4.2 Studies in Zero Magnetic Field....50
4.2.a The Data....50
4.2.b Extrapolation to Zero Temperature....57
4.2.c Critical Exponent....63
4.3 Studies in Various Fixed Magnetic Fields....71
4.3.a The Data in Magnetic Fields....71
4.3.b Interaction Parameter....82
4.3.c Critical Exponent in a Magnetic Field....85
4.4 Magnetoresistance....88
4.4.a Introduction....88
4.4.b Interaction Parameter from Magnetoconductivity....90
4.4.c Interpretation of the Data within Interaction Theory....95
4.4.d Low Field Data and Inelastic Scattering Time....102
4.5 Insulating Samples....114
4.5.a The Temperature Dependence of the Resistivity....114
4.5.b The Magnetoresistance....116

5. Summary and Suggestions for Future Work....121
5.1 Summary....121
5.2 Suggestions for Future Work....124
5.2.a The Hall Coefficient....124
5.2.b The Dielectric Constant....125

5.2.c Stress Tuning of the Transition....125
5.2.d Is Spin-Orbit Scattering Important in the Hopping Regime?....126
References....127

List of Tables

4.1 Characteristics of Si:B samples studied at dilution refrigerator temperatures.....46

4.2 The fitting parameters of conductivity to $\Delta\sigma(T) = mT^{1/2} + BT^{p/2}$...53

4.3 The fitting parameters of conductivity to $\sigma(T) = \sigma(0) + mT^{1/2}$..........60

4.4 The critical exponents ν for some systems studied by other groups.....63

4.5 The parameters ν, σ_0, n_c, and σ_{min} for Si:B, Si:P, Si:As, and Si:(P,B).....69

4.6 The fitting parameters of conductivity to $\sigma(H,T)=\sigma(H,0)+m'T^{1/2}$....80

4.7 The parameters σ_0, n_c, and ν for H=0, 1.0 and 7.5 Teslas................87

4.8 The fitting parameter A_I for five Si:B samples.....99

4.9 Sample designation, boron concentrations, and T'_0 for insulating Si:B samples.....116

List of Figures

3.1 A sketch of the inner part of the dilution refrigerator....................38

3.2 A sketch of the glass mixing chamber and the sample holder......41

4.1(a) ρ(4.2K)/ρ(300K) plotted as a function of ρ(300K) for Si:B samples in the Van der Pauw geometry..48

4.1(b) ρ(4.2K)/ρ(300K) plotted as a function of boron concentration n for Si:B samples in the Van der Pauw geometry..........................48

4.2 Conductivity for ten Si:B samples plotted against temperature...51

4.3 The parameter B versus boron concentration n................................53

4.4 Conductivity for n = 5.01×10^{18}cm-3 plotted against $\sqrt{T}$.................54

4.5 Conductivity for n = $4.86 \times 10^{18} cm^{-3}$ plotted against $\sqrt{T}$.................55

4.6 Conductivity for n = $4.57 \times 10^{18} cm^{-3}$ plotted against $\sqrt{T}$.................56

4.7 Conductivity for ten Si:B samples versus $\sqrt{T}$ for T < 500 mK.........57

4.8 The conductivity slopes m for Si:B samples versus n.......................59

4.9 The conductivity slopes m for Si:P, Si:As, and Si:B plotted as a function of n/n_c 62

4.10(a) Conductivity for two just-insulating samples versus $\sqrt{T}$.........65

4.10(b) Logarithm of the resistivity for two insulating and three metallic samples plotted as a function of $T^{-1/4}$......................66

4.11 Zero T conductivity σ(H=0,T→0) versus concentration n...............68

4.12 Conductivity for n=$5.22 \times 10^{18} cm^{-3}$ versus $\sqrt{T}$ in various magnetic fields...72

4.13 Conductivity for n=$5.01 \times 10^{18} cm^{-3}$ versus $\sqrt{T}$ in various magnetic fields...72

4.14 Conductivity for n=$4.95 \times 10^{18} cm^{-3}$ versus $\sqrt{T}$ in various magnetic fields...73

4.15 Conductivity for n=4.86x10^{18}cm^{-3} versus $\sqrt{T}$ in various magnetic fields.......73

4.16 Conductivity for n=4.72x10^{18}cm^{-3} versus $\sqrt{T}$ in various magnetic fields.......74

4.17 Conductivity for n=4.57x10^{18}cm^{-3} versus $\sqrt{T}$ in various magnetic fields.......74

4.18 Conductivity for n=4.38x10^{18}cm^{-3} versus $\sqrt{T}$ in various magnetic fields.......75

4.19 Conductivity for n=4.30x10^{18}cm^{-3} versus $\sqrt{T}$ in various magnetic fields.......75

4.20 Conductivity for n=4.20x10^{18}cm^{-3} versus $\sqrt{T}$ in various magnetic fields.......76

4.21 Conductivity for n=4.11x10^{18}cm^{-3} versus $\sqrt{T}$ in various magnetic fields.......76

4.22 Conductivity for ten Si:B samples for H = 1 Tesla plotted against $\sqrt{T}$.......77

4.23 Conductivity for ten Si:B samples for H = 7.5 Tesla plotted against $\sqrt{T}$.......79

4.24 The conductivity slopes m' in magnetic fields versus n.......81

4.25 ($\gamma\tilde{F}_\sigma$) and (γF) versus boron concentration n.......83

4.26 Zero T conductivity at fixed fields σ(H,T→0) versus n.......86

4.27 Δσ(H,T) for n = 4.95x10^{18} cm^{-3} plotted against H.......89

4.28 Δσ(H,T) for five Si:B samples versus $H^{1/2}$ at T= 0.31 K.......91

4.29 Δσ(H,T) for a Si:B sample with n = 4.86x10^{18}cm^{-3} versus $H^{1/2}$ at three fixed temperatures.......92

4.30 ($\gamma\tilde{F}_\sigma$) deduced from both *T* and *H* dependences versus n.......93

4.31 The amplitude A in eq. (4.4.3) plotted against $\tilde{F}_\sigma$.......95

4.32 The calculated values of $g_3(h)$ versus $h = g\mu_B H/k_B T$......................96

4.33 $\Delta\sigma(H,T)$ for $n = 5.01x10^{18}$ cm^{-3} versus H with fitted curves.......97

4.34 $\Delta\sigma(H,T)$ for $n = 4.86x10^{18}$ cm^{-3} versus H with fitted curves.......97

4.35 $\Delta\sigma(H,T)$ for $n = 4.57x10^{18}$ cm^{-3} versus H with fitted curves.......98

4.36 $\Delta\sigma(H,T)$ for $n = 4.38x10^{18}$ cm^{-3} versus H with fitted curves.......98

4.37 $\Delta\sigma(H,T)$ for $n = 4.30x10^{18}$ cm^{-3} versus H with fitted curves.......99

4.38 The residual , $-\{[\sigma(H,T)]_{exp.}-[\sigma(H,T)]_{fit}\}$ versus magnetic field H for $n = 4.30x10^{18}$ cm^{-3}..100

4.39 $\Delta\sigma(H,T)$ for a Si:B sample and a Si:P sample versus field H.......102

4.40 $\Delta\sigma(H,T)$ for $n = 4.95x10^{18}$ cm^{-3} versus the square of field H^2..105

4.41 The slope C(T) versus temperature for n= $4.95x10^{18}$ cm^3.........106

4.42(a) $\Delta\sigma(H,T)$ versus magnetic field H for $n = 5.22x10^{18}$ cm^{-3}.......107

4.42(b) $\Delta\sigma(H,T)$ versus square of field H^2 for $n = 5.22x10^{18}$ cm^{-3}...107

4.43(a) $\Delta\sigma(H,T)$ versus magnetic field H for $n = 4.72x10^{18}$ cm^{-3}.......108

4.43(b) $\Delta\sigma(H,T)$ versus square of field H^2 for $n = 4.72x10^{18}$ cm^{-3}....108

4.44(a) $\Delta\sigma(H,T)$ versus magnetic field H for $n = 4.20x10^{18}$ cm^{-3}.......109

4.44(b) $\Delta\sigma(H,T)$ versus square of field H^2 for $n = 4.20x10^{18}$ cm^{-3}....109

4.45(a) $\Delta\sigma(H,T)$ versus magnetic field H for $n = 4.11x10^{18}$ cm^{-3}.......110

4.45(b) $\Delta\sigma(H,T)$ versus square of field H^2 for $n = 4.11x10^{18}$ cm^{-3}....110

4.46 The slope C(T) versus temperature for four Si:B samples..........111

4.47 The hole inelastic scattering rate $1/\tau_{in}$ versus temperature for a Si:B sample with n= $4.95x10^{18}$ cm^3..112

4.48 Ln(ρ) for four insulating Si:B samples versus $T^{-1/2}$.....................115

4.49 $\Delta\rho(H)/\rho(0)$ for four insulating Si:B samples versus magnetic field H at 4.0 K..118

4.50 $\Delta\rho(H)/\rho(0)$ for three insulating Si:B samples versus magnetic field H at 1.6 K..118

4.51 The logarithm of the resistivity for a Si:B sample versus $T^{-1/2}$ at various magnetic fields..119

1. Introduction

An insulator is characterized by a conductivity which vanishes at zero temperature, while the zero T conductivity of a metal has a finite non zero value. There are many materials in which a transition occurs from insulating to conducting behavior. The M-I transition which occurs in doped semiconductors has been studied intensively for many years[1]. If the density of impurities is high enough, a doped semiconductor exhibits metallic behavior. When the impurity density is reduced below a critical value n_c, it becomes an insulator. In addition to varying the density of impurities, a doped semiconductor with a given concentration of impurity may be brought across the transition by application of stress or magnetic field.

Historically, there are two different approaches to the metal-insulator transition. The Mott-Hubbard model[2] treated electron correlations only by considering the on-site repulsion between two electrons on the same impurity center and neglects the randomness of the impurity potential. An alternative and competing mechanism is the localization of electrons due to disorder, called the Anderson transition[3]. In this model, one considers only the randomness of the impurity potential seen by electrons and neglects electron-electron interactions completely.

The roles of these two effects - disorder and electron electron interactions near the metal-insulator transition - is an issue which has been studied for many years, and it is now agreed that both processes play important roles. Measurements[4] performed at very

low temperatures very near the transition have shown that the zero temperature conductivity is continuous as expected in the theory of localization. The minimum metallic conductivity originally expected for a Mott transition appears to be absent in most cases. On the other hand, electron interactions must be invoked to account for the observed temperature dependence of the conductivity in disordered systems[5]. Similarly, it is clear that both electron interactions and localization are necessary to explain the Hall coefficient, the magnetoresistance and other properties.

Despite extensive study of the metal-insulator transitions in doped semiconductors, many problems remain unresolved or not completely understood. One such open question is the value of the critical exponent which characterizes the approach to the transition of the zero T conductivity. In the case of a continuous transition, the zero temperature conductivity can be described by

$$\sigma(T\rightarrow 0) = \sigma_0(n/n_c - 1)^{\nu} \tag{1.1}$$

where ν is the critical conductivity exponent. The first determination of the critical exponent was made on uncompensated n-type Si:P[4,5] and shows $\nu = 1/2$. Subsequent measurements on other uncompensated silicon based n-type systems such as Si:As[6], Si:Sb[7] and Si:(As,P)[8] also give ν values close to 1/2. On the other hand ν values close to 1 have been found in many systems, including most of the amorphous materials studied[1], Ge:Sb[9,10] (both compensated and uncompensated) and compensated silicon Si:(P,B)[11]. The apparent difference in critical exponents between uncompensated n-type silicon and most other systems studied is still a puzzle. Most of

the theories[12,13] developed have predicted an exponent of 1. The only theory[14] which predicts an exponent of 1/2 is for non-interacting electrons in the presence of spin-flip scattering. This does not give satisfactory explanation for the anomalous exponent of 1/2 in n-type uncompensated silicons since the studies of conductivity have shown that interactions are important in these systems. The scaling theory[13] for interacting electrons yield an exponent of 1 for the cases of strong spin-flip scattering, strong spin-orbit scattering or a strong magnetic field. Thus, it is of interest to study the critical exponent of a system in the presence of strong spin-orbit scattering or a strong magnetic field. Other interesting problems such as the effect of compensation on the value of the critical exponent[1], the possible critical behavior of the Hall coefficient as the transition is approached[15], and the possible existence of localized magnetic moments on the metallic side[16] have also drawn much attention.

So far, investigations have centered largely on n-type materials, which are assumed to be typical and representative of all doped semiconductors. There are, however, interesting and important differences for p-type doped semiconductor which merit separate and careful attention. While n-type Si and Ge have six and four degenerate conduction band minima respectively at different equivalent points in the Brillouin zone, their p-type counterparts have degenerate light- and heavy-hole valence band maxima at $k = 0$ and a spin-orbit split hole band shifted downward in energy by spin-orbit coupling. These differences have a number of interesting consequences. For example, the anisotropy of the conduction band

and the effects of intervalley scattering have been invoked to account for some of the observed properties of Si:P and Ge:Sb near the transition[17]. The valence bands, on the other hand, are essentially isotropic, and instead of intervalley scattering one must consider the effect of inter-valence band scattering involving the light and heavy hole bands. Another important difference is that spin-orbit scattering effects are associated in n-type materials with the dopant, and the importance of spin-orbit scattering depends on the dopant mass. In p-type materials, strong spin-orbit scattering derives instead from the structure of the host valence bands[18]. A detailed investigation of the transport behavior of p-type material, and a comparison with its n-type counterpart can thus yield interesting information concerning the role of spin-orbit scattering, anisotropy and other factors associated with the nature of the bands.

We have undertaken a systematic study of the transport and magnetotransport properties of a series of p-type Si:B samples near the metal-insulator transition at temperatures down to 55 mK and in magnetic fields up to 9 Tesla. Through a detailed study of the temperature dependence of the conductivity of a set of carefully chosen Si:B samples, we have determined the critical behavior of the conductivity in the zero temperature limit, and have obtained the critical conductivity exponent. We have also studied the critical conductivity exponent in a strong magnetic field. Through a systematic study of the temperature and magnetic field dependence of the conductivity and a comparison to n-type silicons, we have revealed some of the similarities and differences between *n*- and *p*-type silicons. Some of the work described in this thesis has been

published[19,20]. At the present time we lack a theoretical treatment for the case of *p*-type material, so that detailed explanations of some results must await further theoretical work. However, our results should serve as a comparison for future relevant theories.

The theoretical and experimental background in the field of metal-insulator transition is given in Chapter 2. Chapter 3 describes the experimental procedures used in this study. Chapter 4 presents the experimental results and their analysis. Chapter 5 summarizes the conclusions and suggests some possible directions for future work.

2. Background

This chapter gives a brief review of the theoretical and experimental background in the field of metal-insulator transitions. Since it is impossible to cover all the subjects, the review will concentrate on those aspects which are closely related to the content of this thesis. Since Mott put forward his simple theory on metal-insulator transition, much progress has been achieved in our understanding of the problem both theoretically and experimentally, especially during the past decade.

2.1 Mott Transition, Mott Criterion and Minimum Metallic Conductivity

2.1.a Screening and Mott Transition

The simplest model of a metal-insulator transition was studied by Mott[1] by considering screening. In the effective mass approximation, the Bohr radius of a hydrogenic impurity is

$$a_H = \hbar^2 \varepsilon_0 / m^* e^2 \qquad (2.1.1)$$

where m^* is the electron effective mass and ε_0 is the dielectric constant of the host lattice. Due to the screening by electrons, the Coulomb potential energy of an impurity atom is given by

$$U(r) = -\frac{e^2}{r} e^{-k_s r} \qquad (2.1.2)$$

where k_s is the screening wave vector. In the Thomas-Fermi approximation, the screening length k_s^{-1} is given by

$$k_s^2 = \frac{4\pi e^2}{\varepsilon_0}\frac{3n}{2E_F}. \qquad (2.1.3)$$

At high impurity concentration, the screening is strong (screening length is short), bound states can not be formed and the material is a metal. As the impurity concentration is reduced, the screening will be less effective and at some point bound states can be formed. At zero temperature the material will then be an insulator. The condition under which a metal-insulator transition occurs can be estimated by setting $k_s^{-1} \approx a_H$ and this leads to the well known Mott criterion

$$n_c^{1/3} a_H = 0.25 \qquad (2.1.4)$$

where n_c is the density of impurities at the transition. Despite its very simple derivation, the Mott criterion has been a very good estimate of the critical concentrations for many systems with n_c spanning over many orders of magnitude[2].

2.1.b Hubbard Bands

A more formal treatment of the metal-insulator transition was provided by Hubbard[3]. In this model the electron correlation is included by considering the Coulomb repulsion U between two electrons on the same site. When the impurity density is low, there

is very little overlap between neighboring electron wave functions. In the tight binding model, this corresponds to very narrow energy bands. If the band width B is much smaller than the on-site Coulomb repulsion U, the lower Hubbard band (of singly occupied atomic sites) is separated from the upper Hubbard band (of doubly occupied atomic sites) by a band gap (U-B). At zero temperature, the lower Hubbard band is occupied and the upper Hubbard band is empty and the material is an insulator. As the density of impurities is increased, the overlap also increases and the two bands broaden. At some point the two bands merge and the gap between them vanishes. Thus double occupancy becomes possible and the system becomes a metal.

In the above treatment, only the interactions between electrons on the same site is considered and the possible long range nature of Coulomb interactions is neglected, which turns out to be important for a disordered material[4]. The above model also neglects disorder completely, that is, the randomness of the impurity potential. Disorder is always present and is important in systems such as doped semiconductors.

2.1.c Minimum Metallic Conductivity

Mott[5] predicted that the transition is discontinuous and that there is a minimum metallic conductivity σ_{min}. The idea of a minimum metallic conductivity is based on the Ioffe-Regel criterion[6]. The criterion says that for metallic conduction to occur the electron mean free path l can not be shorter than its wave length λ, which is

approximately the distance d between impurities. Starting from the Boltzmann conductivity

$$\sigma_B = \frac{ne^2\tau}{m^*} = \frac{ne^2 l}{\hbar k_F} \qquad (2.1.4)$$

and setting $l = d$, we obtain the Ioffe-Regel conductivity

$$\sigma_{IR} = \frac{e^2}{3\hbar d} \qquad (2.1.5)$$

Mott further argues that the minimum metallic conductivity should be less than this value due to the reduction of the density of states at the Fermi level caused by disorder. The minimum metallic conductivity derived by Mott is:

$$\sigma_{min} = Ce^2/\hbar d c \qquad (2.1.6)$$

where dc is the average distance between impurities at the transition, and the numerical constant C is predicted to lie between 0.025 and 0.05. While many early experiments were interpreted in terms of σ_{min}, recent very low temperature measurements do not support its existence. The most convincing experiment was done on Si:P by applying uniaxial stress[7], allowing a region very near the transition to be resolved(0.1% of n_c). In that study, zero T conductivities much less than σ_{min} were measured, thereby ruling out the existence of σ_{min}. Mott[8] recently argued that the absence of σ_{min} is due to multiple scattering of electrons by impurities and the quantum interference associated with it. The latter constitutes an

important phenomenon, that is, weak localization, which will be discussed in more detail in section 2.4.

2.2 Anderson Transition

2.2.a Localization

Anderson[9] was the first to introduce the concept of localization in 1958. He considered a regular array of potential wells and then included disorder by introducing random fluctuations in the well depths over an energy range $\pm W/2$. In the tight binding model, the band width is proportional to the overlap integral between nearest neighbors. The overlap integral decreases rapidly as the distance between nearest neighbors increases. The quantity which measures the disorder is the ratio of the energy fluctuation W to the band width B. For sufficiently large values of W/B, all states are localized. There exists a critical value $(W/B)_{cri.}$ at which delocalized states begin to appear in the middle of the band. The wave functions of localized states behave as $\exp(-r/\xi)$, where ξ is the localization length. In this case electrons can not diffuse away. The above can be understood by considering only two wells[10]. Let $\phi_1(\phi_2)$ and $\varepsilon_1(\varepsilon_2)$ be the wave function and energy if the electron is in one of the wells with the other absent. First let the two wells have equal depth, that is $\varepsilon_1 = \varepsilon_2$. The solutions in the presence of both wells will be

$$\psi_1 = \frac{1}{\sqrt{2}}(\phi_1+\phi_2), \quad \psi_2 = \frac{1}{\sqrt{2}}(\phi_1-\phi_2) \tag{2.2.1}$$

The energy difference between the two states is $E_1 - E_2 = 2I$, where I is the overlap integral. In this case the probabilities of finding the electron in either of the two wells are equal. In other words, the electron is not localized no matter how far apart the two wells are. Now let's consider the case where the two wells are not equal in depth, that is, $\varepsilon_1 \neq \varepsilon_2$. The solutions in this case are

$$\psi_1 = c_1\phi_1 + c_2\phi_2, \quad \psi_2 = c_2\phi_1 - c_1\phi_2 \tag{2.2.2}$$

As long as $I/|\varepsilon_1 - \varepsilon_2| >> 1$ (weak disorder), we still have $c_1 \approx c_2$, and the situation is similar to the above. However, in the opposite limit, that is $I/|\varepsilon_1 - \varepsilon_2| << 1$ (strong disorder), we have a very different picture. Now $c_2/c_1 = I/|\varepsilon_1 - \varepsilon_2| << 1$ thus $\psi_1 \approx \phi_1$ and $\psi_2 \approx \phi_2$. The energies are $E_1 \approx \varepsilon_1$ and $E_2 \approx \varepsilon_2$. In each of the two states, the electron is localized in one of the two wells.

2.2.b Anderson Transition

In a doped semiconductor, there is a mobility edge E_c which separates the localized from the extended states. At a low impurity concentration, the Fermi level is below the mobility edge and the material is an insulator. As we increase the impurity concentration, the Fermi level rises and eventually lies above the mobility edge, and a transition occurs from an insulator to a metal[11]. Thus the Anderson transition is a localization transition driven by disorder. In this simple model electron-electron interactions are not taken into account, so that this description is also not complete for doped semiconductors.

In Anderson's model, potential wells of varying depth are located on sites of a regular crystal lattice. There can be another case where identical potential wells are distributed randomly in space. Theoretical work has shown that disorder of this kind also leads to localization[10].

2.3 Scaling Theory and Critical Conductivity Exponent

2.3.a Scaling Theory for Non-Interacting Electrons

The idea of scaling, first suggested by Thouless[12], led to the development of the scaling theory of localization of Abrahams et al[13]. One starts with a hypercube of size L which has a conductance $G(L)$. The corresponding dimensionless conductance is defined by $g(L) = G(L)\frac{\hbar}{e^2}$, where $\frac{\hbar}{e^2} = 2.4\text{x}10^{-4}\ \Omega^{-1}$ is a fundamental conductance unit. One now asks what happens to the conductance if the size of the hypercube is doubled, that is, of dimension $2L$. A hypothesis in the theory is that the conductance $g(2L)$ is determined uniquely by its initial value $g(L)$. The mathematical expression for the above idea is

$$\frac{d\ln(g)}{d\ln(L)} = \beta(g) \tag{2.3.1}$$

where $\beta(g)$ is an unknown function independent of L.

In the limits of $g >> 1$ and $g << 1$, the function $\beta(g)$ can be found from simple physical arguments. For $g >>1$, the disorder is weak and ordinary transport theory is valid. Therefore for a sufficiently large

L, the conductance and conductivity is related by $G = L^{d-2}\sigma$, where d is the dimension of the sample. The value of β in this case can be found easily,

$$\lim_{g\to\infty} \beta(g) = d-2. \tag{2.3.2}$$

At small g the states are localized and the conductance decreases exponentially with L, $g = g_0 e^{-\xi/L}$, where g_0 is a constant of order unity and ξ is the localization length. Thus

$$\lim_{g\to 0} \beta(g) = ln(\frac{g}{g_0}). \tag{2.3.3}$$

For three dimensional systems, β is zero for some conductance g_c, which is called the critical conductance. If $g > g_c$, then the edge doubling procedure will monotonically increase g and metallic behavior will be approached. On the other hand, if $g < g_c$, it will decrease with the doubling of L, and the macroscopic conductivity will be zero. It is important to note that we have a critical conductance instead of a critical conductivity. Near the transition the conductivity is $\sigma(0) = C' \frac{e^2}{\hbar\xi}$, ξ is the correlation length which diverges at the transition $\xi \sim (g-g_c)^{-\nu}$. The exponent ν can be calculated from perturbation theory and is found to be 1. However, the perturbative β function describes the localization transition accurately in $(2+\varepsilon)$ dimensions only for $\varepsilon << 1$. Extending these results to $d = 3$, i.e., for $\varepsilon = 1$ so that ε is not small, depends on the theory outside its range of validity and yields estimates of ν which are not necessarily correct[14].

In order to study the critical behavior of conductivity experimentally, we have to convert δg to some measurable and controllable quantities such as concentration, stress or magnetic field. We assume there exists a smooth and monotonic relationship between g and carrier concentration n in the critical region. We can express δg in terms of δn such that

$$(g-g_c) \approx \frac{dg}{dn}\Big|_{n_c}(n-n_c). \tag{2.3.4}$$

From this we can express zero temperature conductivity in a critical form:

$$\sigma(T\rightarrow 0) = \sigma_0(n/n_c-1)^{\nu} \tag{2.3.5}$$

As mentioned above, the scaling theory for non-interacting electrons predicts $\nu = 1$.

2.3.b Scaling Theory for Interacting Electrons

Following earlier work of Finkelshtein[15], Fermi liquid theory has been applied to a strongly interacting, disordered system of electrons by Castellani, et al[16]. These authors studied the critical behavior within different universality classes determined by the presence of various symmetry breaking fields such as spin-flip scattering, spin-orbit scattering or strong magnetic fields. In all the above cases, weak localization is suppressed, and the theory yields a critical exponent of 1.

2.3.c Experimental Findings

The first study[17] of the critical exponent was made on uncompensated n-type Si:P, where the exponent was found to be near 1/2. Studies utilizing stress to tune the transition confirmed this result[7]. Motivated by the puzzling difference in critical exponents between the measured value of 1/2 in Si:P and the value of 1 predicted by most theories, there has been continued intensive study of the critical exponent at the metal-insulator transition in disordered systems[18]. Most materials studied experimentally exhibit the expected critical conductivity exponent close to 1. This includes all the amorphous metal-insulator alloys studied to date, such as a-Kr:Bi[19], a-Si:Nb[20], a-Si:Au[21], a-Ge:Au[22], a-Si:Mo[23] and many others[16]. An exponent near 1 has also been found in compensated doped semiconductors, such as Ge:Sb[24], Si(P,B)[25] and Ga:As[16], as well as in uncompensated Ge:Sb[26]. On the other hand, all the uncompensated n-type silicon based systems studied so far show exponents near 1/2, namely Si:P[7,17], Si:As[27,28], Si:As+P[29] and possibly Si:Sb[30].

2.4 Weak Localization

Weak localization derives from enhanced back scattering due to quantum interference and has been extensively studied in many systems. Weak localization contributes to physical quantities and offers explanations for some anomalous observations. While the formal diagrammatic treatment of weak localization is very

complicated, Bergmann[29] has provided a physical picture on which the following discussion is based.

In disordered systems such as doped semiconductors, electrons suffer frequent scattering due to the random nature of impurity potentials. The elastic scattering of electrons by impurities does not destroy the phase coherence of the electron's wavefunction. The average distance between elastic scatterings is the electron's elastic mean free path, denoted by l. However, phase breaking mechanism, either spin-flip, spin-orbit, inelastic scattering or magnetic field destroys the phase coherence which is the origin for weak localization. Let's take inelastic scattering as an example. Inelastic scattering can be either electron-electron or electron-phonon scattering. The inelastic mean free path l_{in} is the average distance between inelastic scattering events. In order to calculate the probability of an electron traveling from site r_1 to site r_2, we have to consider all possible paths connecting r_1 and r_2. In general the phase relationship between two different paths is arbitrary. For a bulk sample of size $L >> l_{in}$, quantum theory should give the same answer for the conductivity as the classical one. However quantum interference becomes very important when an electron is scattered back to its starting point. In this case each closed path and its time reversed path have no phase difference between them. Because the two partial waves traveling in the two closed paths interfere constructively, the probability of an electron returning to the origin is larger than it would be if there were no interference effects. This is known as weak localization. Weak localization inhibits the transport of electrons and thus reduces conductivity. Weak

localization is limited by the dominant phase breaking mechanism, either spin-flip, spin-orbit, inelastic scattering or magnetic field. In the case that inelastic scattering is the dominant phase breaking mechanism, since only those closed paths smaller than l_{in} contribute to weak localization, the sum over loops which contribute to the decrease in conductivity is cut off beyond l_{in}.

2.4.a Correction to Conductivity Due to Weak localization

Theory[32,33] predicts a correction to the Boltzmann conductivity caused by weak localization in the following form

$$\sigma(T{=}0) = \sigma_B - \frac{e^2}{\hbar\pi^3}\left[\frac{1}{l} - \frac{1}{L}\right] = \sigma_B\left[1 - \frac{3}{(k_F l)^2}\left(1 - \frac{l}{L}\right)\right] \qquad (2.4.1)$$

where $\sigma_B = \frac{ne^2\tau}{m^*} = \frac{ne^2 l}{\hbar k_F}$ is the Boltzmann conductivity, l is the elastic mean free path and L is the size of the sample.

In the case that inelastic scattering is the dominant phase breaking mechanism, the inelastic scattering of electrons destroys the phase coherence which is the origin for weak localization. The inelastic scattering length is given by $l_{in} = \sqrt{D\tau_{in}}$, where D is the diffusion constant and τ_{in} is the inelastic scattering time. Thus l_{in} becomes the cut off length for weak localization at finite temperatures and we should replace L by l_{in} in the above expression. Because the inelastic scattering time τ_{in} is temperature dependent, so is the correction to the conductivity from weak localization. If we assume that $\tau_{in} = T^{-p}$, we can write

$$\Delta\sigma_L(T) = BT^{p/2}, \tag{2.4.2}$$

where B is a constant. The correction $\Delta\sigma_L(T)$ is positive so that the lower the temperature, the greater the localization due to the diverging nature of l_{in} as $T \to 0$. The value of p depends on the dominant inelastic scattering process. At relatively high temperatures, the inelastic scattering by phonons is dominant and $p = 3$. At low temperatures, electron-electron inelastic scattering is more important. The theoretical predictions are $p = 2$ for a clean metal and $p = 3/2$ for a disordered metal[34]. More recently a value of $p = 1$ has been predicted for samples very near the metal-insulator transition[35].

2.4.b Magnetoresistance Due to Weak Localization

In addition to spin scattering and inelastic scattering, a magnetic field can also destroy weak localization. For a closed path, a magnetic field perpendicular to it introduces a phase shift which is proportional to the magnetic flux ϕ contained within it. The phase difference caused by a field between two time reversed paths is $\Delta\phi = 2\pi\phi/\phi_0$, where $\phi_0 = \hbar/2e$ is a flux quantum. A magnetic field H thus destroys the constructive interference of those closed paths with sizes larger than the magnetic length $l_H = \sqrt{\hbar/eH}$ thus cutting off the sum over loops in much the same way as inelastic scattering processes. A small magnetic field has little effect on the conductivity since the large loops affected by it do not contribute to weak localization anyway. It is only when the magnetic field becomes

large enough to destroy the phase coherence of those loops with sizes smaller than l_{in} that there is a significant increase in the conductivity. Thus, very small magnetic fields such that $l_H >> l_{in}$ do not destroy weak localization but only sense it. As can be seen later, magnetoresistance at very low fields provides a useful tool for determining electron phase breaking lengths.

Magnetoresistance due to weak localization is negative. Theoretical calculations[36] gave the following expression for magnetoconductivity in three dimensions,

$$\Delta\sigma_L(H,T) = \frac{e^2}{2\pi^2\hbar}\left(\frac{eH}{\hbar}\right)^{1/2} f_3(x) \qquad (2.4.3)$$

where $x = 4L_{in}^2/L_H^2$ and $L_H = \sqrt{\hbar/eH}$ is the magnetic length.

The limiting behaviors of the function $f_3(x)$ are

$$f_3(x) = \begin{cases} 0.605 & x >> 1 \\ x^{3/2}/48 & x << 1 \end{cases} \qquad (2.4.4)$$

Weak localization theory predicts no correction to the Hall coefficient.

2.4.c Weak Antilocalization

The above is true when there is no spin-orbit scattering. In the presence of spin-orbit scattering, one has destructive rather than constructive interference, since spin-orbit scattering rotates the spins of the two partial waves in opposite directions, thus leading to what we call weak antilocalization[31]. In contract with weak localization,

the magnetoresistance should be positive in the case of weak antilocalization. Weak localization theory in the presence of strong spin-orbit scattering for p-type cubic semiconductors is not complete at this time. Thus, there is no closed mathematical expression for the magnetoconductivity. According to Altshuler et al[37], the magnetoconductivity for p-type cubic semiconductors due to localization is:

$$\Delta\sigma_L = -\frac{1}{4}\Sigma_0 + \frac{3}{4}\Sigma_1 - \frac{5}{4}\Sigma_2 + \frac{7}{4}\Sigma_3 \quad (2.4.5)$$

where the four terms correspond to the total moment of two holes with values of 0, 1, 2 and 3. Σ_0 is the same as that in the case without spin-orbit scattering[36,37], that is,

$$\Sigma_0 = \frac{e^2}{2\pi^2\hbar}\left(\frac{eH}{\hbar}\right)^{1/2}\frac{1}{2}f_3(x) \quad (2.4.6)$$

where $x = 4L_{in}^2/L_H^2$. However, we do not have mathematical expressions for the other terms. For strong spin-orbit scattering, the first term is the major contribution for small magnetic fields.

2.5 Electron-Electron Interactions

Electron-electron interactions are very important in disordered materials. Due to the frequent scattering of electrons by impurities, the electronic motion is diffusive. This gives more chance for electrons to interact with each other and screening becomes less effective. Theory[4] shows that there is a square root singularity in the density of states at the Fermi level caused by electron-electron

interactions. Electron-electron interactions have important effects on almost all the physical observables in a disordered system including conductivity, magnetoresistance, Hall coefficient, as well as thermodynamic quantities[37,38].

2.5.a Correction to Conductivity from Interactions

The temperature dependent part of the conductivity in zero magnetic field caused by electron-electron interactions is predicted by theory[4,38] to be

$$\Delta\sigma_I(T) = mT^{1/2} \tag{2.5.1}$$

$$m = \alpha\left(\frac{4}{3} - \frac{3\tilde{F}_\sigma}{2}\right) \tag{2.5.2}$$

where $\alpha = \frac{e^2}{\hbar}\frac{1.3}{4\pi^2}\sqrt{k_B/2\hbar D}$, and D is the diffusion constant. $\tilde{F}_\sigma$ is the interaction parameter appropriate for transport properties, which relates to the Fermi-surface average F of the screened electron-electron interactions by[38]

$$\tilde{F}_\sigma = -\frac{32}{3}\,[1- 3F/4 - (1-F/2)^{3/2}]/F. \tag{2.5.3}$$

2.5.b Magnetoconductivity due to Interactions

The temperature and magnetic field dependence of the conductivity due to interaction effects is[14,38,39]:

$$\Delta\sigma_I(H,T) = mT^{1/2} - 0.77\alpha\tilde{F}_\sigma T^{1/2} g_3(h), \tag{2.5.4}$$

where $h = g\mu_B H/k_B T$ and g_3 is defined by

$$g_3(h) = \int_0^\infty d\Omega \frac{d^2}{d\Omega^2}[\Omega N(\Omega)] \left(\sqrt{\Omega+h} + \sqrt{|\Omega-h|} - 2\sqrt{\Omega}\right) \quad (2.5.5)$$

with $N(\Omega) = \frac{1}{e^{\Omega}-1}$.

The limiting behaviors of $g_3(h)$ are,

$$g_3(h) = \begin{cases} \sqrt{h} - 1.3 & h >> 1 \\ 0.053h^2 & h << 1 \end{cases} \quad (2.5.6)$$

A strong magnetic field such that $g\mu_B H >> k_B T$ will result in Zeeman splitting between electrons with opposite spins thus cutting off the diverging triplet channel[16]. The temperature and magnetic field dependence of the conductivity in this case is

$$\Delta\sigma_I(H,T) = m_H H^{1/2} + m' T^{1/2} \quad (2.5.7)$$

where $$m' = \alpha\left(\frac{4}{3} - \frac{\tilde{F}_\sigma}{2}\right), \quad (2.5.8)$$

and $$m_H = -0.77\alpha\sqrt{g\mu_B/k_B}\,\tilde{F}_\sigma. \quad (2.5.9)$$

2.5.c Correction to Hall Coefficient due to Interactions

Interaction theory predicts a similar temperature dependence for the Hall coefficient as that for the conductivity. Specifically, we expect[40]

$$\frac{\Delta R_H(T)}{R_H} = 2\,\frac{\Delta\rho(T)}{\rho}\,. \tag{2.5.10}$$

From theoretical predictions, only interaction effects contribute to the temperature dependence of the Hall coefficient. We may be able to gain some knowledge about interactions by studying the Hall coefficient. In particular, it may be helpful in separating the two mechanisms, namely weak localization and interactions.

3. Experimental

3.1 Samples

3.1.a Obtaining Samples

All the boron doped silicon samples used in this study are nominally uncompensated. They were grown from the melt by the Czochralski method, and obtained from Pensilco Crystals. The impurity concentration in the crystal is determined by the amount of impurity added to the melt. The segregation coefficient χ, which is defined as the equilibrium ratio of the impurity concentration in the crystal to that in the melt, is 0.8 for boron[1] compared with 0.35 for phosphorus[1]. Because the segregation coefficient χ is less than unity, there is always a concentration gradient along the axis. Obviously, the bigger the segregation coefficient, the smaller the concentration gradient if other conditions are fixed. Thus it is easier to grow homogeneous Si:B samples than silicon containing other dopants by the Czochralski method. All theoretical models are derived on the assumption that samples are homogeneous and there is therefore a distinct experimental advantage for Si:B. On the other hand, if one needs a large variation in impurity concentrations among samples, one can not obtain this from a single ingot, and it is necessary to grow a few short ingots with different amounts of impurity added.

Our Si:B wafers obtained from Pensilco were cut from different ingots. They came in 20 groups with 3 or 4 wafers in each group. The boron concentrations of the wafers within a group are very close. All the wafers are about 5cm in diameter and 0.3mm thick with one

face polished. The nominal resistivities range from 1.4 to 1.8 (10^{-3} Ω-cm), which correspond to a variation in boron concentrations from 3.8 to 5.4 (10^{18} cm^{-3}).

3.1.b Cutting and Cleaning Samples

The wafers were cut into pieces of the desired size with a South Bay model 650 diamond wheel. A wafer was mounted onto a plastic plate with wax. Then the plastic plate with the wafer on it was held in the holder of the diamond saw. When the cutting was done, the wax was melted on a hot plate and the Si:B pieces were removed free from stress. The samples were first wiped and rinsed in acetone to get rid of the mounting wax. Then they were cleaned with isopropyl alcohol. It is necessary to remove the damaged surface layer due to machining because this layer can have a higher conductivity than the bulk and can partially short the sample. The damaged surface layer was removed by etching the samples in a modified CP-4 solution. The composition of the solution is 3 parts in HF, 3 parts nitric and 10 parts acetic acids. The etching speed of the solution is about 0.5 mil per minute from each side of the sample. After etching the samples were thoroughly rinsed in distilled water to get rid of the residual acid.

3.1.c Attaching Leads

Making ohmic and low impedance contact to samples is essential for reliable low temperature transport measurements, and this

requirement is more stringent as the temperature is lowered. The usual method of making contact to Si samples is by special arc discharge technique, a method developed and described by R. J. Capik[2]. For Si:P and Si:As samples this has been proven very successful. A good contact is indicated by a very small contact resistance at room temperature which decreases as the temperature is lowered. A minimum requirement is that it increases less rapidly than the sample resistance. If the contact resistance is much bigger than that of the sample, serious heating of the sample due to contact resistance may occur during measurement. Inadequate contact also causes problems with Schottky barriers and non-linear I-V results. For measurements above 1 K, the arc discharge method was adequate for our Si:B samples. The typical contact resistance at room temperature is less than 1 Ω, it increases rapidly as the temperature is lowered, and increases more for samples with smaller carrier concentrations. The contact resistance ratio between 4.2 K and room temperature can be as high as 10. For measurements below 1 K other contact methods were necessary as described later. The contacts as described above were made to freshly etched samples, and finished samples were kept in a vacuum container to reduce oxidation.

3.2 Room T Resistivity and Resistivity Ratio Measurements

3.2.a Introduction

In order to study the dependence of physical quantities such as the zero T conductivity and the Hall coefficient on the dopant concentration, it is necessary to determine systematically the concentrations of all the samples. A very handy and easy way is to measure the room T resistivities and use the established calibration curve. A relation between carrier concentration and room T resistivity for Si:B has been made available by Thurber et al.[4] However, room T resistivity is not a very rapid function of the carrier concentration and the sensitivity of this method is limited. For critical behavior studies the dopant concentrations (in fact it is the relative concentrations) have to be determined accurately, especially for samples very near the transition. On the other hand, the resistivity ratio between 4.2 K and room temperature varies very rapidly with concentration. For samples very close to the transition (but still metallic) a 1% difference in room temperature resistivity corresponds to a 8% change in the ratio. For insulating samples the ratio varies more rapidly as a function of concentration than for metallic samples. Moreover, the resistivity ratio does not depend on the geometry of a sample. Thus measurement of resistivity ratios provides a more accurate determination of the relative dopant concentrations of the samples.

3.2.b Three Kinds of Samples

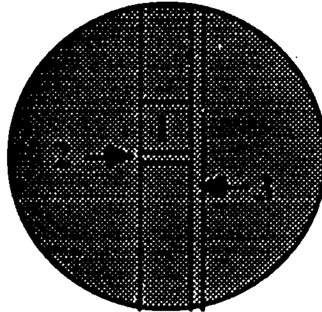

A typical wafer with a thickness about 0.3mm was cut into pieces as indicated above. The square shaped samples (1) of dimensions 8mmx8mm were used for resistivity and resistivity ratio measurements to generate a relation between the ratio and the dopant concentration. The short bar shaped samples (2) of dimensions 1.5mmx8mm were used for low temperature transport measurements. The long bar shaped sample (3) was used for ratio measurements to get a measure of the homogeneity of the wafer.

3.2.c Van der Pauw Geometry and Resistivity Measurements

In 1958 van der Pauw[3] proposed a method for measuring the resistivity and the Hall coefficient of a thin sample of arbitrary shape. For the resistivity determination this involves the measurements of two resistances and the thickness of the sample. The contact and lead configuration is indicated below.

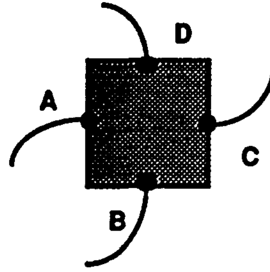

R_1 is defined as V_{CD}/I_{AB} and R_2 as V_{DA}/I_{BC}. In the actual measurements we first pass a current through leads A and B and measure the voltage drop across leads C and D. Then we drive a current through BC and record the voltage across DA. The expression for resistivity derived by Van der Pauw[3] is:

$$\rho = \frac{\pi t}{2\ln 2}(R_1 + R_2)\, f(R_1/R_2) \tag{3.2.1}$$

where f is a function of R_1/R_2 and is given by the equation:

$$\frac{R_1 - R_2}{R_1 + R_2} = \frac{f}{\ln 2} \quad \mathrm{arccosh}\{\frac{\exp(\ln 2/f)}{2}\} \tag{3.2.2}$$

One can not solve for f explicitly, however, the values of f and R_1/R_2 can be tabulated.

If R_1/R_2 is close to unity one obtains f approximately,

$$f \approx 1 - (\frac{R_1 - R_2}{R_1 + R_2})^2 \frac{\ln 2}{2} - (\frac{R_1 - R_2}{R_1 + R_2})^4 \{\frac{(\ln 2)^2}{4} - \frac{(\ln 2)^3}{12}\}. \tag{3.2.3}$$

In my measurements the electrical leads were placed so that $R_1/R_2 \approx 1$, and the above expression was always used.

The thickness t enters into the expression for ρ. The values of t were measured with a thickness indicator with a resolution of 0.2 thousandth of an inch, which is about 2% of the thickness of the

sample. In Van der Pauw[3] geometry errors come mainly from two sources. First is the misplacement of contacts on samples. The requirement of the Van der Pauw method is that the size of the contact must be small and the contact be placed at the outer edge of a sample, and that the thickness t be much smaller than other dimensions (i.e. he assumed 2-D geometry). Small sized contacts were made by melting as short gold wires onto samples as possible. The finite size of the contacts is offset by the relatively large size of the samples. Great care was exercised to make contacts as close to the edge of the sample as possible. The ratios of the other dimensions of a sample to its thickness is about 30, so that the error due to finite thickness is small. A second source of error comes from the determination of the thickness of a sample. This was limited by the resolution of the thickness indicator. The wafers were cut by the manufacturer and are very uniform in thickness. Our experience shows that a small wafer machine like the one in our lab can not produce samples of uniform thickness. The uniformity in thickness of the samples reduces the error in t considerably. Even so, many measurements on different points of a sample were made to eliminate accidental error and to scan the very small variation in thickness with position.

Standard DC methods were used to measure resistivities. A HP model 6181C DC current source was used to provide the constant current. The voltage was measured using a HP model 3478A Voltmeter. A typical current used at room T is 1 mA. The samples were covered during the process of measurement to eliminate thermal effect caused by air flow in the lab. The switching between

the two current-voltage configurations was done manually with a home-made switch box. The measurements at 4.2 K were done by immersing samples directly in liquid helium. This was accomplished by using a stick-shaped sample holder that fits into a liquid helium storage dewar. Around 30 samples were measured to generate a calibration relation between carrier concentrations and resistivity ratios. The absolute boron concentrations of samples were obtained from the measured room *T* resistivity values and by using the results of Thurber et al[4]. The boron concentrations obtained in this way were then related to the measured resistivity ratios. The plots of measured data are shown in Figs. 4.1(a) and 4.1(b).

3.2.d Short Bar Shaped Samples

The short bar shaped samples were used for low *T* measurements. For measurements above 1 K contacts to samples were made by arc discharge gold wire onto them directly. For measurements below 1 K, a different method was necessary for making contacts as described in detail in section 3.4.h. For bar shaped samples it is difficult to accurately determine the geometric factor that enters into the calculation of resistivity. However, the resistance ratio of a bar-shaped sample, which is independent of geometry, can be measured accurately. By using the calibration relation obtained in the above section we can determine both the room *T* resistivity and the boron concentration of a bar shaped sample from resistivity ratio measurements alone.

3.2.f Long Bar Shaped Sample

In order to estimate the degree of inhomogeneity of samples we measured differential resistivity ratios along a long bar shaped piece whose length is equal to the diameter of the wafers. We placed some 12 leads along the bar and measured at both room T and 4.2 K resistances between every 2 adjacent leads except the 2 leads at the ends which were used as current leads. From this we estimate that there are random variations in concentration from point to point on the order of 1 to 2%.

3.3 Measurements above 1.5 K

Measurements above 1.5 K were made in a glass dewar by pumping on ^{4}He. A home made superconducting magnet was used to produce magnetic fields up to 4 Tesla. This system is economical to run in terms of its consumption of liquid helium, and is very useful for preliminary measurements.

3.3.a Glass Dewar

The glass dewar system consists of a liquid nitrogen jacket and a liquid helium dewar. The vacuum shield of the helium dewar is pumped with a diffusion pump just before each run. The helium bath is pumped on by a LH 200 pump to obtain temperatures below 4.2K. The helium volume is about 4 liters.

3.3.b Small Magnet

The superconducting magnet that fits the glass dewar was home-built. About 8.5×10^3 turns of copper coated superconducting wire were wound on a hollow brass cylinder frame with an outer diameter of about $1\frac{1}{4}$" and about $4\frac{1}{2}$" long. The bore diameter is 1". The superconducting wire was commercially bought from Cryomagnetics Inc. The size of the bare wire is 0.011'' and its size is 0.012'' with the copper coating. The wire was wound manually using a lathe which was rotated very slowly. During the test run it was energized to 4 Tesla without quenching. The magnet can be attached to or detached from the sample holder depending on the purpose of a run. The current is supplied by a HP model 6260B power supply.

3.3.c Sample Holder and Electrical Wiring

The sample holder which fits the glass dewar is made of copper. The wires that connect the posts on the holder and the connector outside the dewar are made of constantan. The heater was also wound with constantan wire but the leads to the heater were copper wires. The carbon glass thermometer used for reading and controlling of the temperature was calibrated by and bought from Lake Shore. The temperature was controlled by either the pressure regulator or by the heater and a BTi controller, depending on the temperature range.

3.3.d Mounting of Samples and Effect of Stress

The commonly used method of thermally anchoring samples in low temperature measurements is to apply a material such as GE varnish 7031 or Apiezon grease, which is thermally conducting but electrically insulating, between the sample and sample holder. The above is useful and acceptable for n-type silicon. When I tried to use Apiezon grease for my Si:B samples, I found a big difference in the sample resistance at low T depending on whether or not Apiezon grease was used. Then I found out that it is the stress effect due to Apiezon grease which hardens as it is cooled. Due to the strong piezoelectric properties of *p*-type material like Si:B, the stress applied by grease changes the character of the sample a great deal. For a sample close to the transition, the change in the resistivity at 4.2 K associated with using grease can be as high as 20%. GE varnish 7031 which dries at room *T* has a similar effect on samples, and so does rubber cement. In order to mount samples free from stress, I tried to apply grease only to one end of a sample. The grease had to be limited to the outside of the region between the voltage leads. The thermal conduction between samples and sample holder is limited this way. Further, the contact resistance of Si:B samples is not small, and self heating becomes a problem. The sensitivity to stress and the relatively big contact resistances in Si:B samples make measurements very difficult. In order to avoid stresses and to enhance the thermal conduction, it became necessary to immerse samples directly in liquid helium. This eliminates the stresses

caused by using grease. This also increases the contact area of a sample to the cold environment, making self heating less likely.

3.3.e Temperature Control

The temperature was controlled either by regulating the vapor pressure of liquid helium or by using a heater feedback circuit. For temperatures below 4.2 K, they were controlled with a pressure regulator. The regulator stabilizes the vapor pressure around its set point thus keeping the temperature steady. Samples were directly immersed in liquid helium in this temperature range. During the experiment enough time was given to allow the system to come to thermal equilibrium. The lower the temperature, the longer the time required. The stability of the temperature was monitored by the read-out of the thermometer resistance with a AC bridge. For temperatures above 4.2 K a heater was used to control the temperature using a BTi 1000 Capacitance Bridge/Controller. The sample holder was surrounded by a vacuum space and samples were mounted with application of grease to one end only. Care was exercised to avoid self heating of samples. Different currents were used to ensure ohmic behavior.

3.4 Measurements below 1 K

3.4.a General

Because the Metal-Insulator transition is a phenomenon that occurs at zero temperature, it is essential that measurements be taken to as low a temperature as possible. Temperatures down to about 55mK were obtained in an Oxford Model 75 dilution refrigerator.

3.4.b Designing the Right Sample Holder

A sketch of the insert of the dilution refrigerator is shown below. As indicated in the sketch, the bottom of the mixing chamber is about 12cm from the center of the magnet. In order to measure samples both at low T and in magnetic fields, care must be exercised in the design of the sample holder to insure good thermal conduction and to avoid heating due to eddy current. Our first attempt was to use a bunch of very thin insulated copper wires to connect the bottom of the mixing chamber and samples. The wires were held rigidly by a Teflon frame. This design was chosen in order to minimize eddy currents. Although it was quite effective from this point of view, it provided inadequate thermal contact between the samples and the mixing chamber. Our second version was a sample holder made of copper which was quite massive. A number of slices were made in order to reduce eddy current. The problem of eddy current for this sample holder is not very serious. However, although superior to the teflon holder, the thermal conduction was still unsatisfactory. Its performance was tested by placing a few thermometers at the position of the sample and the mixing chamber. Above about 200 mK, the temperature gradient between the position

of the sample and the mixing chamber is very small. However, below 200 mK there is a sizeable temperature difference between the position of the sample and the mixing chamber. In addition, thermal contact between the samples and the holder required the use of grease which entailed stresses which are not acceptable for Si:B samples as described earlier.

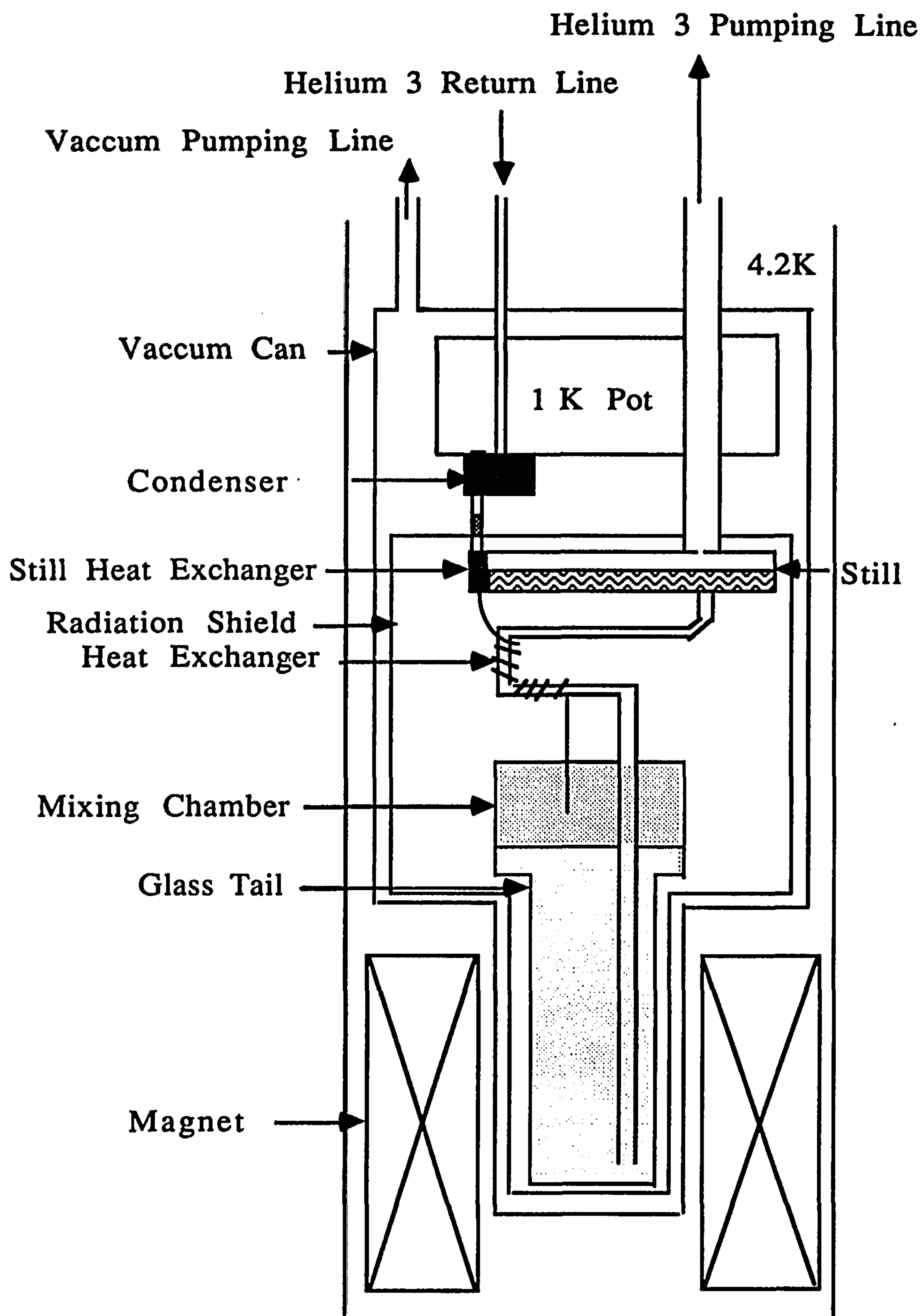

Fig. 3.1 The inner part of the dilution refrigerator.

3.4.c Glass Mixing Chamber

An alternative method for establishing thermal contact is to immerse the samples in the ^3He-^4He mixture in a long glass mixing chamber provided by Oxford which extends to the center of the magnet. The disadvantage of this method is that each time one wants to change samples, one has to detach and attach the mixing chamber. Furthermore, all the electrical leads have to be brought into the mixing chamber and care had to be taken to insure that the feed-through is leak tight each time.

3.4.d Feed-Through

The feed-through to the mixing chamber was made of brass and filled with stycast. Since the thermal contraction of stycast is a little bit larger than that of brass, it is necessary to apply stycast to both the inside and the outside of the brass tube. This way, when the stycast is cooled it will squeeze on the brass and insure that the feed-through is leak-tight. The opening of the brass tube was machined very thin to allow it to yield to stycast during thermal contraction when it is cooled down. A teflon cast was used to hold the stycast outside the tube and to let the stycast form a nice shape. Forty-five copper wires were brought through the feed-through. It was leak tested before and after attaching to the glass chamber both at room and nitrogen temperatures. It has been thermally cycled many times and has not yet leaked.

3.4.e the Sample Holder and Electrical Wiring

The sketch of the sample holder and the supporting rod is indicated below. The supporting rod is made of plastic and its function is to hold the sample holder in the right position(not to touch the bottom and the wall of the glass chamber). The sample holder is made of teflon. There are three main points to note regarding the wiring of a sample holder for use at very low temperatures, namely thermal anchoring, thermal resistance and impedance matching with measuring instruments. The wires were thermally sunk at different stages, at the 1 K pot, at the still, at the heat exchangers and at the top of the mixing chamber. This was done by using heat stations. The heat stations were made of copper tubing with a few turns of wire wound around them and attached to different cold places with screws. The wires from the bottom of the 1 K pot to the feed-through are either superconducting or constantan wires. Their thermal conduction is poor at low T, thus reducing the heat leak to the mixing chamber. The use of superconducting wires served the purpose also of matching the low impedance of the AC bridge used for measurements. The wires from the feed-through to the samples are made of copper where thermal conduction is not a problem. The heater was made with Evanohm wires. Low impedance wires were used as leads to the heater.

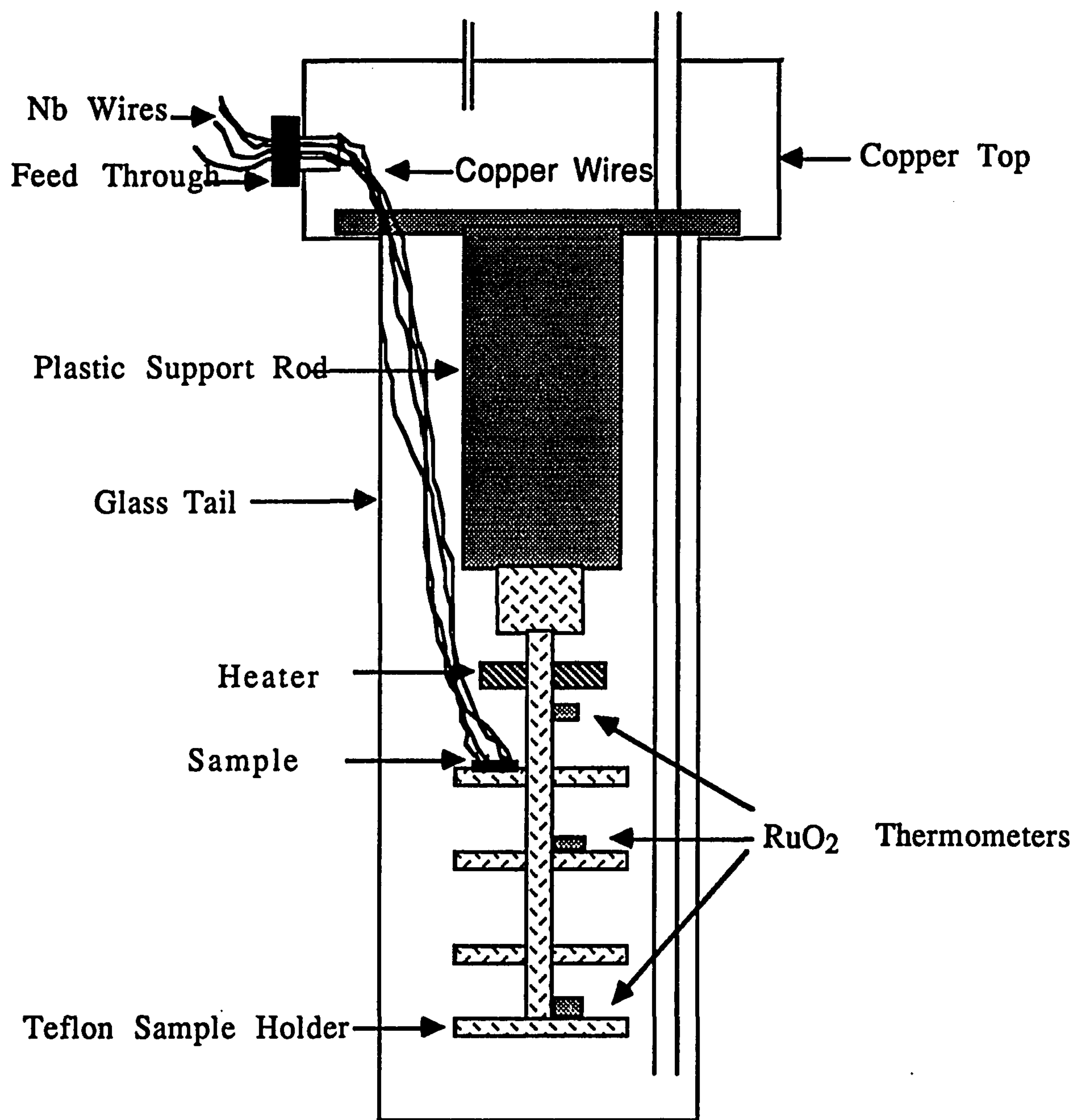

Fig. 3.2 The glass mixing chamber and the sample holder.

3.4.f Temperature Gradient of the Glass Mixing Chamber

At first we attempted to control temperature from the top of the mixing chamber. We put a control sensor and a heater on the top of the mixing chamber which is made of copper. The effect of the magnetoresistance of the thermometer used as the sensor is very small because it is far away from the magnet. However, there are other problems with this arrangement. There is a temperature gradient between top and bottom of the mixing chamber. This gradient is reduced by running the ^{3}He pumping tube all the way down to the bottom of the chamber, but this does not eliminate the problem entirely. We then decided to control temperature at the sample position. The samples are distributed over a vertical distance of about 1.5". Because it is impractical to put a thermometer at each sample position(for the large number of samples), I had to worry about a possible temperature gradient along this 1.5" distance. We found that the heater had to be placed just above the samples in order to minimize the temperature gradient. On the other hand, placing the heater at the bottom of the mixing chamber only made the temperature gradient problem worse. During measurements, the thermometers were very close to the samples so that the temperatures measured should be very close to those of the samples. There is one problem with this arrangement when doing measurements in magnetic fields, namely the magnetoresistance of the thermometer.

3.4.g the Magnet

The dilution refrigerator dewar is equipped with a 9 Tesla magnet, which can be taken to 10 Tesla with the use of a λ point fridge. The power supply for the magnet is a HP model 6260B DC Power Supply. The magnet current is controlled by a Cryomagnetics model 60 Programmer/Monitor. The power supply to the persistent switch heater is a Cryomagnetics model 30.

3.4.h Electrical Contacts

As noted earlier, contacts made with direct arc discharge are not good enough for measurements at very low temperatures. One method for making low impedance contact to p-type silicon is by depositing a thin aluminum film. This method was implemented as follows. Four spot shaped aluminum films were deposited onto each bar shaped freshly etched sample. Then samples were annealed at 450° under vacuum. Finally, gold wires were attached to aluminum films by arc discharge. Contact resistances of samples treated this way are smaller by about one order of magnitude than those made by arc discharge. It was felt, however, that transitions of these contacts between the superconducting and normal states as a function of temperature and magnetic field would cause problems. The best method available is ion implantation. Contacts to samples measured below 1K were therefore all made by ion implantation. Boron ion implants were made by Dr. Alice White of AT&T labs in the shape of four thin strip-like areas on each sample. Gold wires were then attached to the ion implanted areas by arc discharge as electrical leads. Contact resistances made this way are comparable to

those of aluminum film contacts. Samples were attached to the sample holder with dental floss so that their faces were perpendicular to the magnetic field. No grease was necessary because samples were immersed in ^{3}He-^{4}He mixture insuring that measurements were made under stress-free conditions.

3.4.i Thermometery

Thermometers used for measuring and sensing temperatures are RuO_2 thick film thermometers. A calibrated and a number of uncalibrated thick film thermometers were obtained from Cornell University, and we subsequently calibrated a few of them against the calibrated one. The advantages of these thermometers are their stability and low noise, and the fact that the magnetoresistance is also small. The thermometers were calibrated in magnetic fields. The magnetoresistance of the thermometers were measured at fixed temperatures, and the temperatures were indicated by a thermometer on the top of the mixing chamber where the magnetic field is very small. The measurements above about 300 mK were made in our lab with the copper sample holder. Measurements at lower temperatures were made in P. Lindenfeld's lab at Rutgers University by Y. Zhang. The temperatures in magnetic fields were then determined by taking the magnetoresistance of the thermometer into account.

3.4.j AC Measurements

Standard four terminal AC methods were used for measurements below 1K. Both a AVS-46 AC bridge and a PAR 124A lock-in amplifier with a 118 differential preamplifier were employed for the measurements. The frequency of the excitation of the bridge is 15 Hz and the lock-in amplifier was used at a frequency of 17.5 Hz. The lowest excitation of the bridge is 10 uV. For a sample with a resistance of 2Ω this corresponds to a power level of 5×10^{-11}W. At higher temperatures measurements were mainly made with the bridge. Different excitations were used to ensure ohmic behavior of samples. At the lowest temperatures the lock in amplifier was used. The lock-in preamplifier has a input ratio of 10. Excitations as low as 0.1uV were used and gave stable signals. This corresponds to a power level of 10^{-14}W for a 1Ω sample.

4. Results and Discussion

4.1 Introduction

This chapter presents the results of resistivity and magnetoresistance measurements on a series of metallic Si:B samples listed in table 4.1.

name	R(300K) (Ω)	R(4.2K)/R(300K)	ρ(300K) ($10^{-3}\Omega$-cm)	n ($10^{18}cm^{-3}$)
Si:B-1	0.939	2.684	17.0	4.11
Si:B-2	0.790	2.463	16.7	4.20
Si:B-3	1.006	2.270	16.5	4.30
Si:B-4	0.694	2.112	16.2	4.38
Si:B-5	0.762	1.811	15.8	4.57
Si:B-6	0.701	1.620	15.4	4.72
Si:B-7	0.753	1.489	15.1	4.86
Si:B-8	0.662	1.418	14.9	4.95
Si:B-9	0.662	1.384	14.8	5.01
Si:B-10	0.687	1.274	14.3	5.22

Table 4.1 The room temperature resistance, R(300K), room temperature resistivity, ρ(300K), ratios of resistance at 4.2K to that at room temperature, R(4.2K)/R(300K), and boron concentrations n for ten metallic Si:B samples studied at dilution refrigerator temperatures.

All samples were studied in an Oxford Model 75 dilution refrigerator at temperatures between 55 mK and 1.5 K and in magnetic fields up to 9 Tesla. Measurements above 1.5 K were made in a glass ^{4}He dewar in magnetic fields up to 4 Tesla. All the samples used for low temperature study are bar shaped with approximate dimensions of $8x1.5x0.3mm^3$. Their concentrations were determined from the resistivity ratios $\rho(4.2K)/\rho(300K)$ as follows. The room temperature resistivities and the ratios $\rho(4.2K)/\rho(300K)$ were measured for a large number of square shaped samples using the van der Pauw geometry as shown in Fig. 4.1(a). Using the Thurber[1] calibration curve, the ratio $\rho(4.2K)/\rho(300K)$ was plotted versus boron concentration n in Fig. 4.1(b), which is then used to determine n of the bar shaped samples directly from measurements of the ratio $\rho(4.2K)/\rho(300K)$. The error in measuring the resistivity is estimated to be about 2% stemming mainly from the uncertainty in the determination of sample thickness.

The uncertainty in the values of resistance and resistance ratio listed in table 4.1 is limited only by the measuring instrument, and errors less than 0.1% can be easily achieved. The errors in resistivity and concentration are larger, again due mainly to the uncertainty in the thickness of the square shaped samples. However, the resistivities and concentrations of bar shaped samples are obtained from ratio measurements and the use of Fig. 4.1, which was determined by averaging over many samples. This reduces the error somewhat, and we estimate the error in $\rho(300K)$ and n for bar shaped samples to be about 1%.

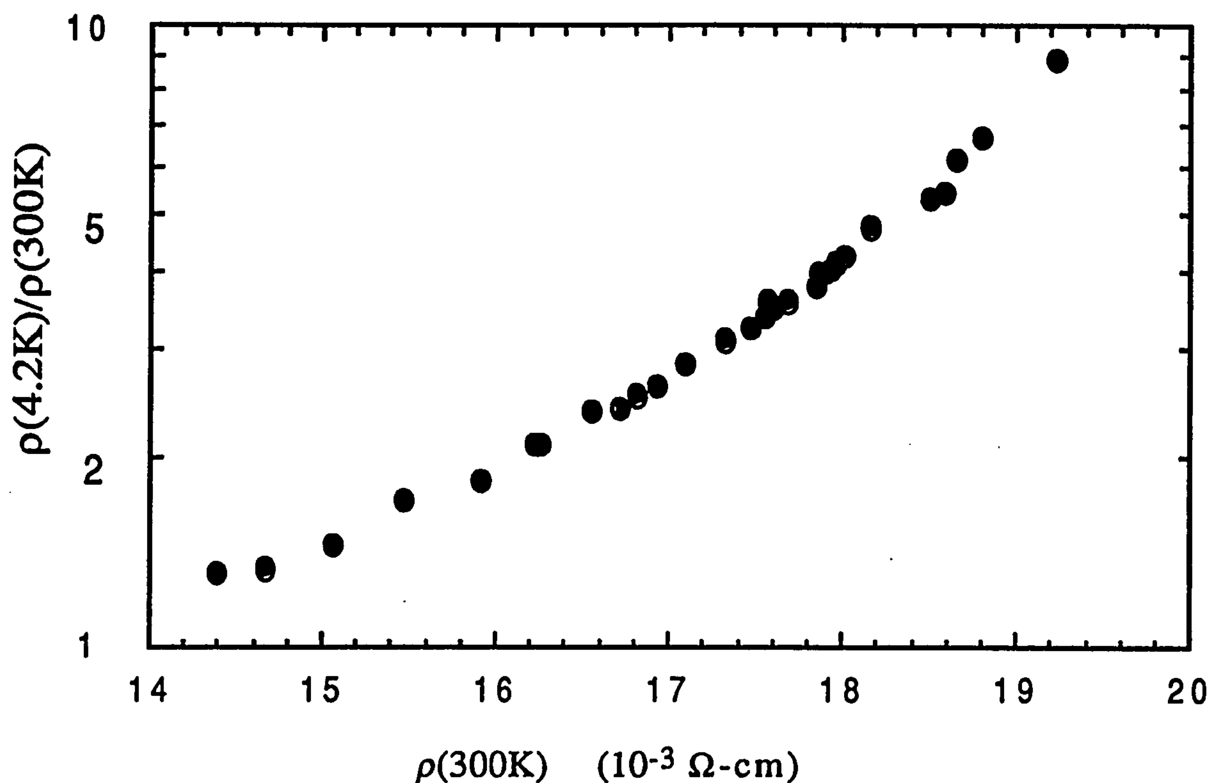

Fig. 4.1(a) Resistivity ratio ρ(4.2K)/ρ(300K) plotted as a function of the room temperature resistivity ρ(300K) on a semilogarithmic scale.

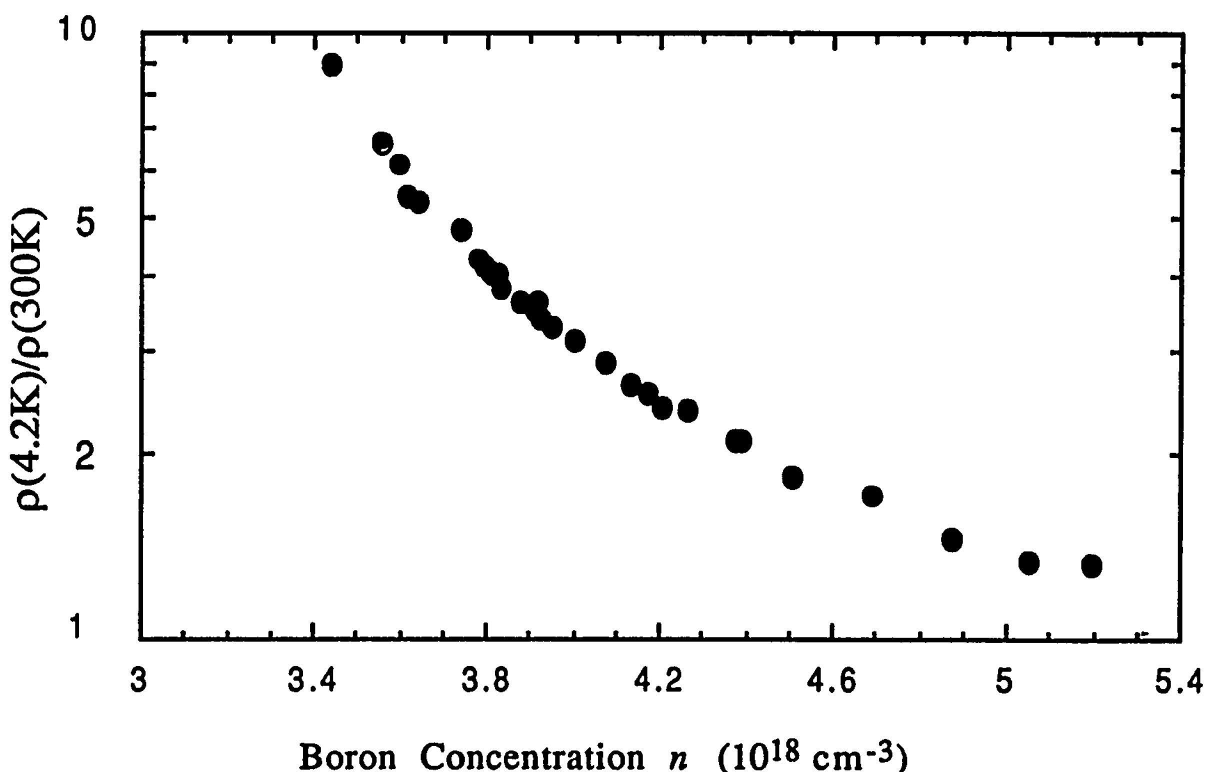

Fig. 4.1(b) Resistivity ratio ρ(4.2K)/ρ(300K) plotted as a function of boron concentration n obtained from Thurber et al[1], again on a semilogarithmic scale.

The resistivity ratios for all samples in this study are larger than one and vary rapidly with concentration near the transition, so that this is a more sensitive function of boron concentration than the room temperature resistivity. An additional advantage is that the dimensions of a sample do not enter the ratio measurement, and therefore the ratio provides a very accurate determination of the relative concentrations among samples. This is particularly important for the study of the critical exponent of the zero temperature conductivity.

4.2 Studies in Zero Magnetic Field

4.2.a The Data

The conductivities of ten metallic Si:B samples measured between 55 mK and 4.2 K in zero magnetic field are plotted in Fig. 4.2 as a function of temperature. The conductivities for samples with boron concentrations $n \geq 4.38 \times 10^{18} cm^{-3}$ increase as the temperature is lowered, as is characteristic for a good metal. However, the conductivities of those samples with $n \leq 4.30 \times 10^{18} cm^{-3}$ decrease as the temperature is decreased.

The temperature dependence of the conductivity at low T derives mainly from two different sources, namely localization and electron-electron interactions. The contribution from electron-electron interactions[2,3] is

$$\Delta\sigma_I(T) = m\sqrt{T} \qquad (4.2.1)$$

where the slope m depends on the diffusion constant D and interaction parameter F_σ, and will be discussed in more detail in the next section. The contribution from localization[4,5] is:

$$\Delta\sigma_L(T) = B\,T^{p/2} \qquad (4.2.2)$$

where B is a constant. The localization contribution is derived from a temperature dependent dephasing time τ_ϕ. In the case of inelastic scattering, $\tau_{in} \propto T^{-p}$, with p = 2 for a clean metal and p = 3/2 in the case of a disordered metal[6].

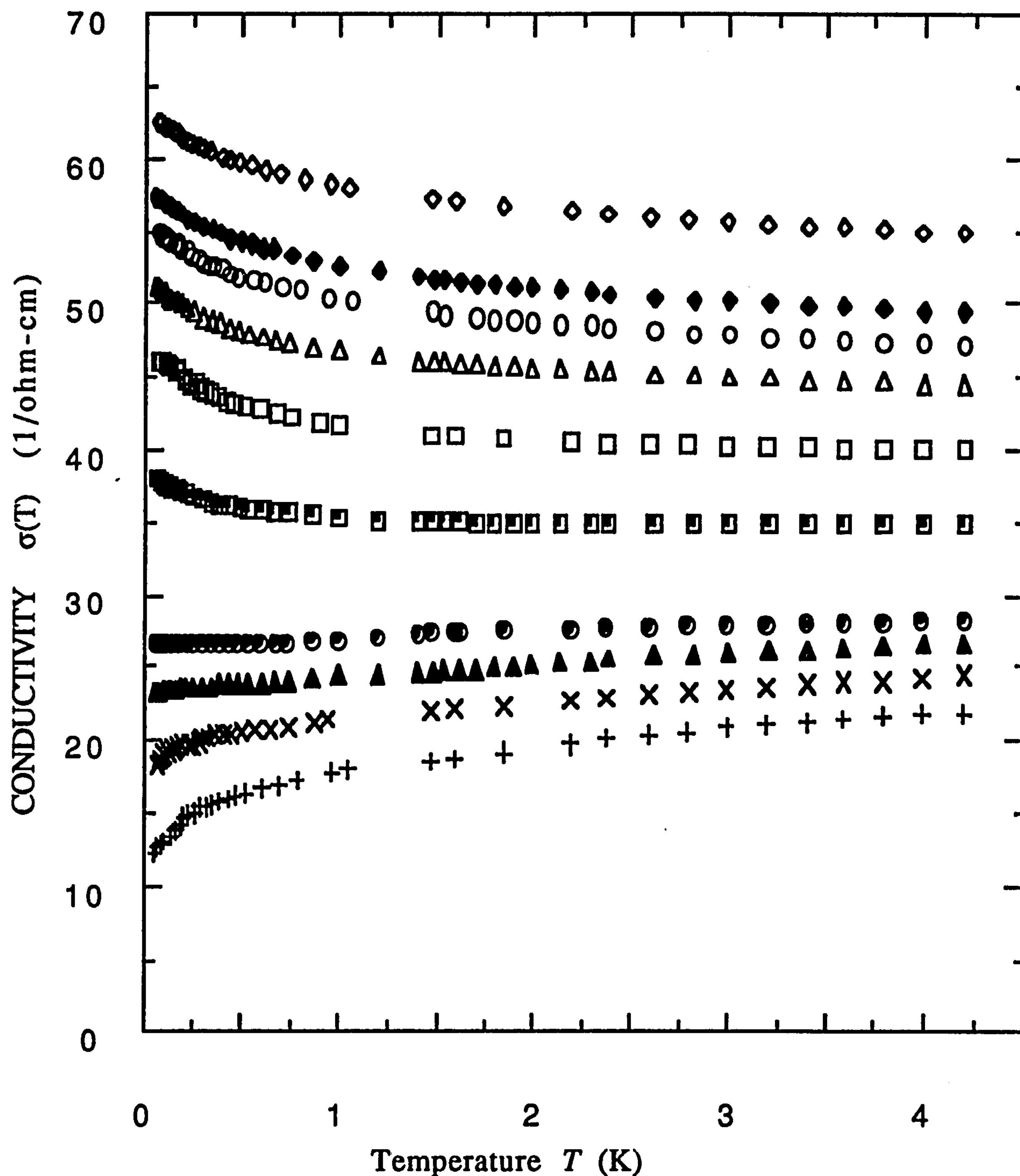

Fig. 4.2 The conductivities for ten metallic Si:B samples plotted against the temperatures. In units of 10^{18} cm^{-3}, their boron concentrations are: ◇ 5.22, ◆ 5.01, ○ 4.95, △ 4.86, □ 4.72, ■ 4.57, ● 4.38, ▲ 4.30, × 4.20, + 4.11.

The conductivity over the whole measured range of temperatures was fitted to the combination of interaction and localization effects expressed in the following,

$$\sigma(T) = \sigma(0) + mT^{1/2} + BT^{p/2} \qquad (4.2.3)$$

Here p was allowed to float, and its best value was between 1.3 and 1.65, depending on the sample. We therefore chose the value $p=3/2$, which is the value appropriate for a disordered metal. The parameters m and B derived from these fits are listed in table 4.2.

The above expression fits the data reasonably well for samples with negative values of $d\sigma/dT$. It should be noted, however, that the values of m and B depend rather strongly on the range of the temperature used, indicating that a fit to three terms, eq. (4.2.3), is not sufficient to describe the data very well. For those samples with positive $d\sigma/dT$, the fits are not good. Moreover, the fitted values of B are positive, which is not understood.

The values of the parameter B are plotted in Fig. 4.3. In the study of Ge:Sb, Thomas et al[7] fitted their data to eq. (4.2.3) with a value of $p = 2$ over a narrower temperature range (T $\leq$ 500 mK). The behavior of the parameter B in their case is similar to that shown in Fig. 4.3.

Name	n (10^{18} cm^{-3})	m ($(\Omega$–cm-K$^{1/2})^{-1}$)	B ($(\Omega$–cm-K$^{3/4})^{-1}$)
Si:B-4	4.38	-3.2	3.1
Si:B-5	4.57	-9.3	4.9
Si:B-6	4.72	-14.3	6.9
Si:B-7	4.86	-12.2	5.5
Si:B-8	4.95	-12.8	5.4
Si:B-9	5.01	-12.0	4.9
Si:B-10	5.22	-11.4	4.5

Table 4.2 The parameters for samples with negative values of $d\sigma/dT$ by fitting to eq.(4.2.3), $\sigma(T) = \sigma(0) + mT^{1/2} + BT^{p/2}$.

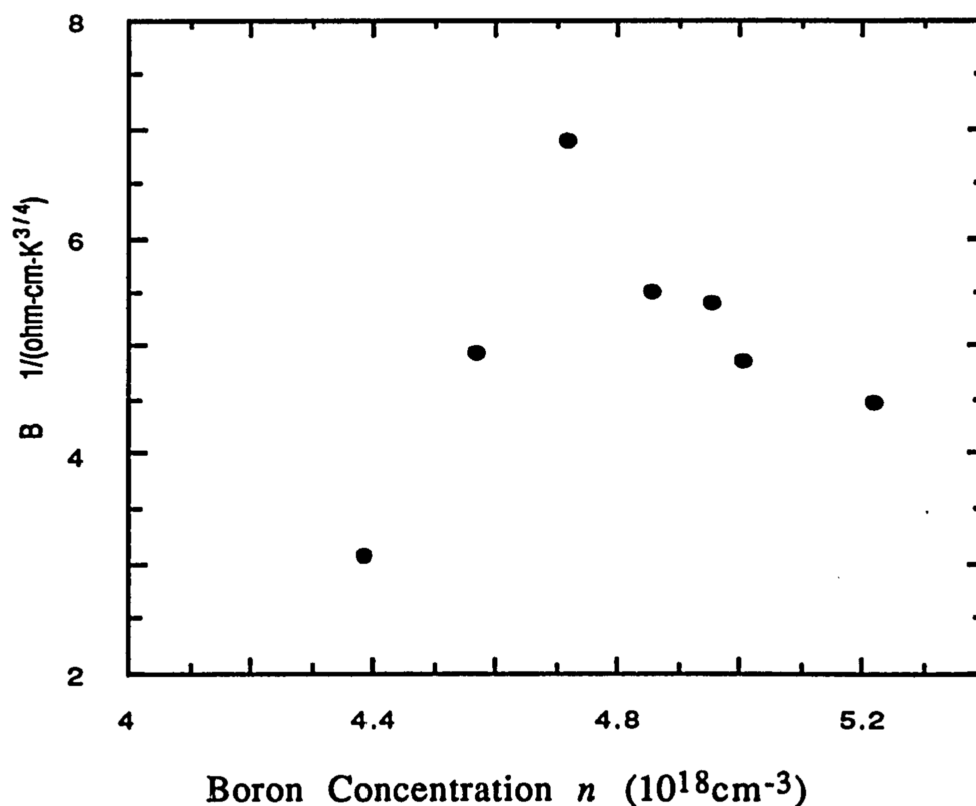

Boron Concentration n (10^{18}cm^{-3})

Fig. 4.3 The parameter B in eq.(4.2.3) plotted versus boron concentration.

The data for three metallic samples with negative values of $d\sigma/dT$ are plotted in Figs. 4.4, 4.5 and 4.6 respectively, along with the fits obtained using eq. (4.2.3).

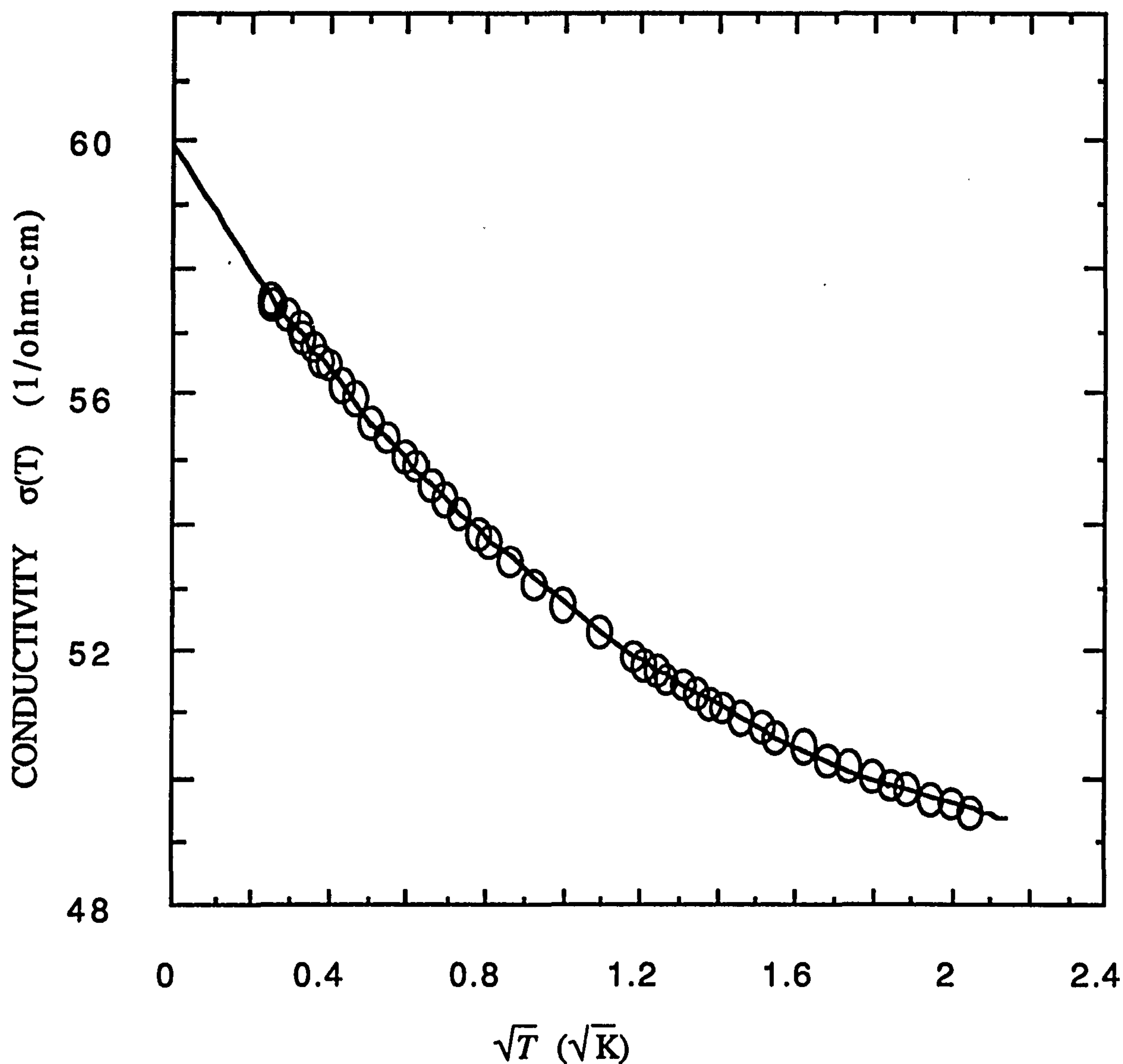

Fig. 4.4. The conductivity of a Si:B sample with boron concentration n = 5.01x10^{18}cm-3 plotted against $\sqrt{T}$. The solid line is a fit to eq. (4.2.3) with m = -12.2(Ω-cm-K$^{1/2}$)$^{-1}$, B =5.51(Ω-cm-K$^{3/4}$)$^{-1}$.

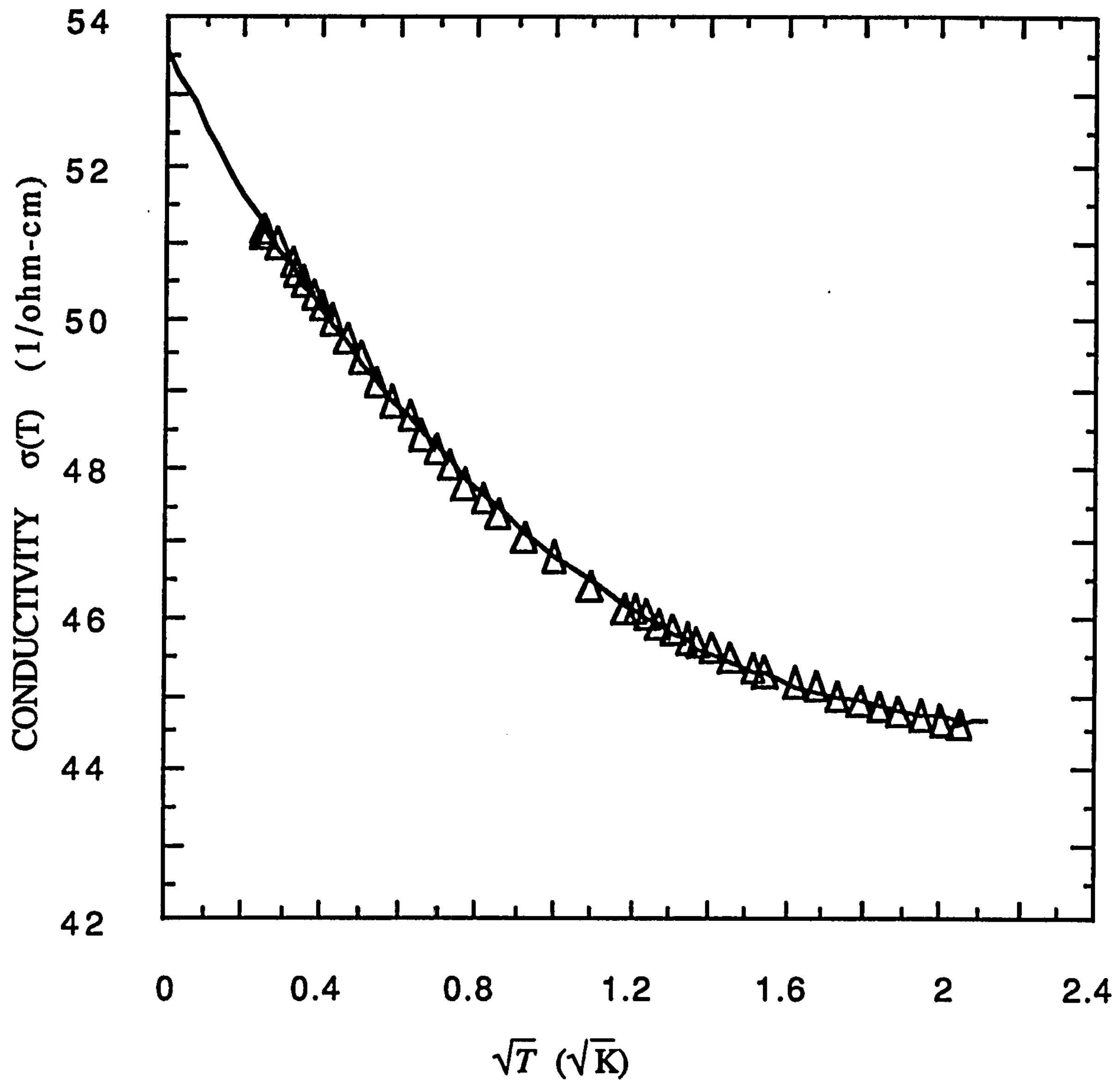

Fig. 4.5. The conductivity of a Si:B sample with boron concentration $n = 4.86\text{x}10^{18}\text{cm}^{-3}$ plotted against $\sqrt{T}$. The solid line is a fit to eq. (4.2.3) with $m = -9.31(\Omega\text{-cm-K}^{1/2})^{-1}$, $B = 4.94(\Omega\text{-cm-K}^{3/4})^{-1}$.

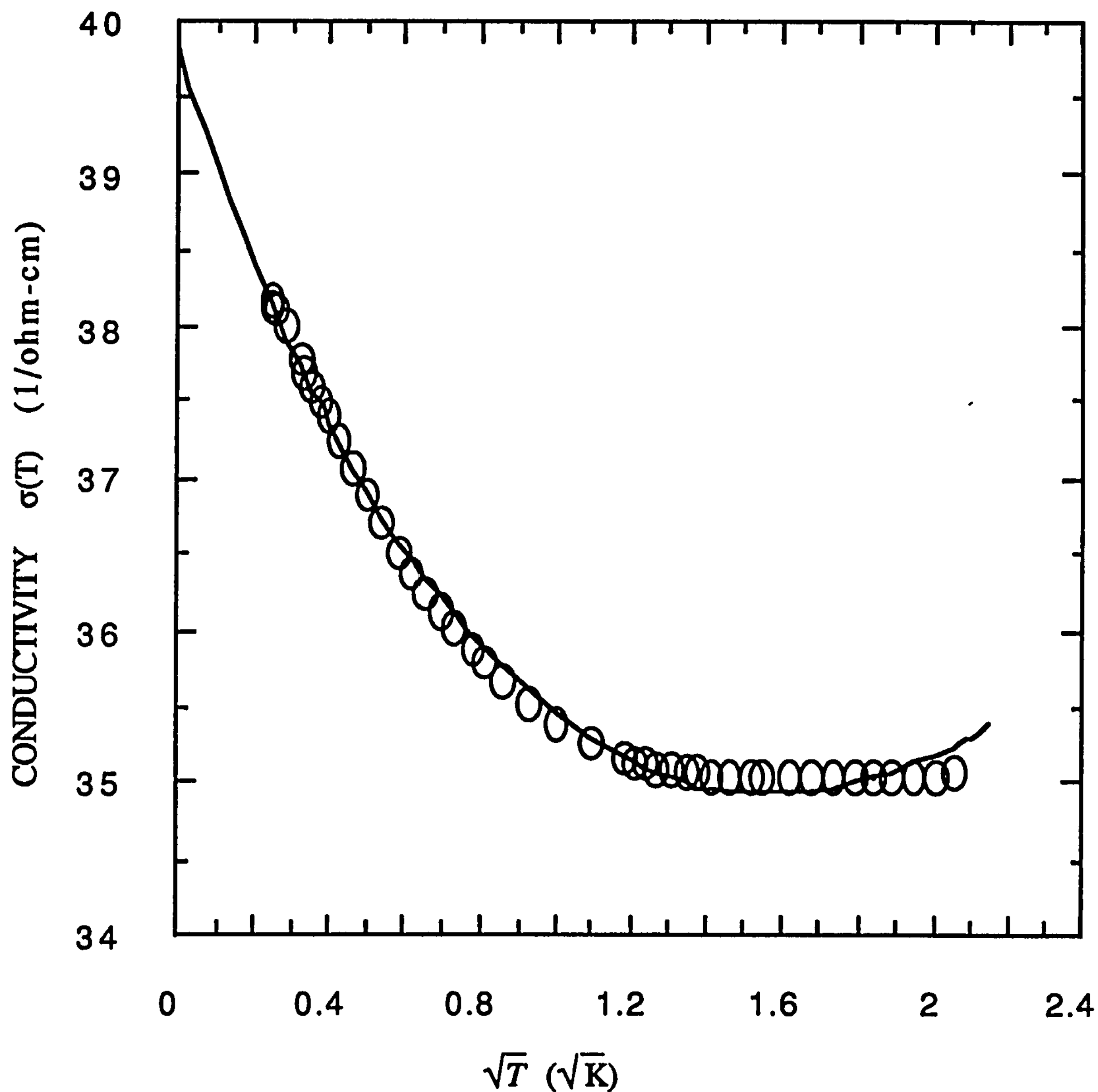

Fig. 4.6. The conductivity of a Si:B sample with boron concentration n = 4.57x10^{18}cm^{-3} plotted against $\sqrt{T}$. The solid line is a fit to eq. (4.2.3) with m = -12.0(Ω-cm-K$^{1/2}$)$^{-1}$, B =4.85(Ω-cm-K$^{3/4}$)$^{-1}$. The fit for this sample is not good at the high T end.

4.2.b Extrapolation to Zero Temperatures

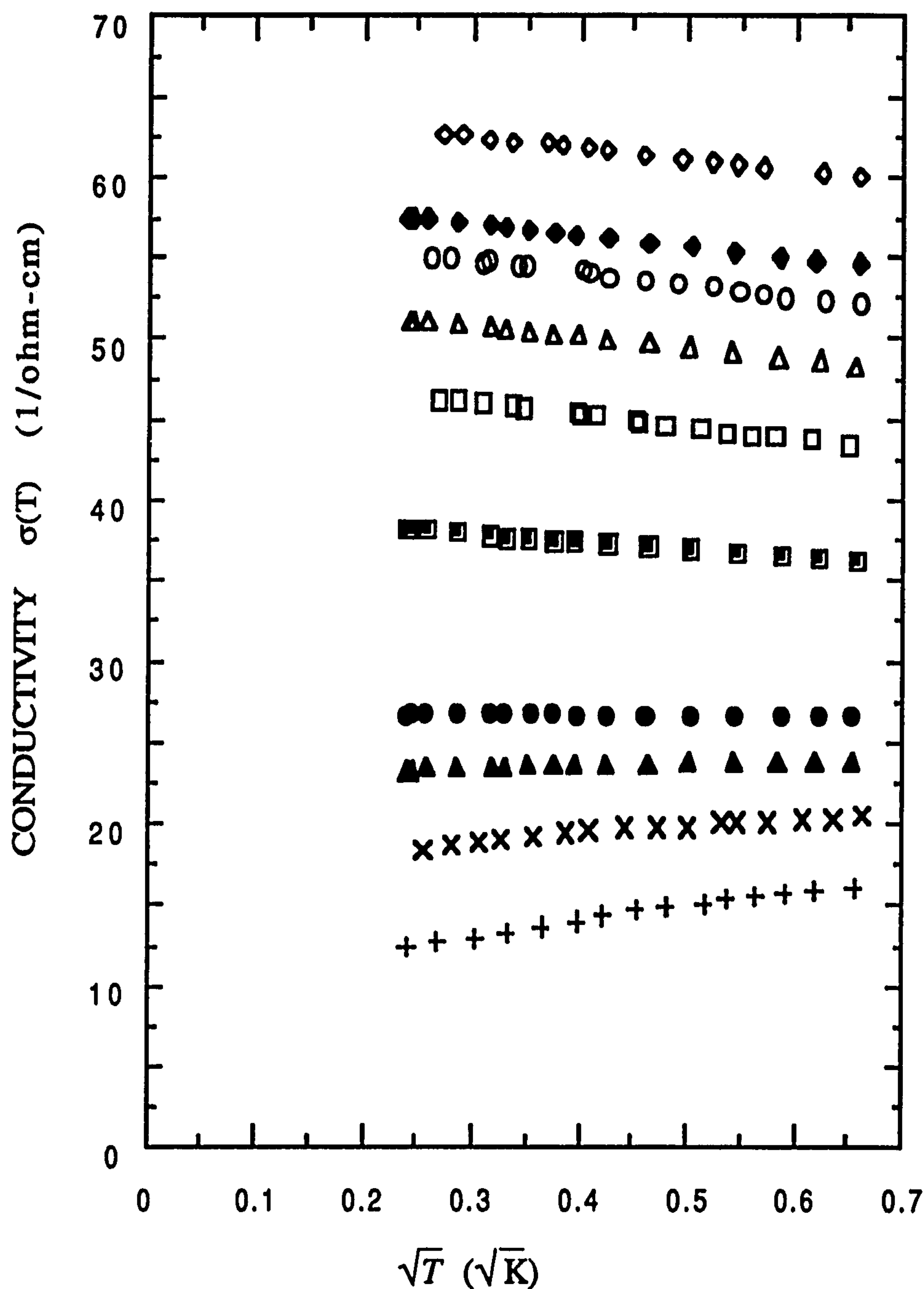

Fig. 4.7 The conductivities for ten metallic Si:B samples plotted as a function of $\sqrt{T}$ for temperatures below 500 mK. In units of $10^{18}cm^{-3}$, their boron concentrations are: ◇ 5.22, ◆ 5.01, ○ 4.95, △ 4.86, □ 4.72, ▣ 4.57, ● 4.38, ▲ 4.30, × 4.20, + 4.11.

In order to study the critical behavior, the zero temperature conductivities have to be deduced by extrapolation from measurements at finite temperatures.

The conductivities for ten Si:B samples in zero magnetic field are plotted as a function of $\sqrt{T}$ at the lower end of the temperature range ($T <$ 500 mK) in Fig. 4.7. The conductivity data can be described by a $\sqrt{T}$ dependence at low enough temperatures as indicated by Fig. 4.7. This implies that interactions are the dominant contribution at low T. We fitted the data to

$$\sigma(T) = \sigma(0) + m\sqrt{T} \tag{4.2.4}$$

at the lower end of the temperature range where a $\sqrt{T}$ dependence is observed. The temperature ranges over which good fits can be obtained depend on how close a given sample is to the transition. For more metallic samples, good fits could be obtained up to about 500 mK. However, for the two samples very near the transition, fits could only be made for $T \leq 200$ mK. The parameters obtained from these fits are listed in table 4.3 and the slopes are plotted as a function of boron concentrations in Fig. 4.8. One should note that the absolute values of the parameter m obtained here are smaller than those obtained by fitting the data to eq.(4.2.3) over a much wider temperature range as discussed in the previous section 4.2.a. Similar differences in m were obtained for Ge:Sb[12], indicating neither eq.(4.2.3) nor eq.(4.2.4) offers a completely satisfactory description of the data.

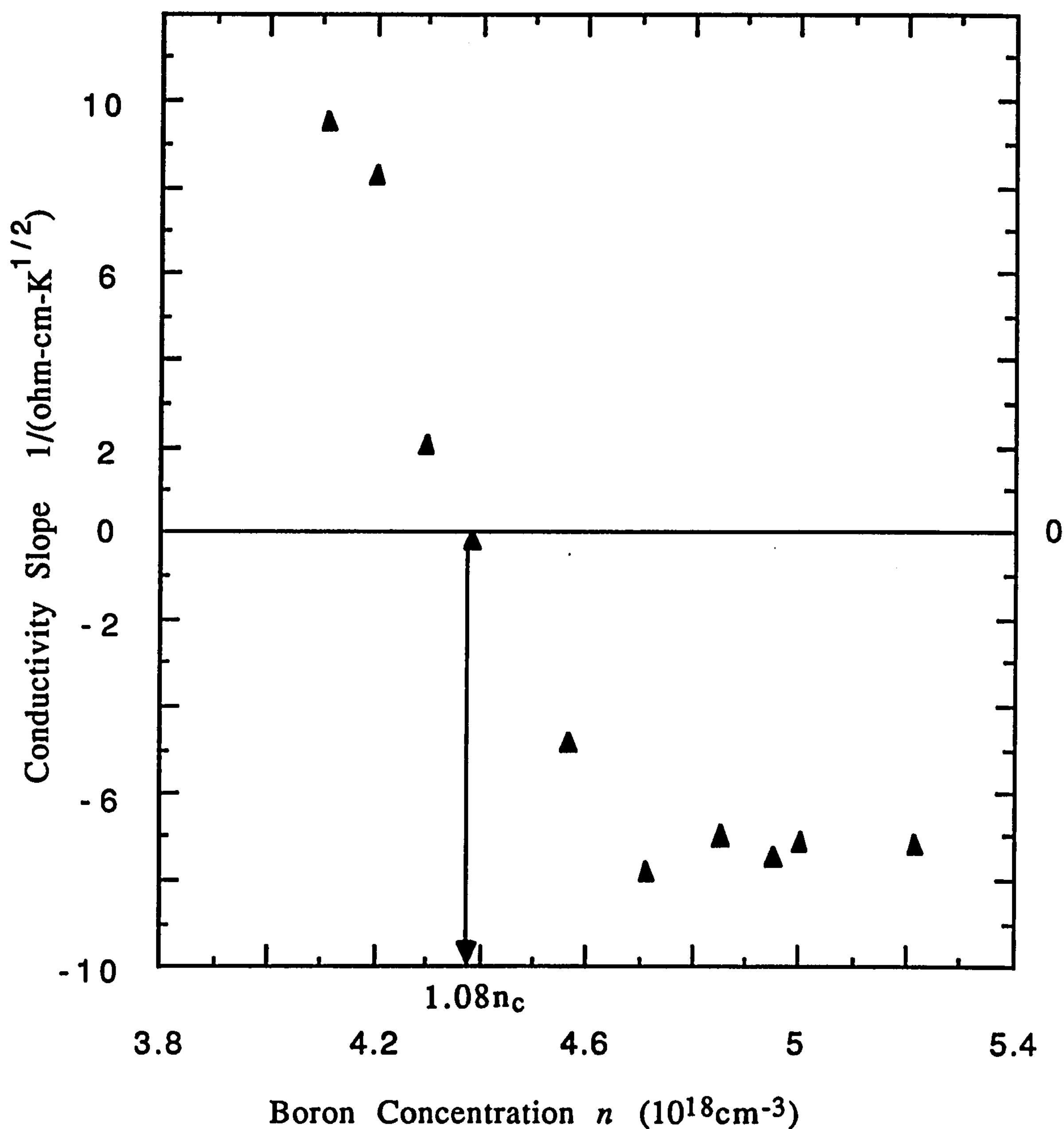

Fig. 4.8 The fitted values of m plotted as a function of boron concentrations. The critical concentration $n_c = 4.06\text{x}10^{18}\text{cm}^{-3}$ (see next section).

name	n (10^{18}cm^{-3})	$\sigma(H=0,T=0)$ (Ω–cm)$^{-1}$	m (ΩcmK$^{1/2}$)$^{-1}$
Si:B-1	4.11	10.2	9.5
Si:B-2	4.20	16.3	8.3
Si:B-3	4.30	22.9	2.1
Si:B-4	4.38	26.8	-0.14
Si:B-5	4.57	39.3	-4.8
Si:B-6	4.72	48.5	-7.8
Si:B-7	4.86	52.9	-7.0
Si:B-8	4.95	57.1	-7.4
Si:B-9	5.01	59.2	-7.1
Si:B-10	5.22	64.7	-7.2

Table 4.3 The slopes and intercepts of conductivities obtained through the above fitting procedure.

The slope m in eq. (4.2.4) in zero magnetic fields is given by[2,3],

$$m = \alpha\left(\frac{4}{3} - \gamma\frac{3\tilde{F}_\sigma}{2}\right) \tag{4.2.5}$$

where $\alpha = \frac{e^2}{\hbar}\frac{1.3}{4\pi^2}\sqrt{k_B/2\hbar D}$, D is the diffusion constant, and $\tilde{F}_\sigma$ is the interaction parameter appropriate for transport properties.

According to Bhatt and Lee[8], the value of γ depends on the mass anisotropy and intervalley scattering. In the isotropic case, the value of γ is 1 for a single valley, and is 6 in the case of n-type silicon without intervalley scattering since there are 6 equivalent valleys in

the conduction band. According to the theory[2,3] , the value of m can either be positive or negative depending on the value of $\tilde{F}_{\sigma}$. As shown in Fig. 4.8, m is negative for more metallic samples, which, in the theoretical framework proposed by Castellani et al.[9], is attributable to the diverging triplet channel. As the transition is approached, m becomes positive at a boron concentration of n = 4.30×10^{18} cm^{-3} . The change of numerical sign for m very near the transition has been observed in a number of systems[7,10] and is not completely understood. In these earlier studies[7,10], the sign reversal was attributed to a diverging screening length which leads to a vanishing interaction parameter, when the transition is approached.

While the theory describes the data qualitatively, the absolute value of the slope m observed in Si:P is several times smaller than that predicted by theory for the case of no anisotropy and intervalley scattering. This was explained by taking anisotropy and intervalley scattering into account[8], and the case of moderate anisotropy and no intervalley scattering in the Bhatt and Lee[8] treatment best fits the data for Si:P. For p-type Si:B, anisotropy is small, and intervalley scattering is not an issue. However, there are heavy and light hole bands and interband scattering should be important. These effects has not been calculated.

As a comparison, the conductivity slopes m in $\sigma(T) = \sigma(0) + m\sqrt{T}$ for Si:B, Si:P[10,11] and Si:As[12] in zero magnetic field are plotted in Fig. 4.9. Despite the differences between the conduction and valence bands of silicon, the behaviors as well as the magnitude of m for n and p-type silicon as a function of reduced concentration n/n_c are very similar(the value of n_c for Si:B is determined in next section

4.2.c). For Si:P and Si:As, the sign reversal occurs at about n/n_c =1.04, while for Si:B it occurs at about n/n_c =1.08. Since the behaviors of n- and p-type silicon are expected to reflect substantial differences such as different anisotropy and different scattering, it is surprising that the m's are so similar. Further, it is interesting to note that if we use the upper bound of n_c ($4.18 \times 10^{18} cm^{-3}$ corresponding to $\nu = 0.51$, see next section 4.2.c) for Si:B, even this small difference disappears.

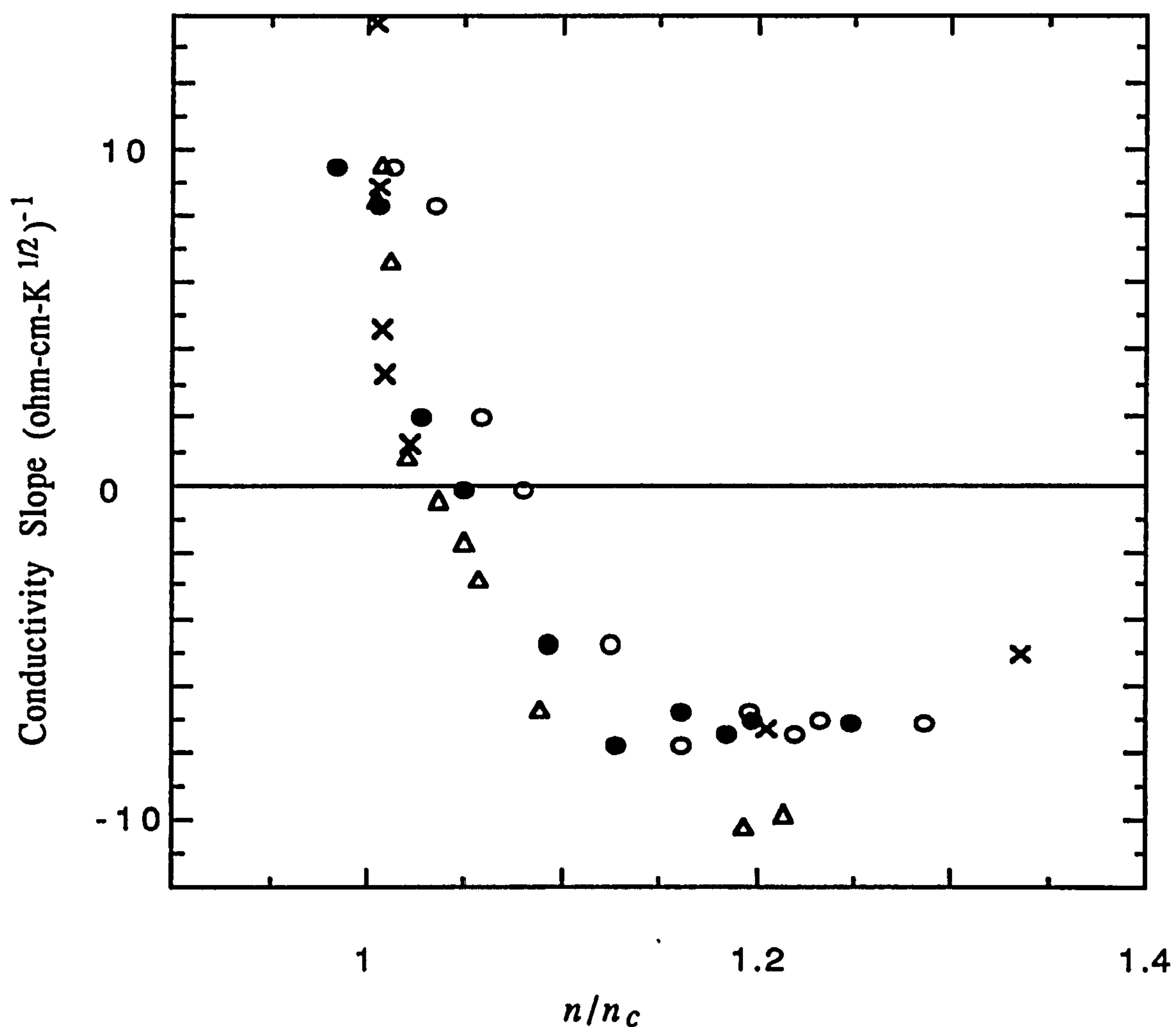

Fig. 4.9 The conductivity slopes m in $\sigma(T) = \sigma(0) + m\sqrt{T}$ plotted as a function of reduced concentration n/n_c. × Si:P; ▵ Si:As; ○ Si:B, with $n_c = 4.06 \times 10^{18} cm^{-3}$; ● Si:B, with $n_c = 4.18 \times 10^{18} cm^{-3}$.

4.2.c Critical Exponent

One of the main goals of this study is to determine the critical conductivity exponent ν in the expression $\sigma(T\rightarrow0) = \sigma_0(n/n_c-1)^{\nu}$. It is particularly interesting to study the critical exponent for Si:B. On the one hand, Si:B is an uncompensated silicon based system and all the uncompensated silicon based systems studied[13] show exponents near 1/2. On the other hand, Si:B is p-type, and spin-orbit scattering is believed to be strong so that theory[14] would predict an exponent near 1.

The following table lists the results for some systems studied by other groups.

System	Ref.	ν	System	Ref.	ν
Si:P	10	0.55 ± 0.1	compen. Ge:Sb	18	1
Si:As	12,15	0.60 ± 0.05	Si:(P,B)	19	0.9 ± 0.08
Si:Sb	16	0.49 ± 0.09	compen. Ga:As	13	1
Si:P,As	17	0.7 ± 0.2	uncompen Ge:Sb	20	0.9

Table 4.4 The critical exponents for some systems studied by other groups.

As can be seen from table 4.4, all the uncompensated silicon based systems show similar critical exponents which are near 1/2, while the critical exponents for all compensated systems as well as uncompensated Ge:Sb are found to be near 1.

The system used in the present study is uncompensated p-type Si:B. The charge carriers are holes and their wave functions are derived from the valence band edge. In silicon the heavy and light hole bands (J=3/2) are degenerate at k=0. The spin-orbit split hole band is below these two shifted by an energy Δ of 44meV. The hole states are p like with l = 1. Strong spin-orbit scattering is usually associated with heavy mass elements, rather than a light element like boron. The strong spin-orbit scattering in Si:B, however, is related instead to the valence band structure of silicon. The good quantum numbers in this case are J and M_J. As has been shown by Elliott[21] and Kawabata[22], scattering by impurities can cause transitions among states with different values of M_J between the heavy and light hole bands very easily.

The most direct evidence for strong spin-orbit coupling is a g-factor very different from 2 (free electron value). For Si:B[23,24] g = 1.2 so that spin-orbit coupling is indeed strong. The fact that spin-orbit scattering is strong in p-type materials is also supported by magnetoresistance measurements. When there is no spin-orbit scattering there is weak localization, and the magnetoresistance is negative in this case because of delocalization by magnetic fields. On the other hand, if strong spin-orbit scattering is present, we have instead weak anti-localization, and the magnetoresistance in the latter case is positive. Both our studies and an earlier study[25] show that the magnetoresistance is always positive for Si:B. Further, the magnetoresistance of p-type Ge[26,27] and Si:B[28] becomes negative under uniaxial stress, which lifts the degeneracy of the valence band thus reducing spin-orbit scattering.

The zero T conductivities for all the samples were determined as described in section 4.2.b. The error bars of $\sigma(0)$ are typically 1% except for samples very close to the transition where uncertainties are relatively large. This is because very near the transition the temperature range over which a good fit can be obtained is limited and also the behavior of $\sigma(T)$ is less well known. In order to obtain a more precise determination of the critical concentration at which the transition occurs, we also measured a few just-insulating samples down to low temperatures. Data for two such samples are plotted in Fig. 4.10(a). The negative intercepts indicate that they are indeed on the insulating side of the transition.

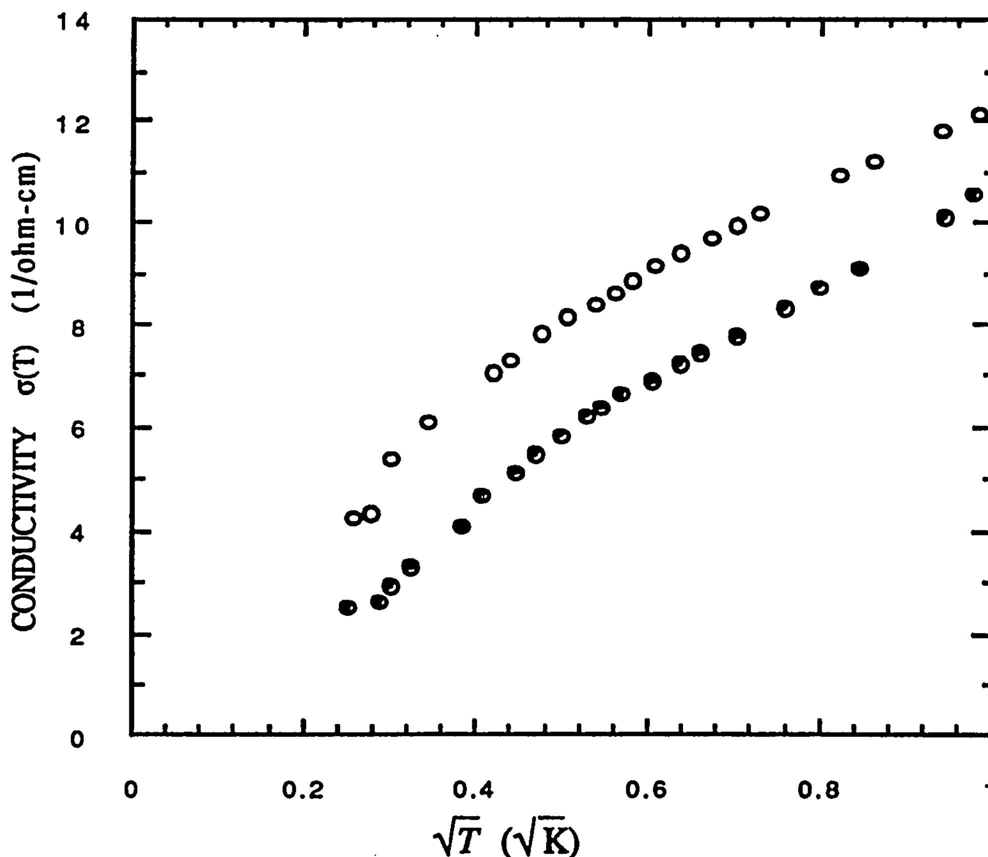

Fig. 4.10(a) The conductivities of two just-insulating samples plotted as a function of $\sqrt{T}$. ○ n = 3.95x10^{18}cm^{-3}; ● n = 3.90 x10^{18}cm^{-3}.

The logarithm of the resistivities of the two just-insulating samples and of the three metallic ones with positive values of $d\sigma/dT$ are plotted as a function of $T^{-1/4}$ on a semilogarithmic scale in Fig. 4.10(b). Within the range of temperature of our measurements, there is a clear difference between the samples we designated as just-insulating and the barely metallic ones. However, it would be desirable and very interesting to follow the two metallic samples, which are near the transition, to even lower temperatures to detect any possible change in their behavior.

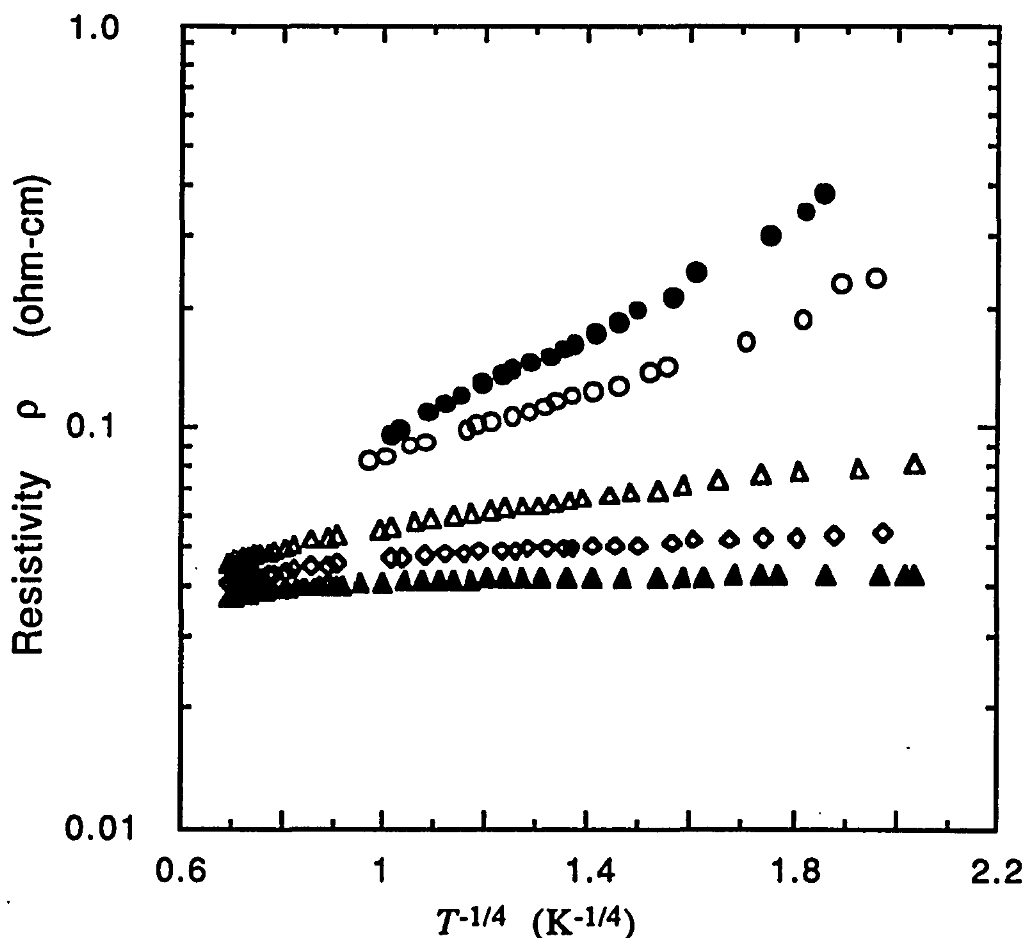

Fig. 4.10(b) The logarithm of the resistivities for two insulating samples and the three metallic samples with positive values of $d\sigma/dT$ plotted against $T^{-1/4}$. In units of 10^{18} cm^{-3}, their boron concentrations are: ● 3.90, ○ 3.95, △ 4.11, ◇ 4.20, ▲ 4.30.

The zero T conductivities for all the samples measured at low temperatures were plotted against boron concentrations in Fig. 4.11 A nonlinear least squares fit of the resultant $\sigma(0)$ values by the expression:

$$\sigma(T \to 0) = \sigma_0(n/n_c - 1)^{\nu} \tag{4.2.6}$$

yields a prefactor $\sigma_0 = 152 \pm 10$ $(\Omega\text{-cm})^{-1}$, a critical concentration $n_c = (4.06 \pm 0.02) \times 10^{18}$ cm^{-3}, and an exponent $\nu = 0.65 \pm 0.05$, where the quoted errors for each fitting parameter correspond to one standard deviation with the other two parameters allowed to vary freely. One should note, however, that $\sigma(0)$ becomes increasingly uncertain near the transition, owing to the fact that progressively lower temperatures are required for a reliable determination of $\sigma(0)$ as the transition is approached, and to a lack of a complete theoretical understanding of the temperature dependence expected for the conductivity very near the transition. It has been found[29], for example, that samples of n-type compensated GaAs very near the transition exhibit a $T^{1/3}$ rather than a $T^{1/2}$ dependence as predicted by Altshuler et al.[3]; Analysis of our data using this form for the three metallic samples with the lowest dopant concentrations yields essentially the same value $\nu = 0.64$. Omitting the two points closest to the transition entirely due to this uncertainty yields $\nu = 0.51$. If one enlarges the error bars to include this possibility, one obtains:

$$\nu = 0.65^{+0.05}_{-0.14}, \sigma_0 = 152^{+10}_{-18}\,(\Omega\text{-cm})^{-1}, n_c = (4.06^{+0.12}_{-0.02}) \times 10^{18}\ \text{cm}^{-3}.$$

An exponent of $\nu = 1$ is inconsistent with the experimental data.

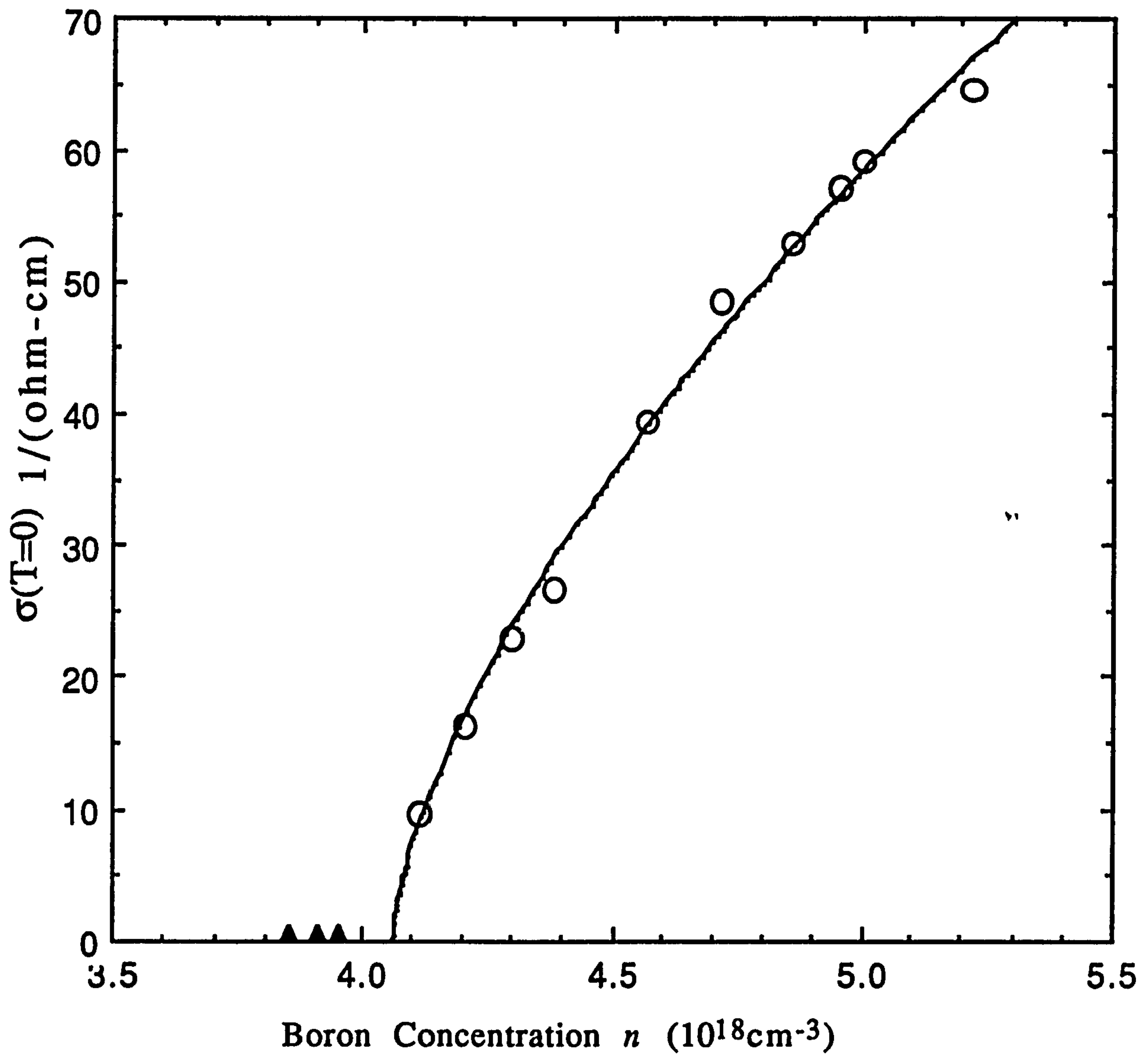

Fig. 4.11 The zero temperature conductivities plotted as a function of boron concentration. The line is the fitted curve to eq. (4.2.6).

As shown in Fig. 4.11, a sample with a boron concentration $n=3.95\times10^{18}$ cm^{-3} is insulating and thus sets a lower bound for n_c. A best straight line fit of the data points (corresponding to $\nu = 1$) would cross the x axis at about $n = 3.5\times10^{18}$cm^{-3}, which is clearly ruled out by the three insulating samples shown in Fig. 4.11.

Now let's compare briefly the results for some silicon based systems. The following table lists the parameters, namely the critical exponent ν, the prefactor σ_0, the critical concentration n_c, and the Mott minimum metallic conductivity σ_{min} for Si:B, Si:P[10], Si:As[12,15], and Si(P,B)[19].

System	Ref.	ν	σ_0 $(\Omega\text{-cm})^{-1}$	n_c (10^{18}cm^{-3})	σ_{min} $(\Omega\text{-cm})^{-1}$
Si:P	10	0.55 ± 0.1	$260 = 13\sigma_{min}$	3.75	20
Si:As	12,15	0.60 ± 0.05	$376 = 15\sigma_{min}$	8.55–8.60	25
Si:(P,B) (K=0.35–0.52)	19	0.9 ± 0.08	140	4.49	
Si:B	This Work	$0.65^{+0.05}_{-0.14}$	$152 = 8\sigma_{min}$	$4.06^{+0.12}_{-0.02}$	20

Table 4.5 The parameters ν, σ_0, n_c, and σ_{min} for Si:B, Si:P, Si:As, and Si:(P,B). The values of σ_{min} are calculated from $\sigma_{min} = 0.05e^2/hd_c$ with $d_c = n_c^{-1/3}$.

The prefactor for Si:B is 152, which is smaller than that of Si:P(260) and Si:As(376), but is comparable to that of compensated silicon Si:(P,B). In terms of the calculated value of σ_{min}, the prefactor σ_0 is quite similar for the two n-type materials Si:P and Si:As, and is

considerably smaller in Si:B. This is presumably due to differences between the conduction and valence bands.

Despite strong spin-orbit scattering, our results indicate that Si:B has a critical exponent near 1/2, which is very similar to that of uncompensated *n*-type silicon based systems, in contrast with a value near 1 for compensated silicon Si:(P,B). This implies that the physical processes which govern the transition must be similar or the same for both *n*- and *p*-type uncompensated silicon based semiconductors. It is interesting to note that the critical exponent for uncompensated Ge:Sb[20] is found to be near 1, where the low field magnetoresistance is negative[30] indicating that spin-orbit scattering is relatively weak. Our result seems to rule out the possibility that spin-orbit scattering is important in determining the critical exponents, at least for silicon based semiconductors.

4.3 Studies in Various Fixed Magnetic Fields

4.3.a The Data in Magnetic Fields

The temperature and magnetic field dependence of the conductivities were studied systematically for all the samples. Figs. 4.12 through 4.21 show the conductivity data for ten Si:B samples measured in fixed magnetic fields between zero and 1 Tesla. For the more metallic samples, the slope of the conductivity which is negative at high temperatures becomes positive at lower temperatures, and maxima occur at about $g\mu_B H = 2k_B T$ (g=1.2 for Si:B). Similar results have been obtained in Si:P by Paalanen and Bhatt[31] and by Lohneysen et al.[32], and may be accounted for in terms of Zeeman splitting[33,34] in a strong magnetic field, such that $g\mu_B H >> k_B T$. This presumably suppresses the diverging triplet channel which are responsible for the negative slope in zero magnetic field. For samples closer to the transition which have positive $d\sigma/dT$, the curves become steeper in a magnetic field.

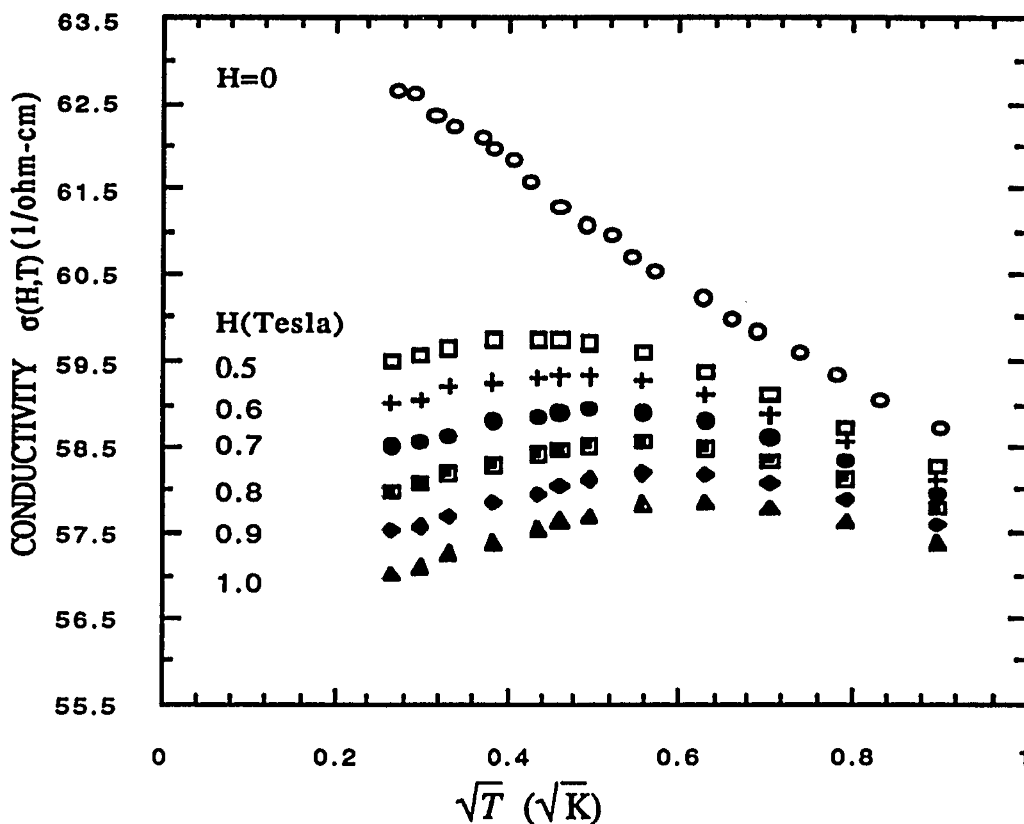

Fig. 4.12. Conductivity for a Si:B sample with boron concentration n=5.22x10^{18}cm^{-3} plotted against $\sqrt{T}$ in various magnetic fields

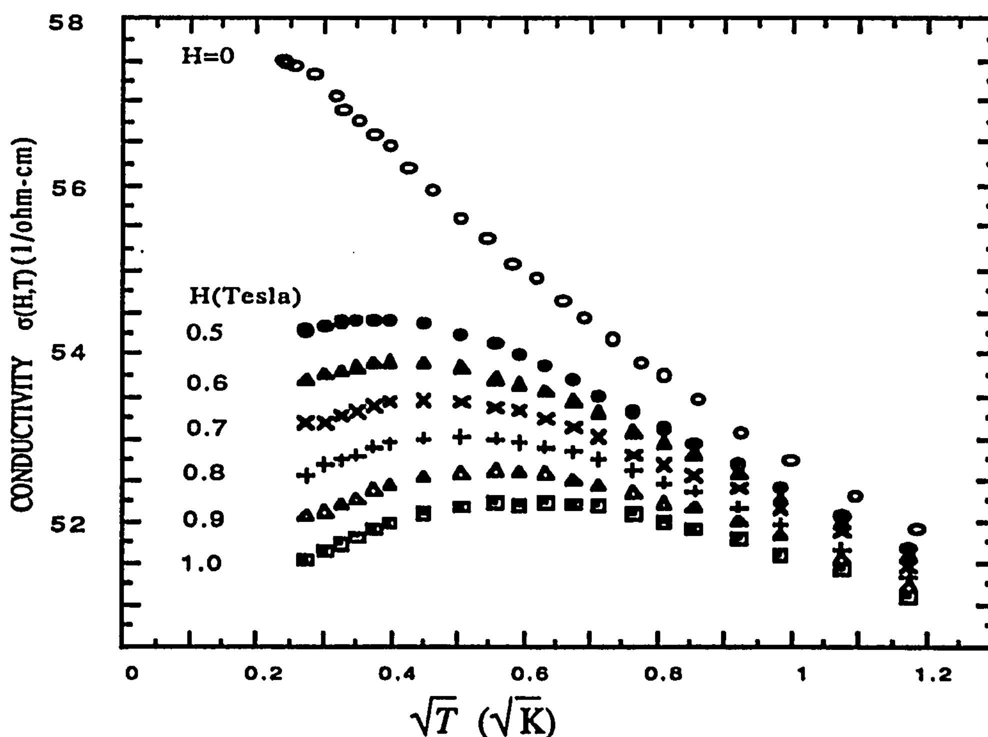

Fig. 4.13 Conductivity for a Si:B sample with boron concentration n=5.01x10^{18}cm^{-3} plotted against $\sqrt{T}$ in various magnetic fields

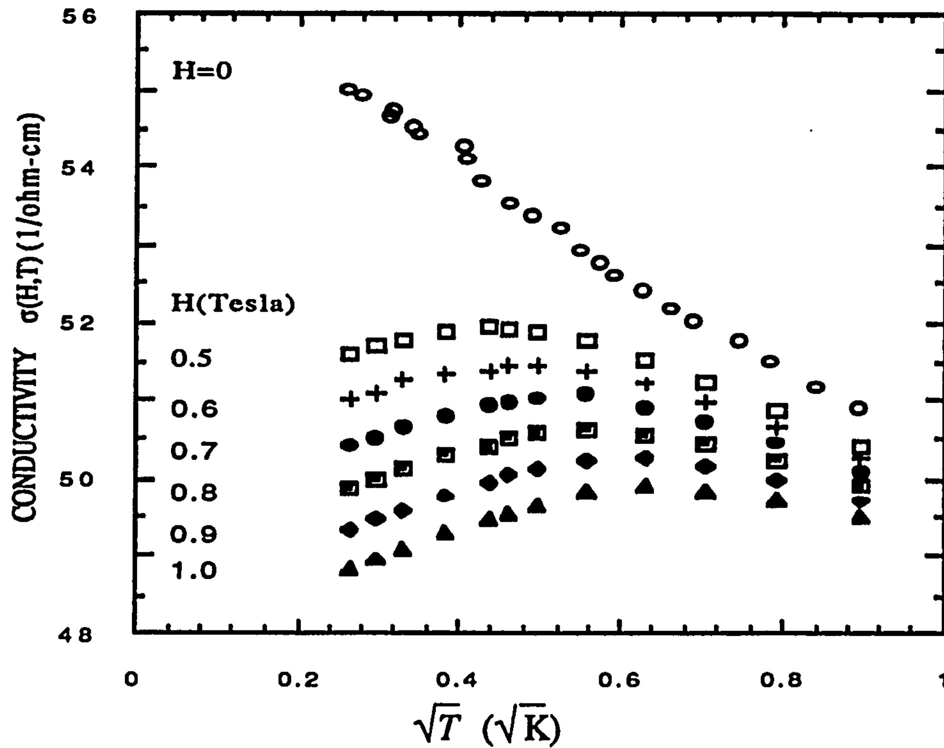

Fig. 4.14 Conductivity for a Si:B sample with boron concentration n=4.95x10^{18}cm^{-3} plotted against $\sqrt{T}$ in various magnetic fields

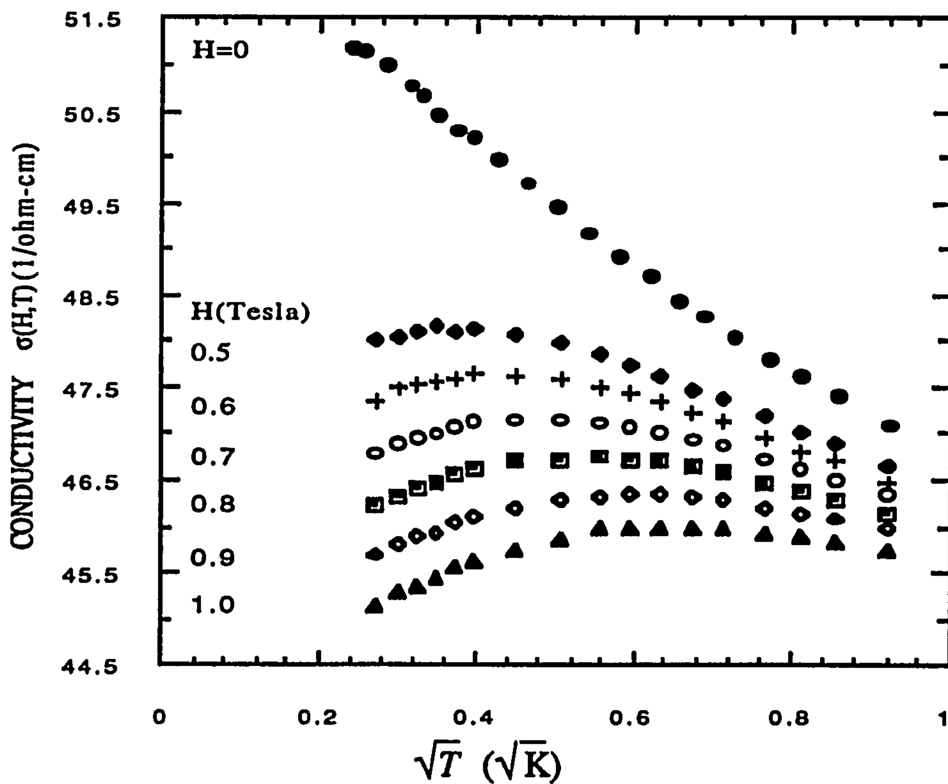

Fig. 4.15 Conductivity for a Si:B sample with boron concentration n=4.86x10^{18}cm^{-3} plotted against $\sqrt{T}$ in various magnetic fields

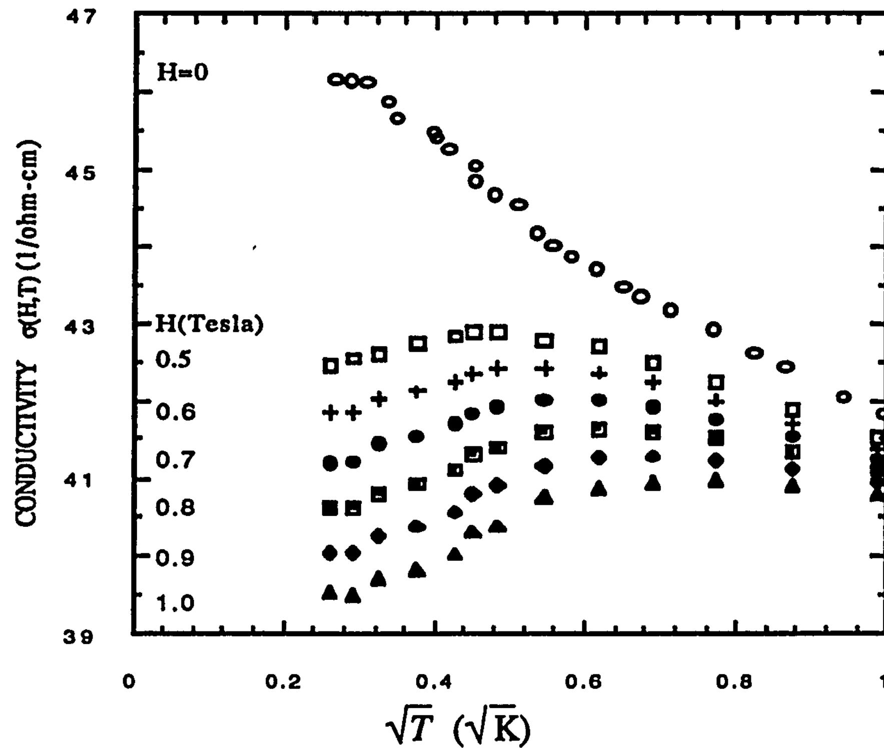

Fig. 4.16 Conductivity for a Si:B sample with boron concentration n=4.72x10^{18}cm^{-3} plotted against $\sqrt{T}$ in various magnetic fields

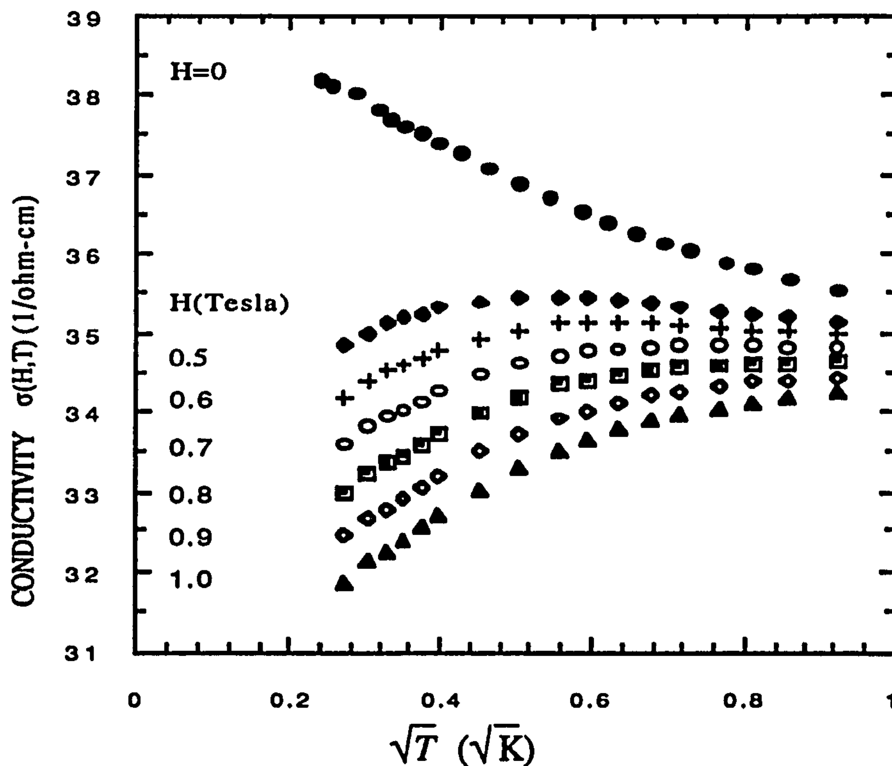

Fig. 4.17 Conductivity for a Si:B sample with boron concentration n=4.57x10^{18}cm^{-3} plotted against $\sqrt{T}$ in various magnetic fields

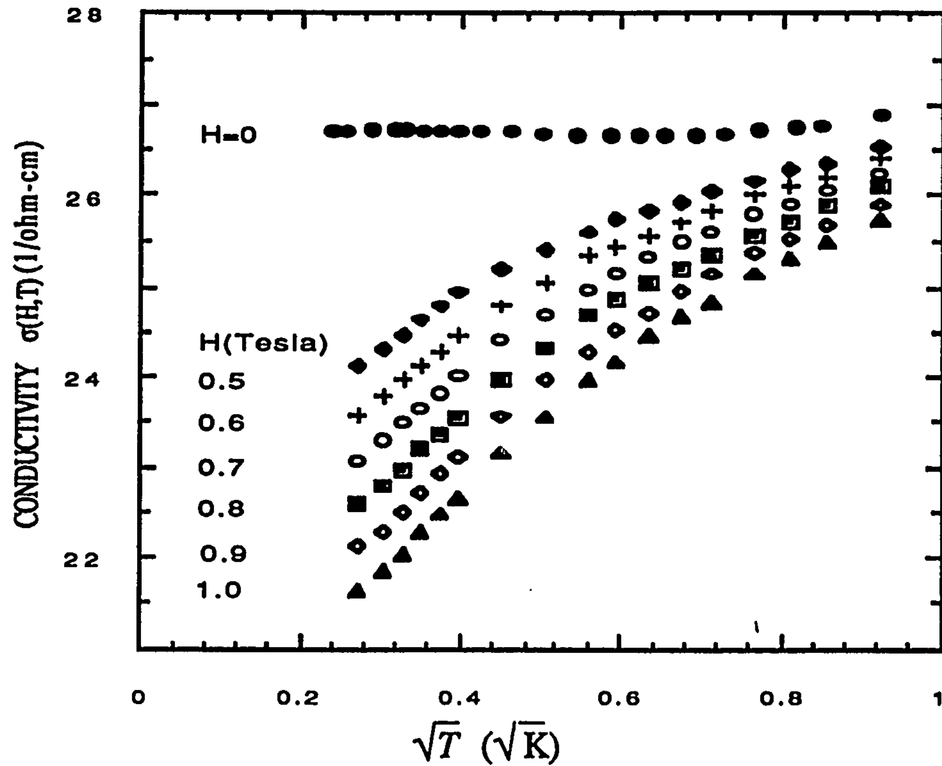

Fig. 4.18 Conductivity for a Si:B sample with boron concentration n=4.38x10^{18}cm^{-3} plotted against $\sqrt{T}$ in various magnetic fields

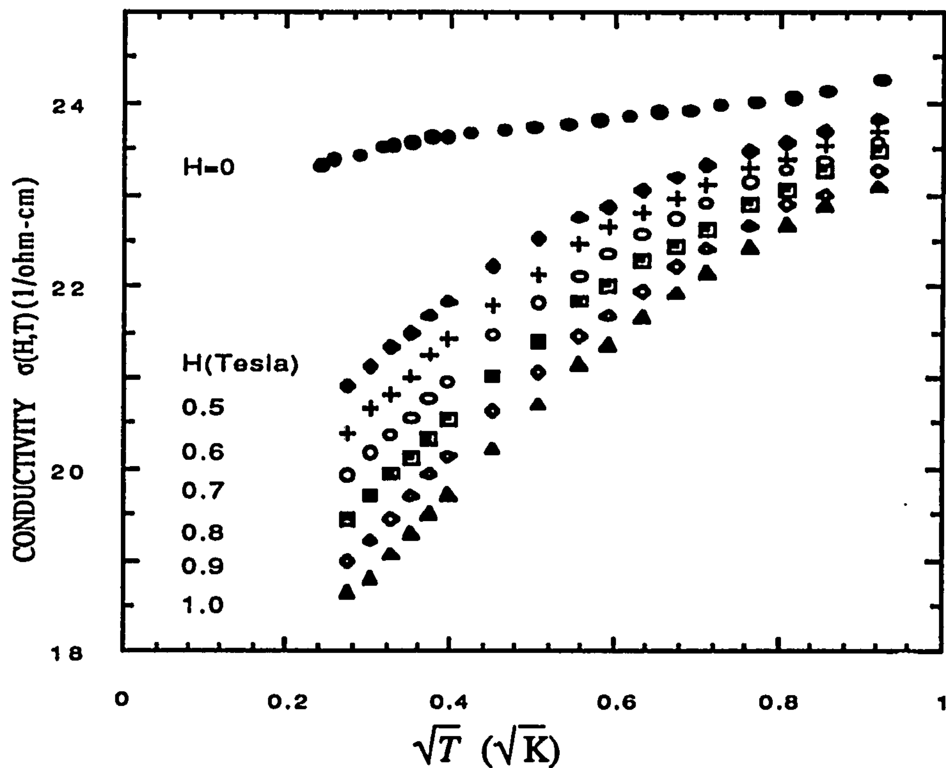

Fig. 4.19 Conductivity for a Si:B sample with boron concentration n=4.30x10^{18}cm^{-3} plotted against $\sqrt{T}$ in various magnetic fields

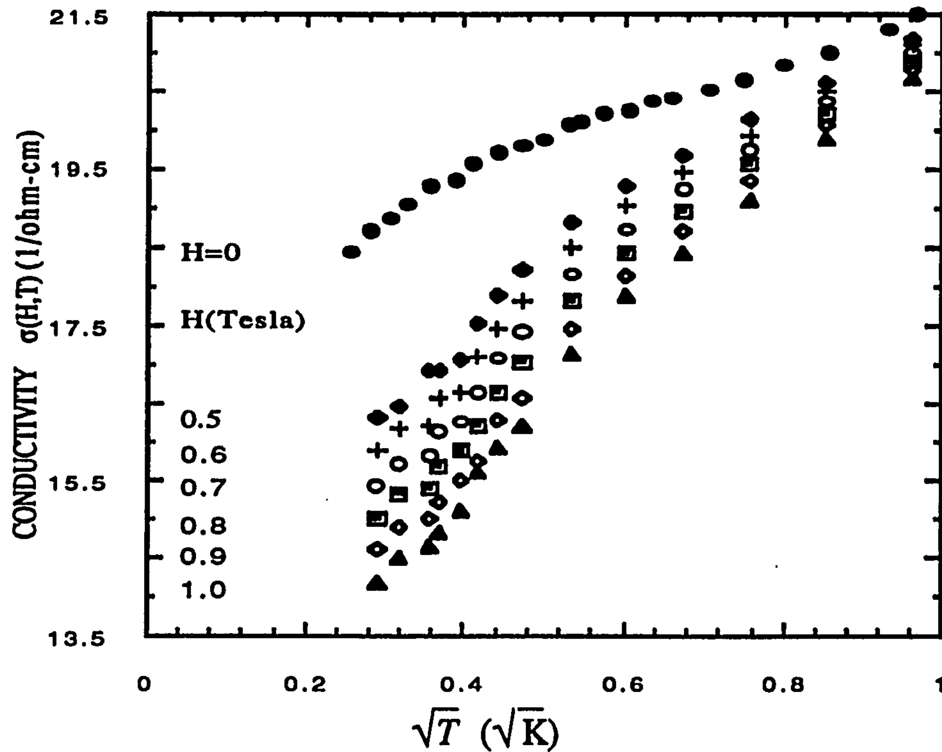

Fig. 4. 20 Conductivity for a Si:B sample with boron concentration n=4.20x10^{18}cm^{-3} plotted against $\sqrt{T}$ in various magnetic fields

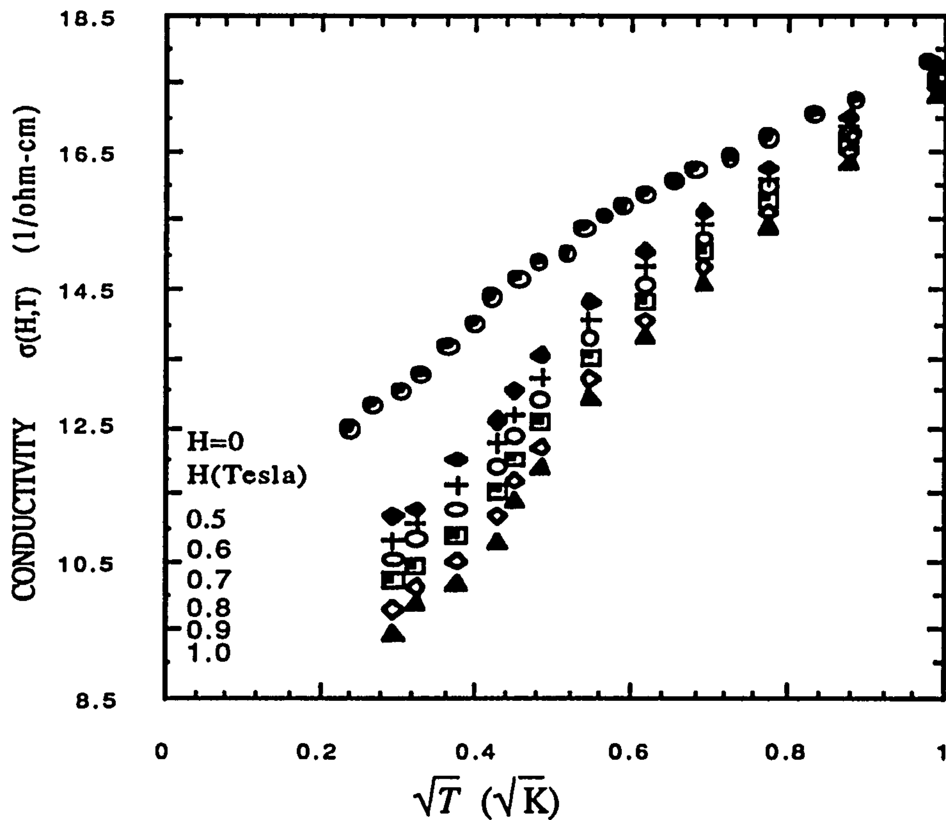

Fig. 4.21 Conductivity for a Si:B sample with boron concentration n=4.10x10^{18}cm^{-3} plotted against $\sqrt{T}$ in various magnetic fields

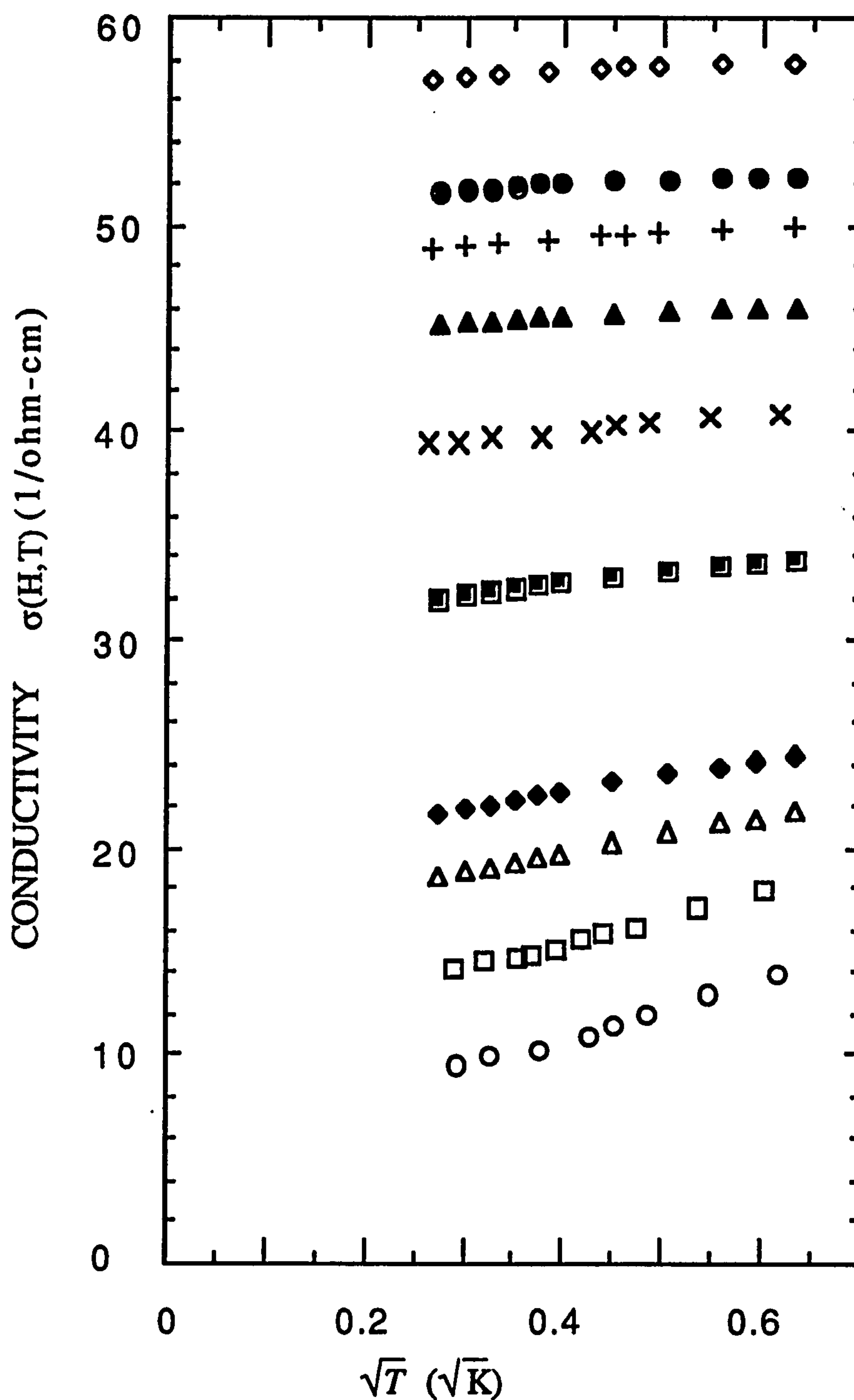

Fig. 4.22 The conductivity for ten Si:B samples in a fixed magnetic field of 1 Tesla plotted against $\sqrt{T}$. In units of 10^{18} cm^{-3}, their boron concentrations are: ◇ 5.22; ● 5.01; + 4.95; ▲ 4.86; × 4.72; ◼ 4.57; ◆ 4.38; △ 4.30; □ 4.20; ○ 4.11.

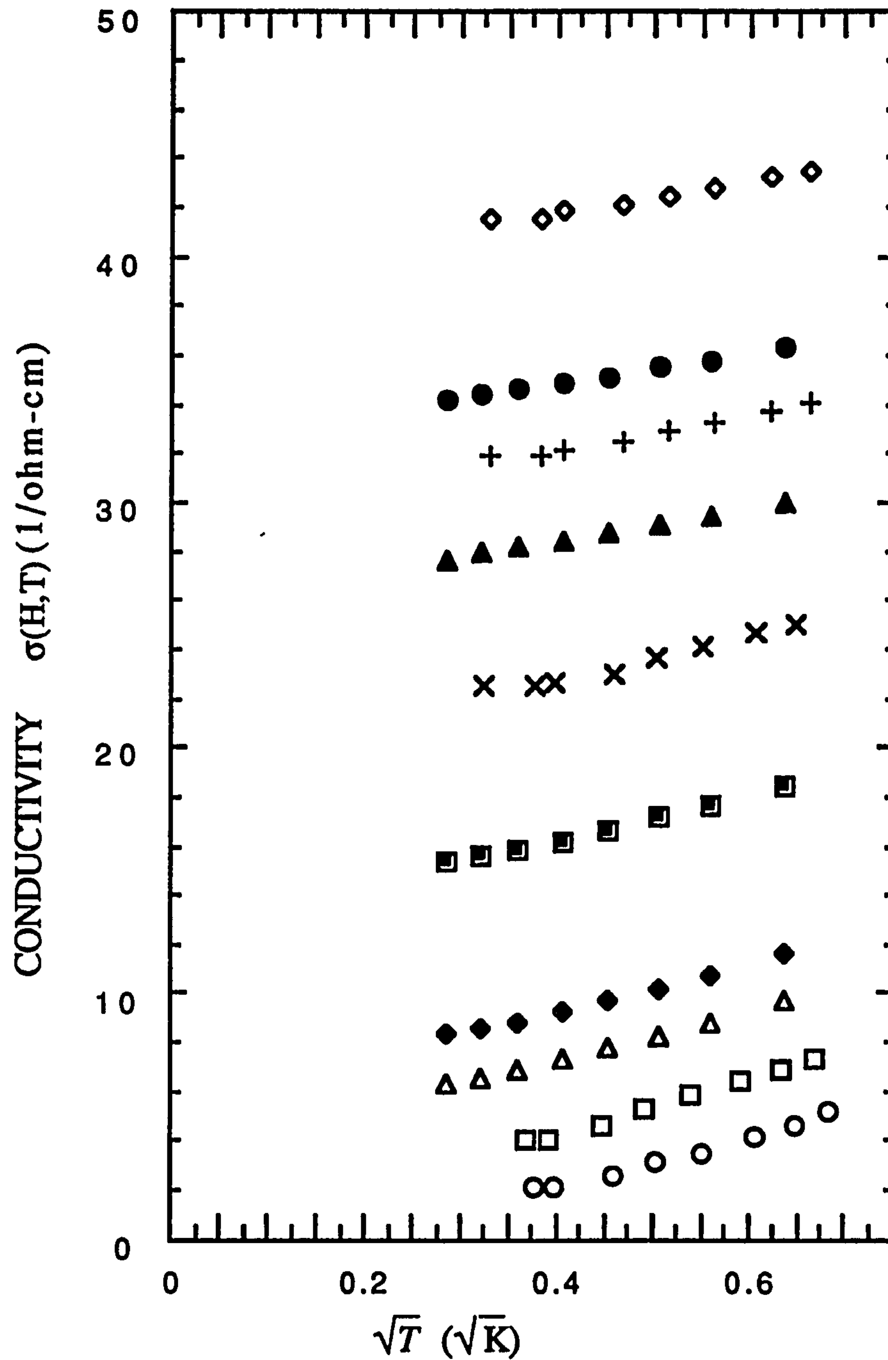

Fig. 4.23 The conductivity for ten Si:B samples in a fixed magnetic field of 7.5 Tesla plotted against $\sqrt{T}$. In units of 10^{18} cm^{-3}, their boron concentrations are: ◇ 5.22; ● 5.01; + 4.95; ▲ 4.86; × 4.72; ◪ 4.57; ◆ 4.38; △ 4.30; □ 4.20; ○ 4.11.

The conductivities for ten Si:B samples in magnetic fields of 1.0 and 7.5 Teslas are plotted as a function of $\sqrt{T}$ at the lower end of the temperature range ($T <$ 500 mK) in Figs. 4.22 and 4.23, respectively.

According to theory[33,34], the temperature dependence of the conductivity in a strong field such that $g\mu_B H >> k_B T$ should be:

$$\sigma(H,T) = \sigma(H,T{=}0) + m' \sqrt{T} \qquad (4.3.1)$$

where $$m' = \alpha\left(\frac{4}{3} - \gamma\frac{\tilde{F}_\sigma}{2}\right) \qquad (4.3.2)$$

For comparison, the conductivity slope m in zero field is given by[2,3]

$$m = \alpha\left(\frac{4}{3} - \gamma\frac{3\tilde{F}_\sigma}{2}\right) \qquad (4.3.3)$$

where $\alpha = \frac{e^2}{\hbar}\frac{1.3}{4\pi^2}\sqrt{k_B/2\hbar D}$, $\tilde{F}_\sigma$ is the interaction parameter, and the value of γ depends on anisotropy and intervalley scattering[8].

The T dependence of the conductivity in fixed magnetic fields of 1 and 7.5 Teslas, plotted in Figs. 22 and 23 were fitted to eq.(4.3.1) within the relevant temperature ranges where $g\mu_B H > 2k_B T$ is satisfied. A field of 1 Tesla offers only a limited range of temperatures over which a fit can be made. However, a field of 7.5 Tesla provides a much wider temperature range. The intercepts and slopes in Figs. 22 and 23 obtained by fitting the data to eq. (4.3.1) are listed in table 4.6.

name	$m'(H{=}1.0\ T)$ $(\Omega cmK^{1/2})^{-1}$	$m'(H{=}7.5\ T)$ $(\Omega cmK^{1/2})^{-1}$	$\sigma(H{=}1T, T{=}0)$ $(\Omega{-}cm)^{-1}$	$\sigma(H{=}7.5T, 0)$ $(\Omega{-}cm)^{-1}$
Si:B-1	10.1		5.61	0.00
Si:B-2	9.77		11.5	0.00
Si:B-3	9.56	9.45	15.9	3.68
Si:B-4	8.70	9.31	19.1	5.71
Si:B-5	6.25	8.87	30.1	12.9
Si:B-6	4.37	7.92	38.4	18.7
Si:B-7	3.17	6.53	44.1	25.8
Si:B-8	3.41	6.70	47.6	28.7
Si:B-9	3.81	6.06	50.5	32.5
Si:B-10	3.38	6.08	56.9	39.1

Table 4.6 The conductivity slopes and zero T conductivities for ten samples in magnetic fields of 1 and 7.5 Teslas deduced from Figs. 21 and 22.

The slopes m' at magnetic fields of 1 and 7.5 Teslas are plotted in Fig 4.24. The slopes m' in a strong magnetic field are always positive, unlike the slopes m in zero magnetic field where both positive and negative values observed. In addition, the slope in a strong field varies less rapidly as a function of concentration than it does in weak and zero fields.

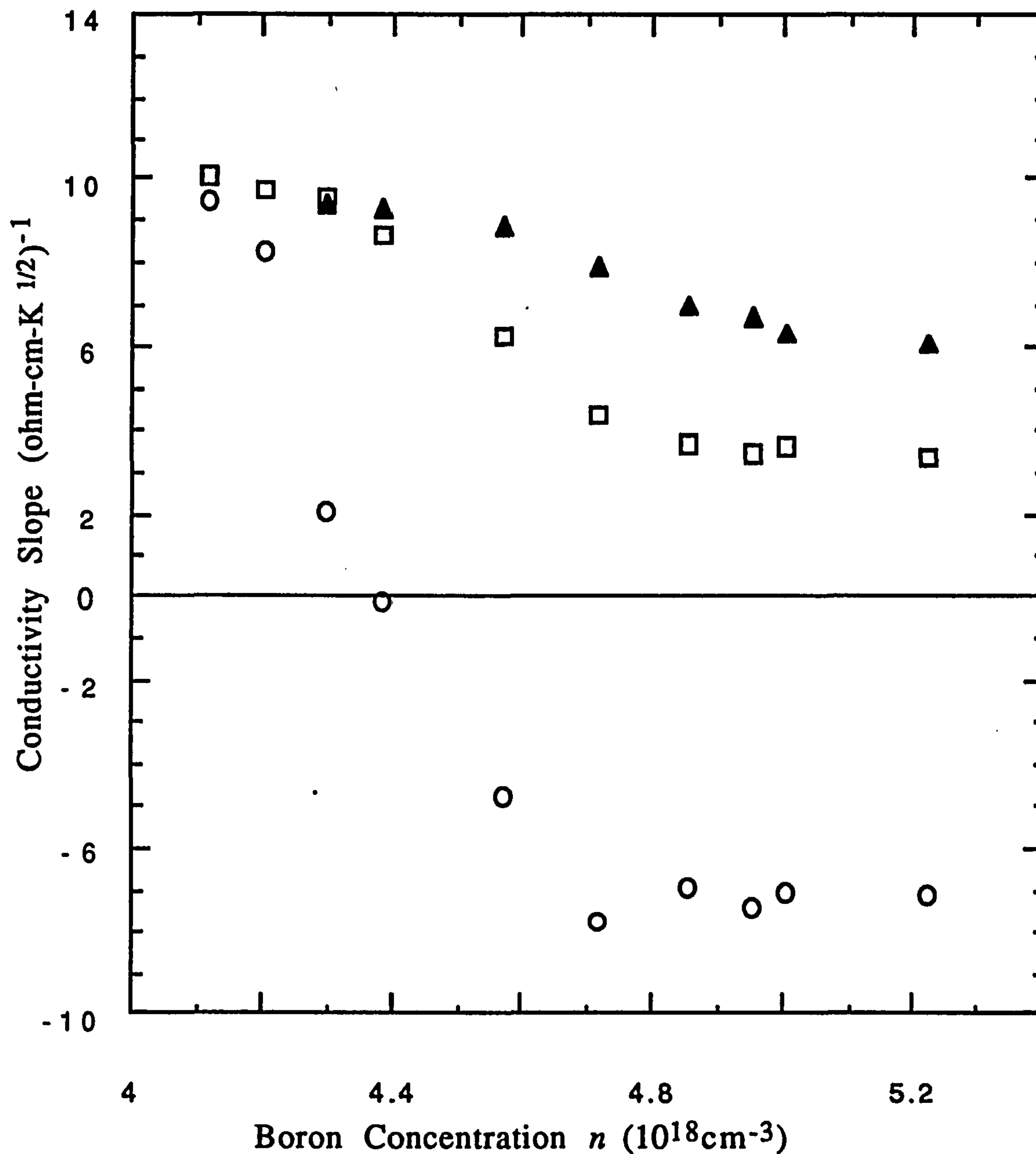

Fig. 4.24 The slopes of conductivities for ten Si:B samples in magnetic fields of H=0(○), H=1 Tesla(□) and H=7.5 Tesla(▲) plotted against boron concentration.

4.3.b Interaction parameter

The interaction parameter is an important quantity which characterizes interaction effects. If one considers only the particle-hole channel, the contributions from interactions to transport, as well as to thermodynamic properties depend on only one Fermi-liquid interaction parameter F, which is the Fermi-surface average of the screened electron-electron interactions[3,34]. The relation between F and the interaction parameter $\tilde{F}_\sigma$ appropriate for transport properties is given by[3,34]:

$$\tilde{F}_\sigma = -\frac{32}{3}\,[1 - 3F/4 - (1 - F/2)^{3/2}]/F \qquad (4.3.4)$$

In this study, we deduce interaction parameter from the temperature dependence of the conductivity in both zero and strong magnetic fields. Since both m and m' can be obtained experimentally, the values of $(\gamma\tilde{F}_\sigma)$ as well as the prefactor α can be deduced for each sample directly from eqs. (4.3.2) and (4.3.3). We note that eqs. (4.3.2) and (4.3.3) were derived for weak disorder, that is $k_F l >> 1$. The fact that the low T conductivities for samples near the transition still show $\sqrt{T}$ behavior may imply that the theory is applicable in the transition region. We deduce $(\gamma\tilde{F}_\sigma)$ and α simultaneously, neglecting any possible change in the value of α (and thus the diffusion constant D) due to the application of a magnetic field. The values of m' at a field of 7.5 Tesla were used in the calculation, so that the high field condition is well satisfied, that is $g\mu_B H >> k_B T$, within our temperature range. It should be noted, however, that details involving light and heavy holes in Si:B and the

effect of interband scattering are likely to be important, and have not been taken into account. Therefore there is no detailed knowledge about the value of γ for Si:B in eqs.(4.3.2) and (4.3.3). Further, we assume the value of γ is not changed by the application of a magnetic field.

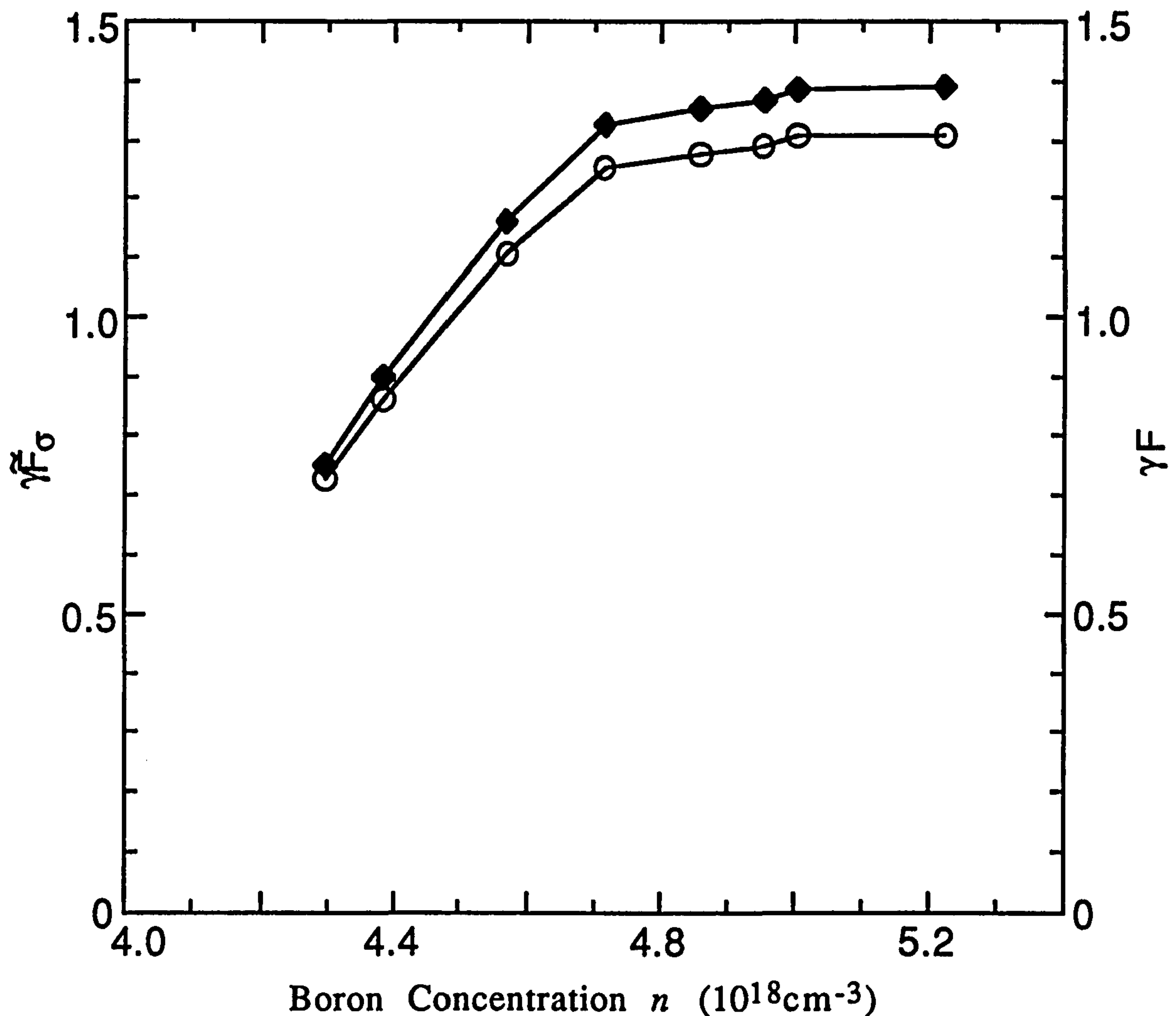

Fig. 4.25 The quantities $\gamma\tilde{F}_\sigma$ (◆) and γF (○) plotted against boron concentrations. The values of F are calculated from eq.(4.3.4) by assuming $\gamma = 2$. The lines are a guide to the eye.

Fig. 4.25 is a plot of the product of γ and $\tilde{F}_\sigma$, $(\gamma\tilde{F}_\sigma)$, against boron concentrations. The values of F are calculated from eq.(4.3.4) by assuming $\gamma = 2$, and the quantity γF is also plotted in Fig. 4.25. The behavior of the interaction parameter has been studied in a few cases. In those studies[7,10] the interaction parameter calculated within the Thomas-Fermi approximation was used to explain the behavior of the slope m.

The interaction parameter has been written as[7,10]:

$$F = \frac{1}{\chi}\ln(1+\chi) \qquad (4.3.5)$$

with $\chi = (2k_F/k_S)$, where k_F is the Fermi wave vector and k_S is the Thomas-Fermi screening wave vector. The screening length k_S^{-1} becomes very large near the transition, and one expects that F (as well as $\tilde{F}_\sigma$) will therefore decrease toward zero as the transition is approached[7,10], which is qualitatively consistent with our result shown in Fig. 4.25.

One should bear in mind that the validity of this analysis depends on the assumption that D and γ remain unchanged in a magnetic field. Further, the expressions for m and m' used to deduce $\tilde{F}_\sigma$ were derived for weak disorder, so that it is by no means clear that the theory is applicable very near the transition.

For two dimensional systems, the temperature dependence of the Hall coefficient has been used to estimate the values of interaction constants[35].

4.3.c Critical Exponent in a Magnetic Field

Weak localization is suppressed in the presence of a strong magnetic field and in this case an exponent $\nu = 1$ has also been predicted by theory[14]. The zero temperature conductivities deduced in the above section are plotted as a function of boron concentration in Fig. 4.26. The data were again fitted to the expression:

$$\sigma(H,T\rightarrow 0) = \sigma_0(H)[n/n_c(H)-1]^{\nu} \tag{4.3.5}$$

with a nonlinear least squares fitting procedure in order to determine the critical exponent. The fitted results are listed in table 4.7 along with those in zero field . The errors for the parameters are determined by enlarging the error bars to reflect the uncertainties associated with samples very close to the transition, as discussed in section 4.2.c. A strong magnetic field causes a shift toward more insulating behavior, as evidenced by the increase in the critical concentration n_c and the fact that some of the samples which are metallic in the absence of a field are insulating in a field of 7.5 Tesla, as shown in Fig. 4.26. Most interesting is the fact that the application of a magnetic field causes a shift of the critical exponent ν toward a higher value near 1. Spin-orbit scattering is strong in Si:B and therefore there is weak anti-localization. Although we do not have an estimate of the spin-orbit scattering time τ_{so}, it is expected to be approximately independent of temperature.

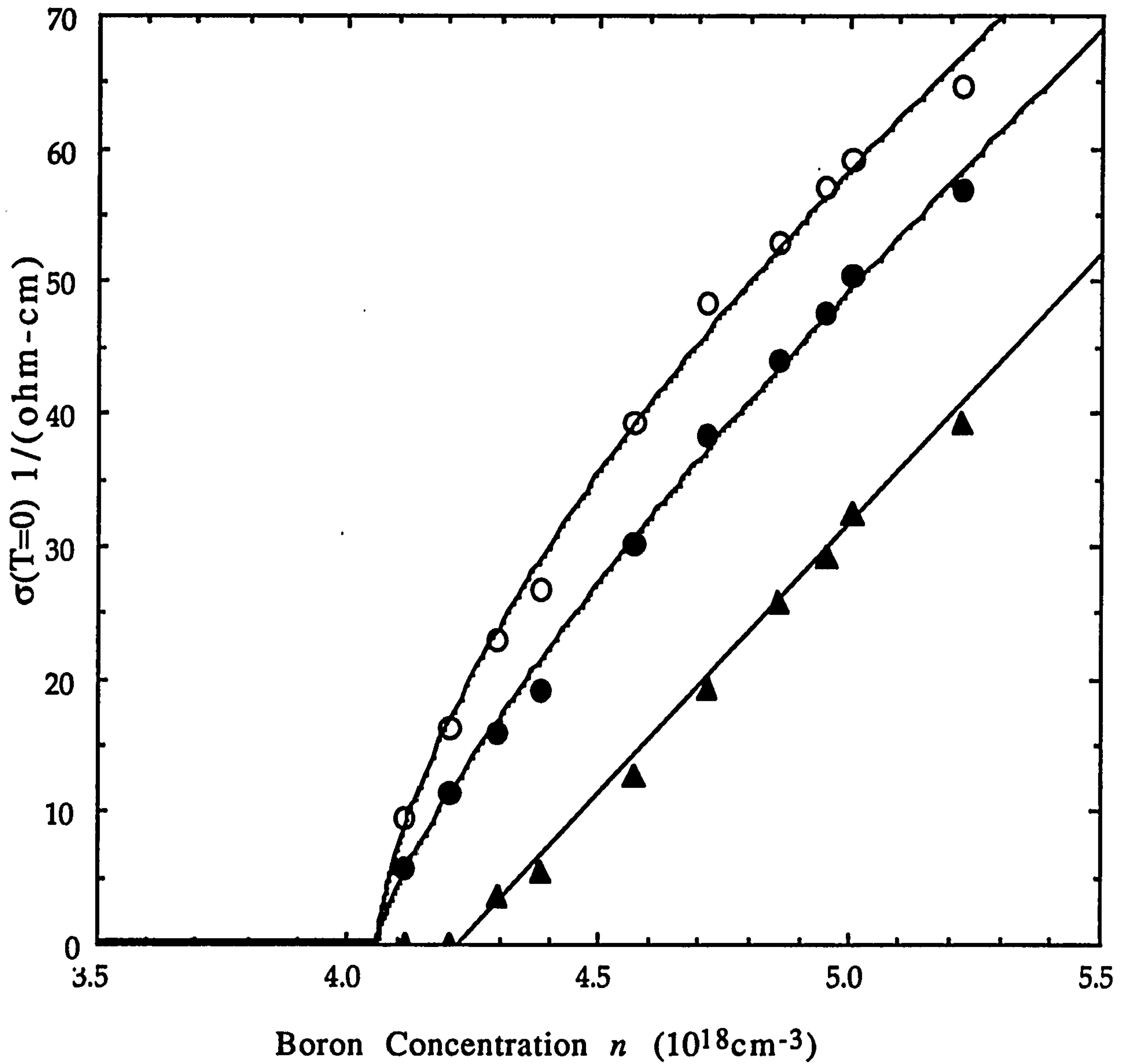

Fig. 4.26 The zero temperature conductivities plotted as a function of boron concentrations. ○ $H = 0$; ● $H = 1.0$ Tesla; ▲ $H = 7.5$ Tesla. The lines are the fitted curves to the expression

$$\sigma(H,T\to 0) = \sigma_0(H)[n/n_c(H)-1]^{\nu}$$

In our case the conditions under which the slope of the conductivity changes sign in a magnetic field are set only by the ratio H/T as discussed earlier and shown in Figs. 12 through 21, implying that the temperature rather than spin-orbit scattering determines the crossover field. In order to cause Zeeman splitting, we need a field such that $g\mu_B H >> k_B T$. For Si:B this gives $H/T >> 1.24$ (Tesla/Kelvin). Obviously a field of 1 Tesla only meets this condition marginally, thus offering a fairly restricted range of temperature from which the extrapolated value $\sigma(H,0)$ is determined within our measurements. When the above condition is clearly met in a field of 7.5 Tesla, a critical exponent near 1 was found.

Magnetic Field	σ_0 (Ω-cm)	n_c (10^{18} cm^{-3})	ν
0	152^{+10}_{-18}	$4.06^{+0.12}_{-0.02}$	$0.65^{+0.05}_{-0.14}$
1.0 T	155^{+12}_{-18}	$4.06^{+0.10}_{-0.03}$	$0.80^{+0.06}_{-0.14}$
7.5 T	171^{+23}_{-25}	$4.22^{+0.12}_{-0.05}$	$1.0^{+0.10}_{-0.20}$

Table 4.7 The parameters in $\sigma(H,T\to 0) = \sigma_0(H)[n/n_c(H)-1]^\nu$ obtained through a non-linear least square fitting procedure for Si:B samples at different magnetic fields.

Other attempts have been made to determine the effect of a magnetic field on the critical exponents. Ootuka et al[20] determined the critical exponent of uncompensated Ge:Sb in a magnetic field of 4 Tesla and found $\nu = 1$. In that case, however, the critical exponent in zero field is 0.9 which is already close to 1, and thus the shift is not obvious.

4.4 Magnetoresistance

4.4.a Introduction

The magnetoresistance of the Si:B samples was studied in magnetic fields up to 9 Tesla and at various temperatures. The two main contributions to the magnetoresistance in a disordered metal arise from weak localization and electron-electron interactions. The sign of the magnetoresistance due to localization can be either negative or positive, depending on whether spin-orbit scattering is weak or strong. The fact that strong spin-orbit scattering leads to positive magnetoresistance in two dimensional systems has been established both theoretically[36] and experimentally[37]. Theory[38,39] also predicts a positive magnetoresistance in the presence of strong spin-orbit scattering for three dimensional systems and is confirmed by experiments[40].

The magnetoconductivity for a Si:B sample studied in magnetic fields between zero and 1 Tesla at various fixed temperatures is plotted in Fig. 4.27. The magnetoresistance for our Si:B samples is found to be positive (negative magnetoconductivity) within the ranges of temperatures and magnetic fields of our measurements, in agreement with an earlier study by Roth et al[25]. This provides additional evidence for strong spin-orbit scattering in p-type Si:B. For n-type systems such as Si:P, the magnetoresistance due to weak localization is negative, and a separation into contributions arising from localization and interactions has been possible since they are of opposite sign[31,41].

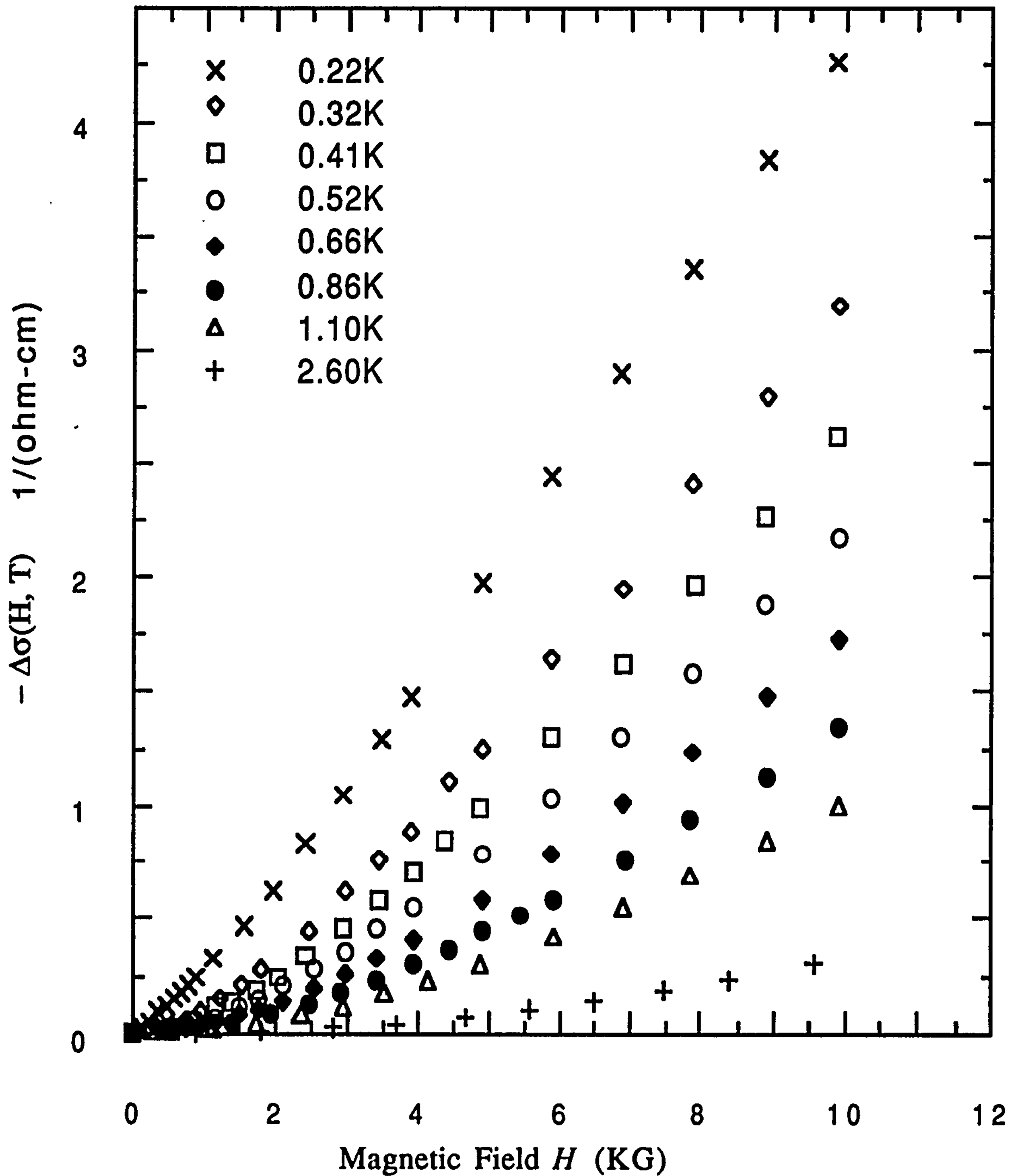

Fig. 4.27 The negative of $\Delta\sigma(H,T)$ for a Si:B sample plotted versus magnetic fields at several fixed temperatures. The boron concentration for this sample is $n = 4.95 \times 10^{18}$ cm^{-3}.

For Si:B, however, the contributions from localization and interactions have the same sign, and it is therefore difficult to separate one from the other.

4.4.b Interaction Constant from Magnetoconductivity

Five Si:B samples were studied in magnetic fields up to 9 Tesla at various fixed temperatures. The magnetoconductivities of the five samples at a fixed temperature of 0.31 K are plotted in Fig. 4.28 as a function of $\sqrt{H}$, while the magnetoconductivity of a single sample at three fixed temperatures is plotted in Fig. 4.29.

The conductivity in strong magnetic fields such that $g\mu_B H >> k_B T$ is given by[33,34]

$$\Delta\sigma(H,T) = m_H H^{1/2} + m' T^{1/2} \tag{4.4.1}$$

where $$m_H = -\,0.77\alpha\sqrt{g\mu_B/k_B}\,\gamma\tilde{F}_\sigma \tag{4.4.2}$$

At a fixed temperature and in strong magnetic fields, the conductivity follows a $\sqrt{H}$ behavior in agreement with the theoretical prediction[33,34], except at the high end of the field range where as shown in Figs. 4.28 and 4.29 there are deviations from $\sqrt{H}$ dependence. We note the slope m_H of the $\sqrt{H}$ dependence is again related to the interaction constant $\tilde{F}_\sigma$. We can now examine if the theory based on electron-electron interactions describes the dependence of the conductivity on both temperature and magnetic field self consistently.

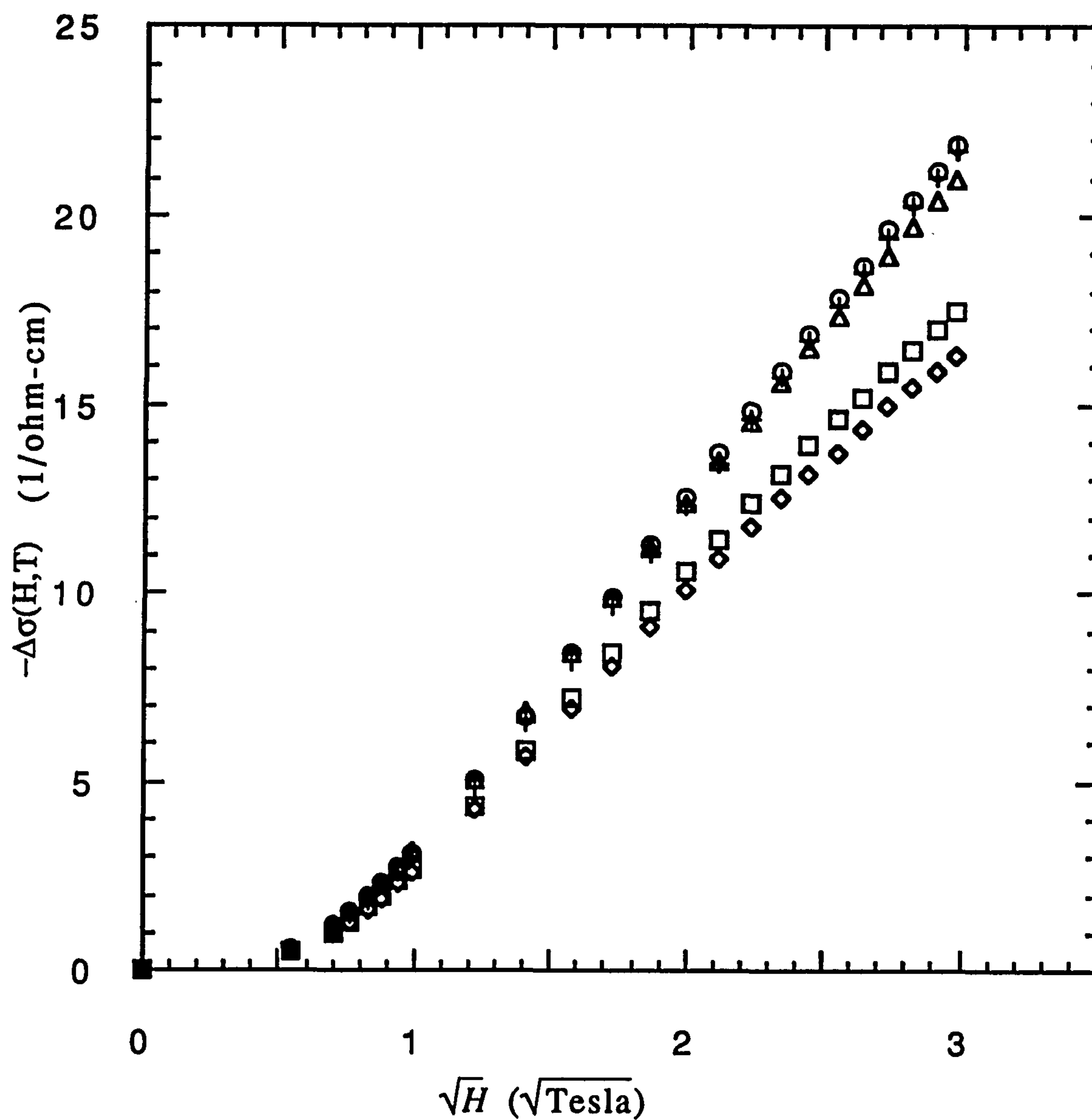

Fig. 4.28 The negative of $\Delta\sigma(H,T)$, $-[\sigma(H,T)-\sigma(H=0,T)]$, plotted as a function of the square root of magnetic field for five Si:B samples at a fixed temperature of 0.31 K. In units of 10^{18} cm^{-3}, their boron concentrations are: + 5.01, ○ 4.86 , △4.57 , □ 4.38, ◇4.30.

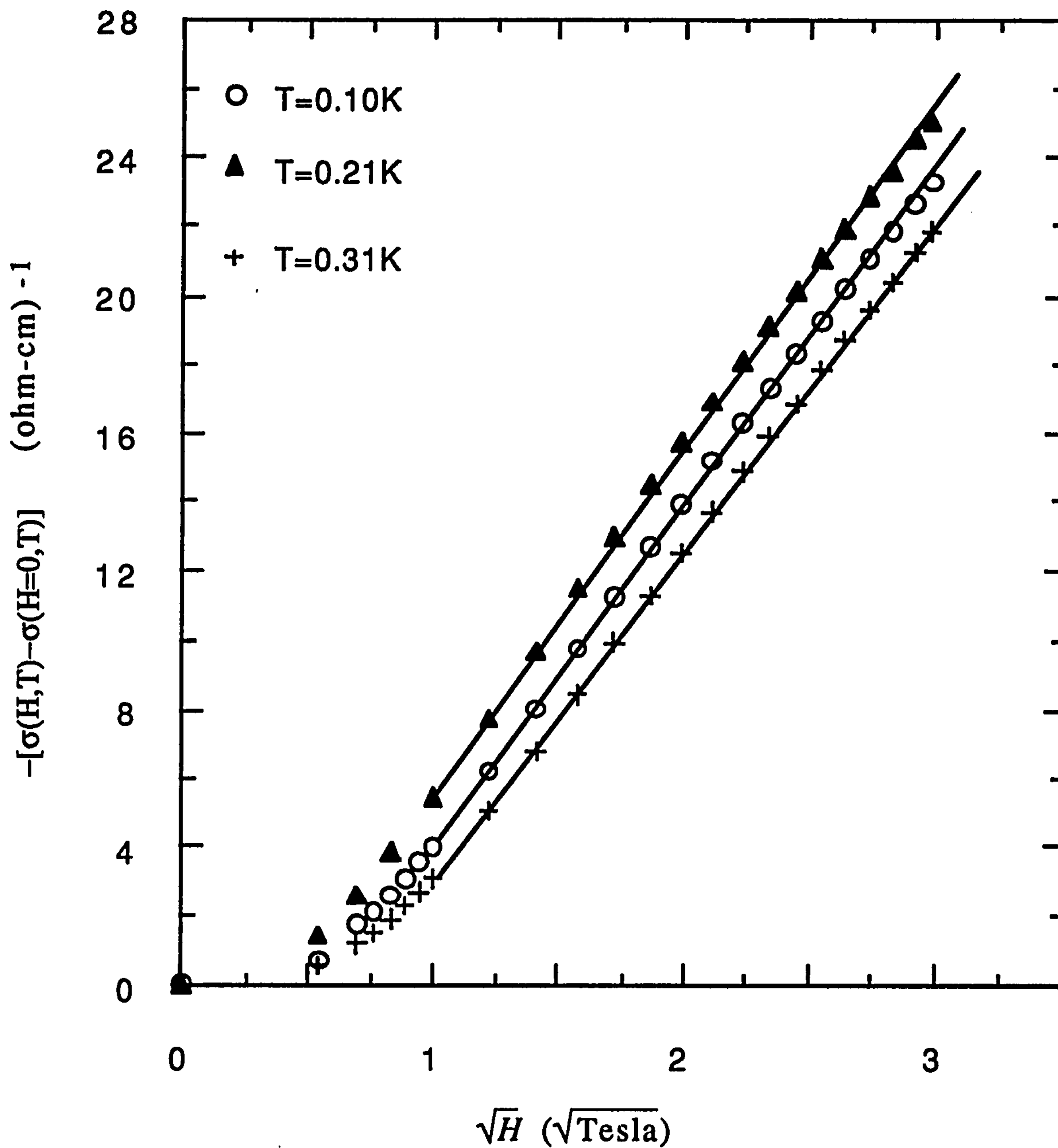

Fig. 4.29 The negative of $\Delta\sigma(H,T)$, $-[\sigma(H,T)-\sigma(H=0,T)]$, plotted as a function of the square root of magnetic field for a single Si:B sample at three fixed temperatures. The boron concentration for this sample is $n = 4.86\times10^{18}\text{cm}^{-3}$. The straight lines are guides to the eye.

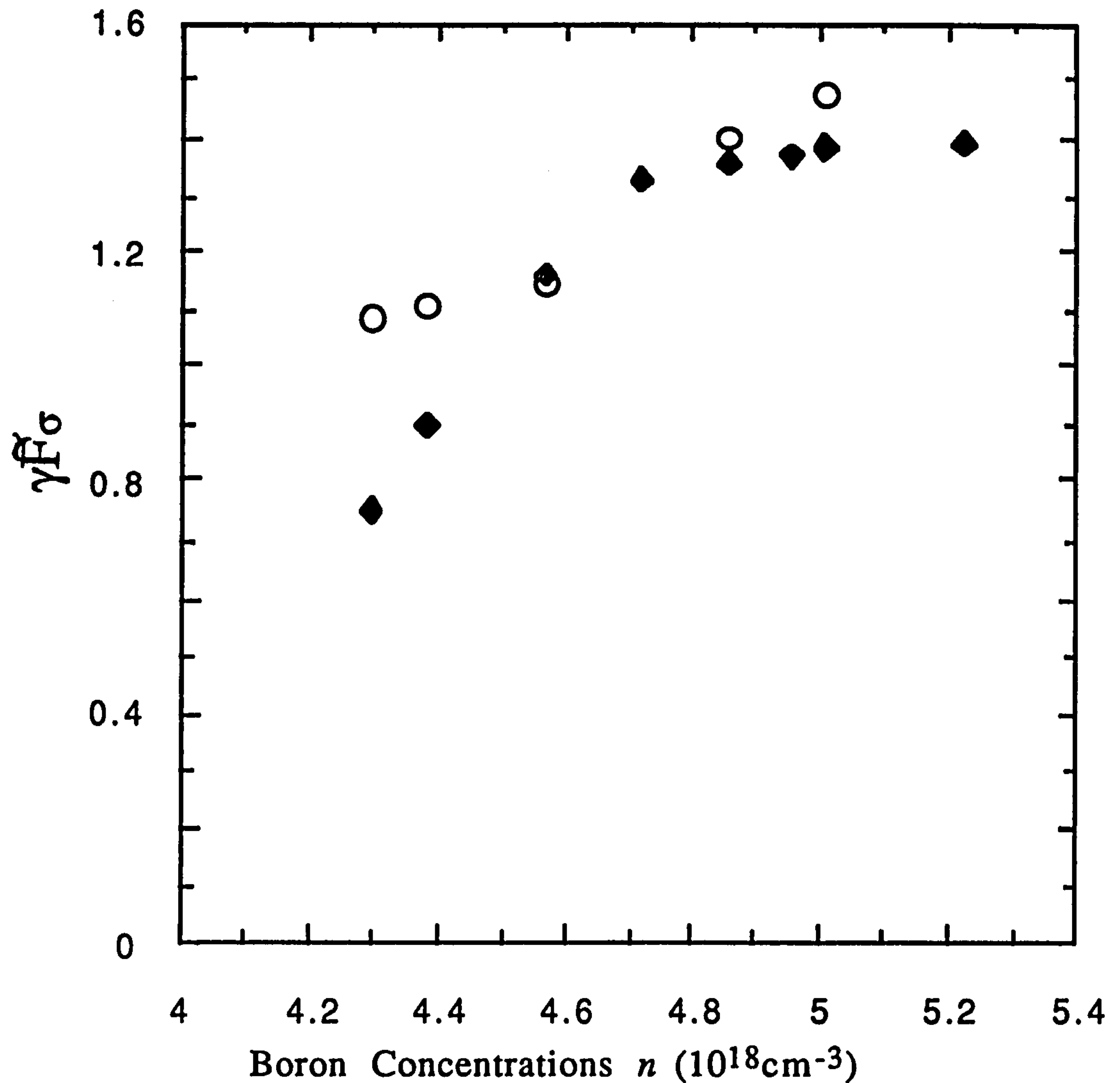

Fig. 4.30 The product of γ and $\tilde{F}_\sigma$, $(\gamma\tilde{F}_\sigma)$, deduced from both the T and H dependence plotted versus boron concentration. ◆ from T dependence; ○ from H dependence.

Using the values of α obtained from m and m' in section 4.3.b and the slopes m_H determined experimentally, we calculated $(\gamma\tilde{F}_\sigma)$ from eq. (4.4.2) and plotted the values in Fig. 4.30 along with those obtained in sections 4.3.a and 4.3.b from the temperature dependence of the conductivity.

As shown in Fig. 4.30, the value of $(\gamma\tilde{F}_\sigma)$ obtained from the two methods agree with each other fairly well for samples not near the

transition, but for samples close to the transition the agreement is not as good. This is not surprising, since the theory is not expected to be valid very near the transition. The localization contribution to the magnetoconductivity, which has not been taken into account, may also add to the discrepancy. Thus, the uncertainty in the value of $(\gamma\tilde{F}_\sigma)$ for samples very near the transition may be large. The approximate agreement between the experimental data and interaction theory implies, however, that the high field magnetoresistance can be accounted for largely by interaction effects, and that the contribution due to localization may be relatively less important.

More recent calculations by Raimondi et al.[42] showed that $\tilde{F}_\sigma$ in eq. (4.4.2) should be replaced by a different multiplicative factor A which relates to $\tilde{F}_\sigma$ by

$$A = 4x[1 + 2x^2 ln(x)/(1-x^2)] \qquad (4.4.3)$$

where $x = 1 - \tilde{F}_\sigma/2$. The values of $(\gamma\tilde{F}_\sigma)$ deduced using the new theory[42] depend on the value of γ which is not known, and generally lie below those shown in Fig. 4.30. However, the concentration dependence of $(\gamma\tilde{F}_\sigma)$ deduced using the new theory[42] is not very different from that shown in Fig. 4.30.

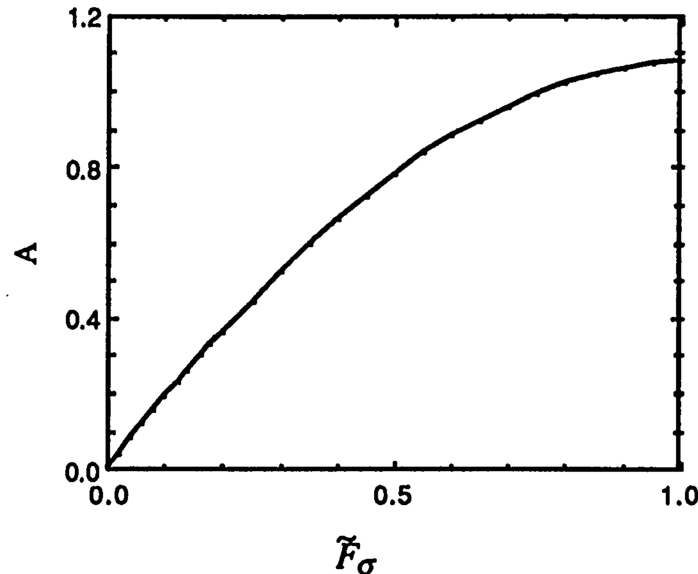

Fig. 4.31 The multiplicative factor A of eq. (4.4.3) plotted against $\tilde{F}_\sigma$.

4.4.c Interpretation of the Data within Interaction Theory

Motivated by the rough agreement between the high field magnetoresistance and the prediction of interaction theory as discussed in the above section, we first attempt to fit the full field-dependence of the magnetoresistance data assuming interaction effects only.

The full expression for the magnetoconductivity due to interactions is given by:[33,34]

$$\Delta\sigma_I(H) = -\,0.77\alpha\,\gamma\tilde{F}_\sigma T^{1/2} g_3(h) \qquad (4.4.4)$$

where $\alpha = \frac{e^2}{\hbar}\frac{1.3}{4\pi^2}\sqrt{k_B/2\hbar D}$, $h = g\mu_B H/k_B T$ and g_3 is defined by

$$g_3(h) = \int_0^\infty d\Omega\,\frac{d^2}{d\Omega^2}[\Omega N(\Omega)]\,(\sqrt{\Omega+h}+\sqrt{|\Omega-h|}-2\sqrt{\Omega})$$

with $N(\Omega) = \frac{1}{e^{\Omega}-1}$.

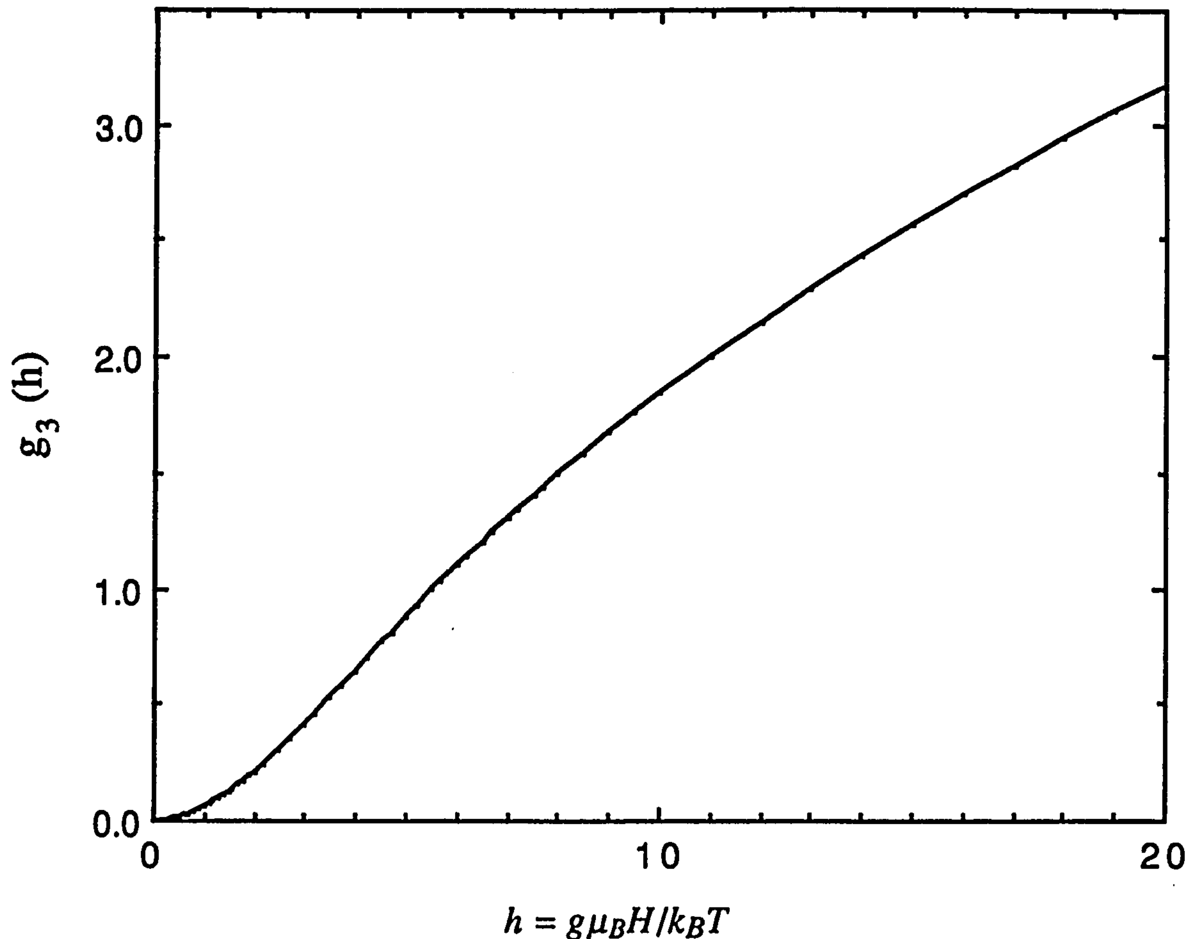

Fig. 4.32 The numerically calculated values of $g_3(h)$ plotted as a function of $h = g\mu_B H/k_B T$.

The magnetoconductivity data for five Si:B samples at three different temperatures are plotted versus magnetic fields in Figs. 4.33, 4.34, 4.35, 4.36 and 4.37 respectively. Assuming that electron-electron interactions completely determine its behavior, the magnetoconductivity over the whole field range is fitted to the expression:

$$\Delta\sigma(H,T) = -A_I\, g_3(g\mu_B H/k_B T) \qquad (4.4.5)$$

with A_I as an adjustable parameter and a g-factor of 1.2 for Si:B. The lines drawn in Figs 4.33 through 4.37 represents the fits obtained for the various samples at different temperatures.

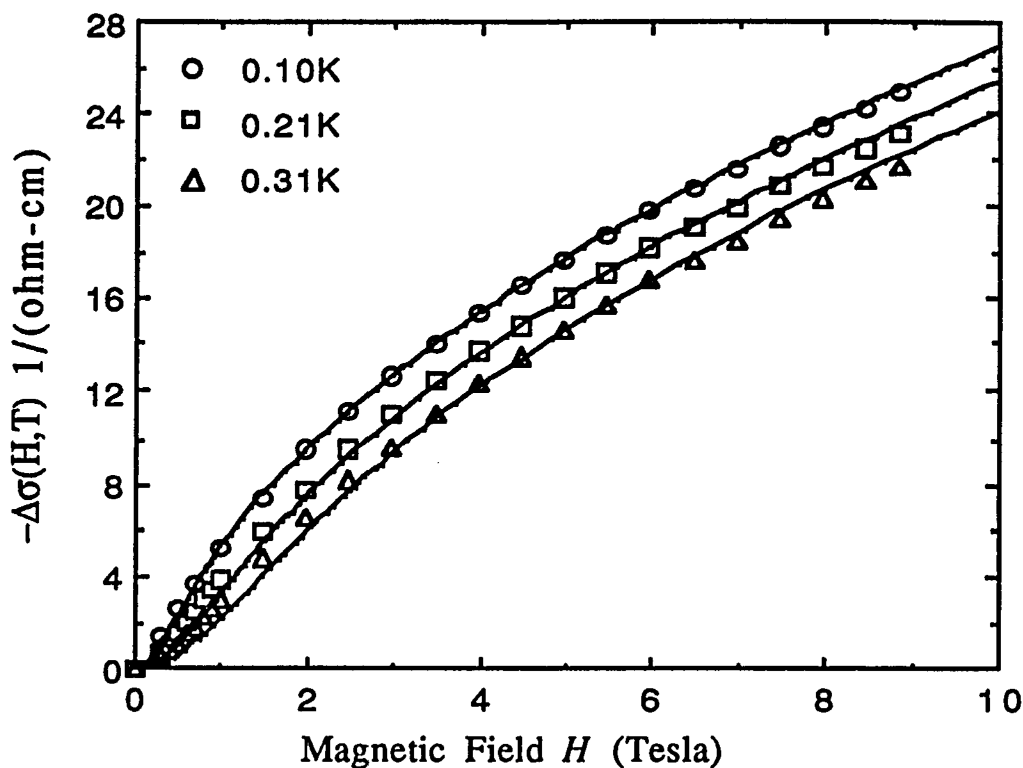

Fig. 4.33 $-\Delta\sigma(H,T)$ for a sample with $n = 5.01 \times 10^{18}$ cm^{-3} plotted against magnetic field. The solid cures are fits to eq. (4.4.5).

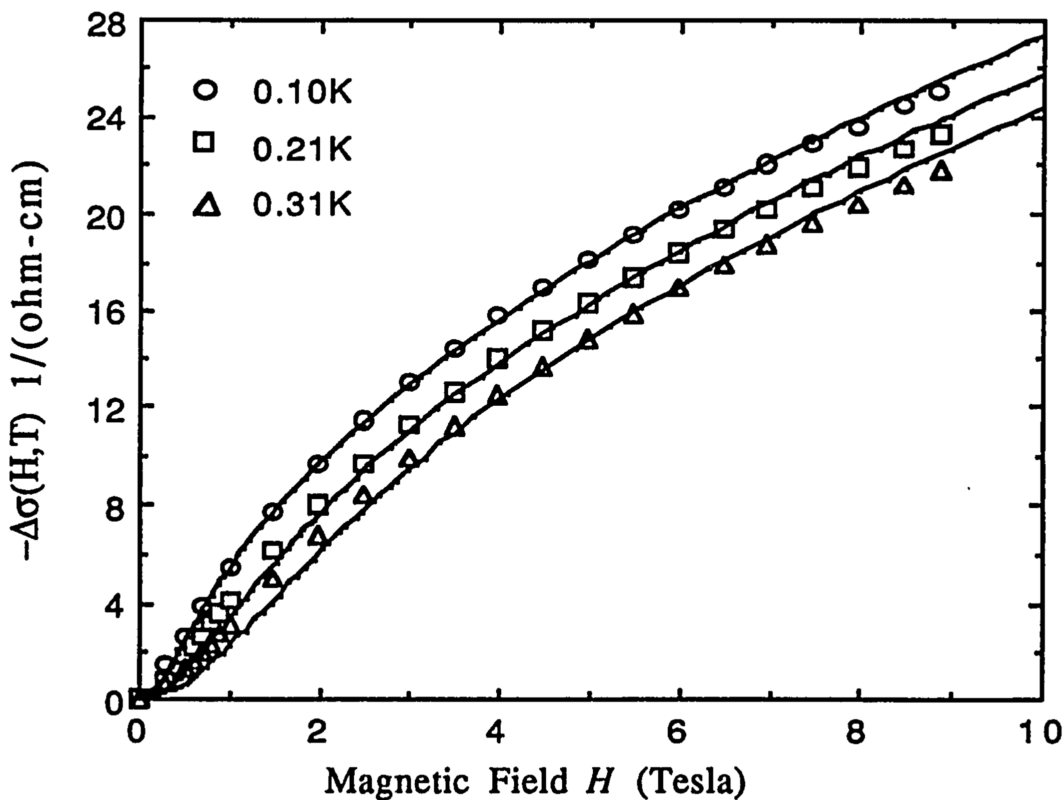

Fig. 4.34 $-\Delta\sigma(H,T)$ for a sample with $n = 4.86 \times 10^{18}$ cm^{-3} plotted against magnetic field. The solid cures are fits to eq. (4.4.5).

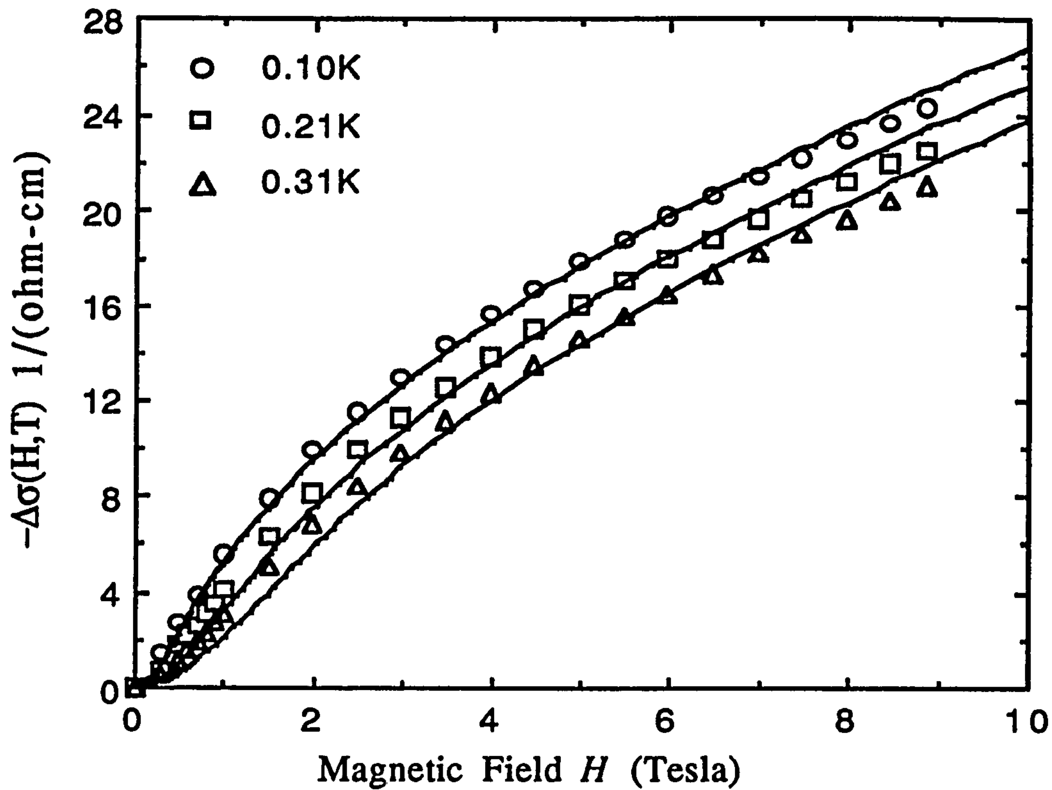

Fig. 4.35 -$\Delta\sigma(H,T)$ for a sample with n = 4.57x10^{18} cm^{-3} plotted against magnetic field. The solid cures are fits to eq. (4.4.5).

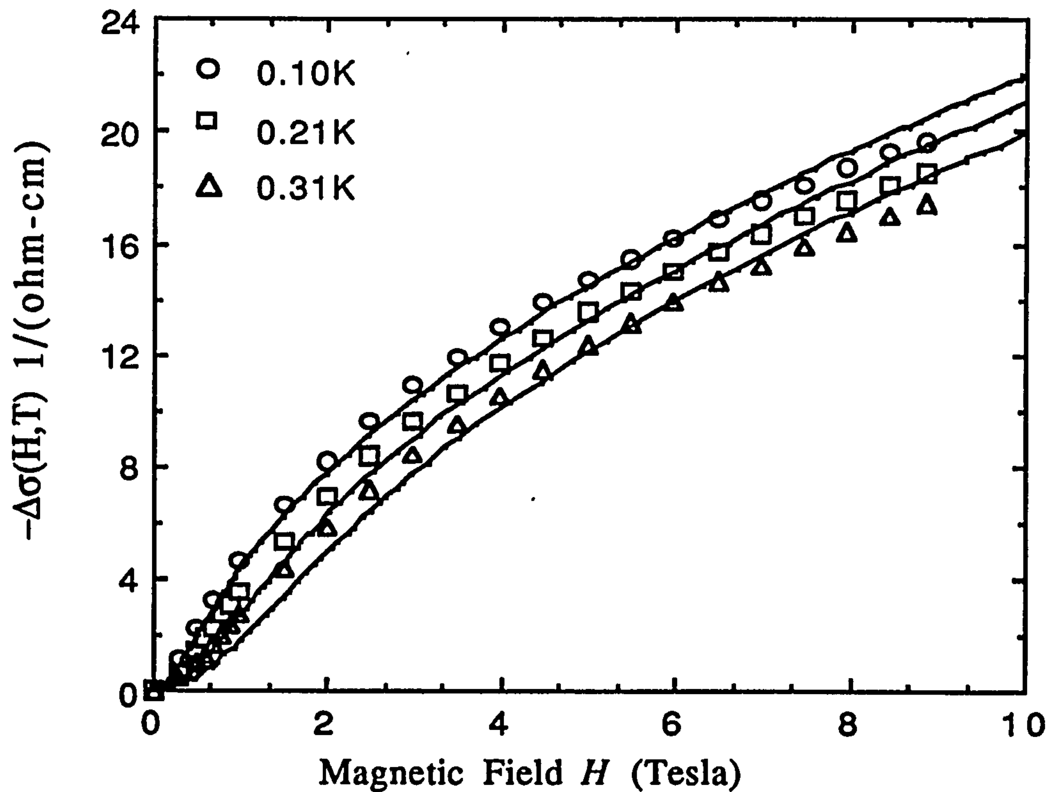

Fig. 4.36 -$\Delta\sigma(H,T)$ for a sample with n = 4.38x10^{18} cm^{-3} plotted against magnetic field. The solid cures are fits to eq. (4.4.5).

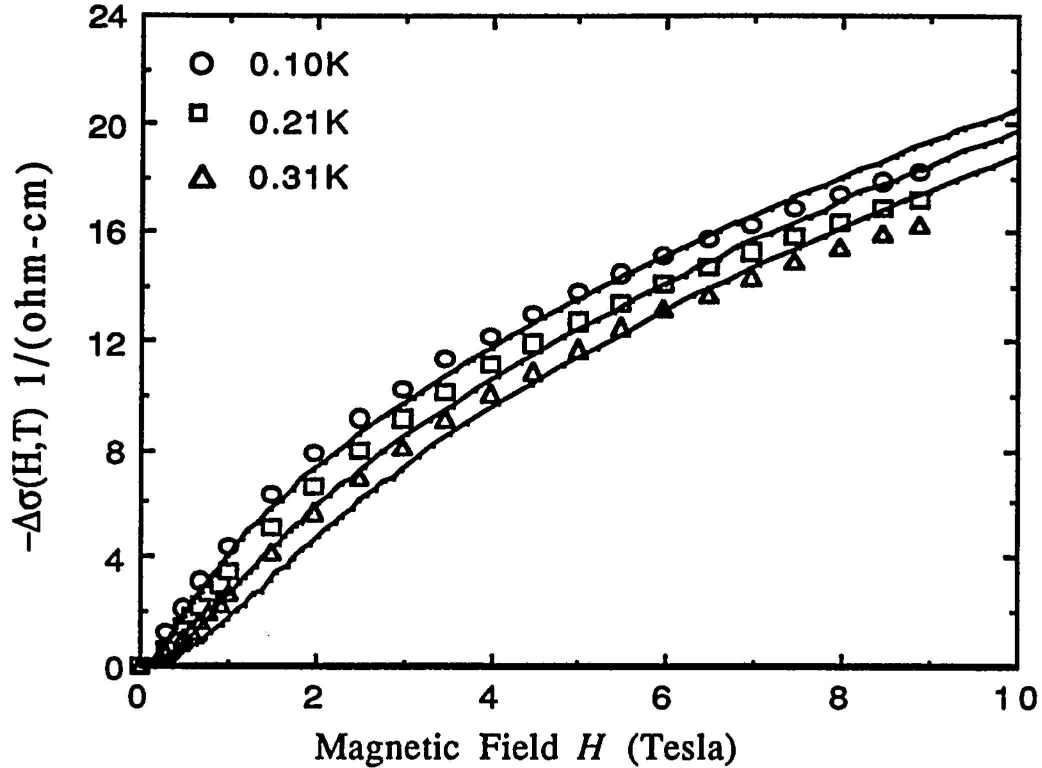

Fig. 4.37 $-\Delta\sigma(H,T)$ for a sample with n = 4.30x10^{18} cm^{-3} plotted against magnetic field. The solid cures are fits to eq. (4.4.5).

The values of A_I obtained from the non-linear fitting procedure are listed in table 4.8.

n (10^{18} cm^{-3})	A_I T=0.10K	A_I T=0.21K	A_I T=0.31K
5.01	3.50	5.11	6.19
4.86	3.56	5.18	6.26
4.57	3.49	5.07	6.09
4.38	2.86	4.22	5.12
4.30	2.67	3.96	4.84

Table 4.8 The values of the fitting parameter A_I by using eq.(4.4.5) for five Si:B samples at three temperatures.

For a given sample, the fitting parameters at different temperatures are proportional to $\sqrt{T}$, which is consistent with theoretical prediction expressed in eq. (4.4.4).

As can be seen from the plots, the fits for samples not very near the transition are reasonably good. However, the fits get worse as the transition is approached. This again may imply that the theory is not valid very close to the transition, or that the contribution due to localization becomes increasingly important and can not be neglected. In any case, there are serious discrepancies at low fields, and there is also systematic deviation at the high field end.

The residuals, $-\{[\sigma(H,T)]_{exp.}-[\sigma(H,T)]_{fit}\}$, for some of the fits are plotted in Fig. 4.38.

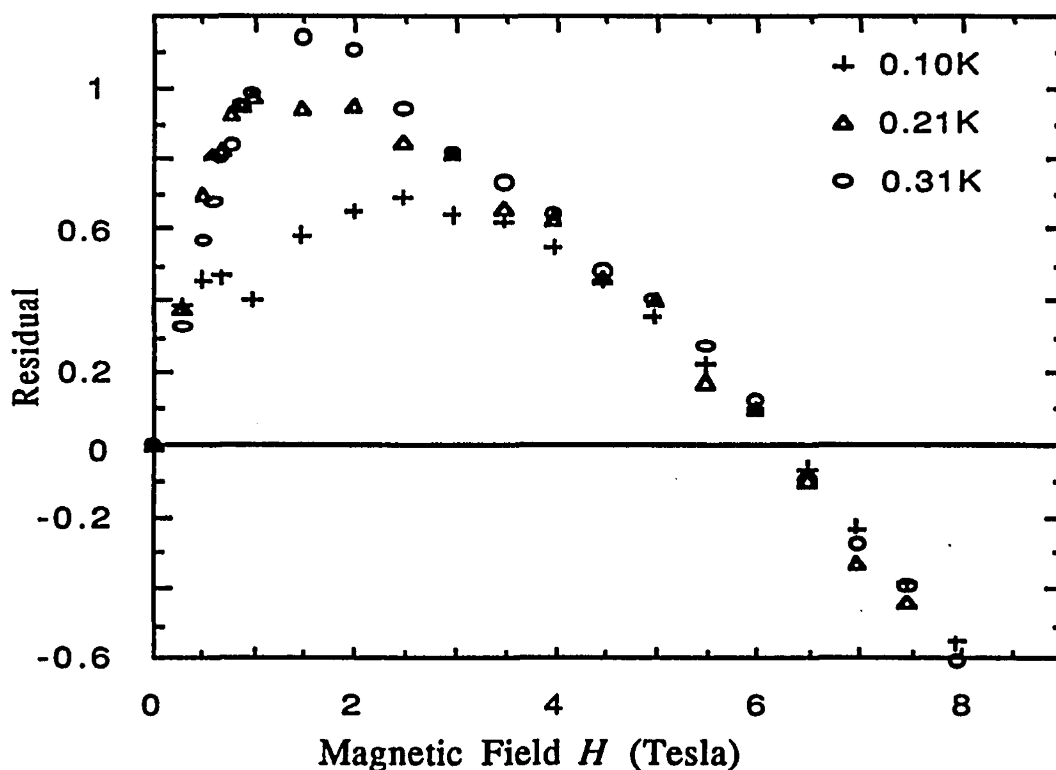

Fig. 4.38 The residual of $-\Delta\sigma(H,T)$, that is, $-\{[\sigma(H,T)]_{exp.}-[\sigma(H,T)]_{fit}\}$ plotted versus magnetic fields for a sample with n = 4.30x10^{18} cm^{-3}. The fits were made by using eq. (4.4.5).

The residual resembles the magnetoconductivity which has been found experimentally in other materials[37,40,43] in the presence of spin-orbit scattering, and where interaction effects are relatively weak. At small magnetic fields, the magnetoresistance is positive. A maximum then appears as the field increases. As the magnetic field increases further such that it becomes larger than

$$H_{so} = \frac{\hbar}{eD\tau_{so}} \tag{4.4.6}$$

the magnetoresistance eventually becomes negative[44]. Since the size of the interaction effects is not precisely known, we can not determine the spin-orbit scattering time quantitatively. Further, since the positions of the maxima shown in Fig. 4.38 vary with temperature rather than remaining fixed, this interpretation should not be regarded too seriously.

While the magnetoresistance of n-type silicon such as Si:P[31,41] has a negative component due to weak localization, the magnetoresistance of Si:B is always positive due to strong spin-orbit scattering. The magnetoconductivity for a Si:B and a Si:P samples with similar values of n/n_c at the same constant temperature of 0.1K is plotted in Fig.4.39. The absolute value of the magnetoconductivity of the Si:B sample is several times bigger than that of the Si:P sample at the same temperature and magnetic field. The dramatic difference in the overall size of the magnetoresistance is probably associated with details of the band structure, and is also due to the fact that the contributions of localization and interactions are of opposite sign in Si:P, while in Si:B the contributions are additive.

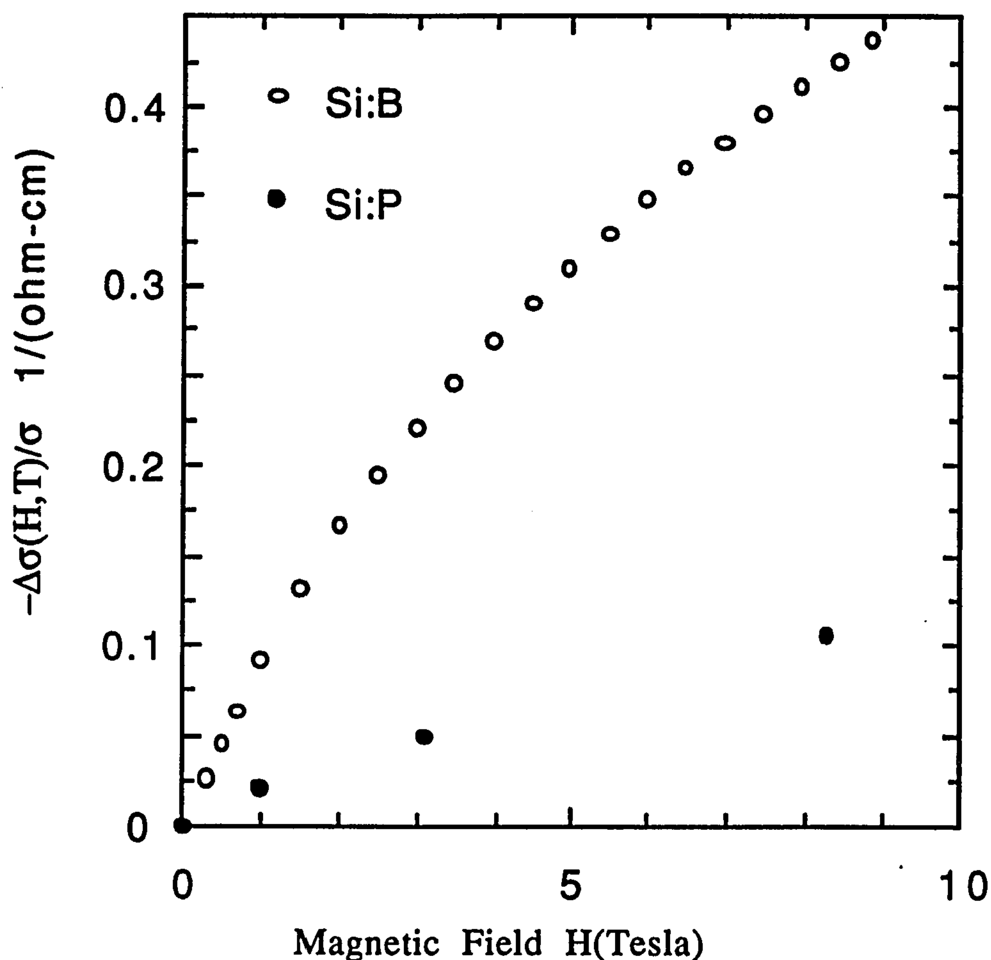

Fig.4.39 -[σ(H,T)-σ(0,T)]/σ(0,T) for a Si:B sample (○ n/n_c=1.23), and a Si:P sample[31] (● n/n_c=1.25) at a constant temperature of 0.1 K plotted against magnetic field H.

4.4.d Low Field Data and Inelastic Scattering Time

Weak localization theory in the presence of strong spin-orbit scattering for p-type cubic semiconductors is not complete at this time. Thus, there is no closed mathematical expression for the magnetoconductivity. According to Altshuler et al[38,44], the magnetoconductivity for p-type cubic semiconductors due to localization is:

$$\Delta\sigma_L = -\frac{1}{4}\Sigma_0 + \frac{3}{4}\Sigma_1 - \frac{5}{4}\Sigma_2 + \frac{7}{4}\Sigma_3 \qquad (4.4.7)$$

where the four terms correspond to the total moment of two holes with values of 0, 1, 2 and 3. Σ_0 is the same as that in the case without spin-orbit scattering[38,44], that is,

$$\Sigma_0 = \frac{e^2}{2\pi^2 \hbar}\left(\frac{eH}{\hbar}\right)^{1/2}\frac{1}{2}f_3\left(\frac{H}{H_i}\right). \qquad (4.4.8)$$

However, we do not have mathematical expressions for the other terms. For strong spin-orbit scattering, the first term is the major contribution for small magnetic fields. The magnetoconductivity due to weak anti-localization for low magnetic fields can be written as:

$$\Delta\sigma_L \approx -\frac{1}{4}\frac{1}{12\pi^2}\frac{e^2}{\hbar}\left(\frac{e}{\hbar}\right)^2 D^{3/2}\tau_{in}^{3/2}H^2 \quad (H \ll H_i) \qquad (4.4.9)$$

where $H_i = \frac{\hbar}{4De}\tau_{in}^{-1}$ and $\tau_{in}^{-1} \ll \tau_{so}^{-1}$, τ_{in} is the inelastic scattering time and τ_{so} is the spin-orbit scattering time.

On the other hand, interaction theory predicts a magnetoconductivity due to Zeeman splitting[33,34],

$$\Delta\sigma_I = -0.041\ \alpha\left(\frac{g\mu_B}{k_B}\right)^2 \gamma\tilde{F}_\sigma T^{-3/2}H^2 \quad (g\mu_B H \ll k_B T) \qquad (4.4.10)$$

The above two contributions have very similar magnetic field dependences and are of the same sign, and it is therefore not easy to separate one from the other.

Following the work of Rosenbaum et al.[41] and Paalanen et al.[31], we assume that the two contributions are additive so we have

$$\Delta\sigma(H) = \Delta\sigma_L(H) + \Delta\sigma_I(H). \tag{4.4.11}$$

Further we assume the weak localization contribution for low magnetic fields is known, and is approximately given by eq.(4.4.9). Even so, the magnetoconductivity at low fields involves two unknowns, τ_{in} and the prefactor of the interaction contribution, which is $\alpha\gamma\tilde{F}_\sigma$. We therefore use the value of $\alpha\gamma\tilde{F}_\sigma$ obtained from the high field magnetoresistance data, where it was assumed that the high field magnetoresistance is due entirely to interaction effects.

In this work, we succeeded in measuring the magnetoresistance at very low magnetic fields from which we were able to deduce the slope of the initial H^2 dependence which contains information about the electron's inelastic scattering time. The change of the conductivity $\Delta\sigma(H,T)=\sigma(H,T)-\sigma(0,T)$ for one of the samples studied is plotted against the square of magnetic fields in Fig 4.40. As can be seen from the plot, the magnetoconductivity is always negative(positive magnetoresistance), and starts as a function of H^2 at small fields. As the temperature gets lower the magnetic field range over which $\Delta\sigma(H)$ follows a H^2 dependence gets shorter.

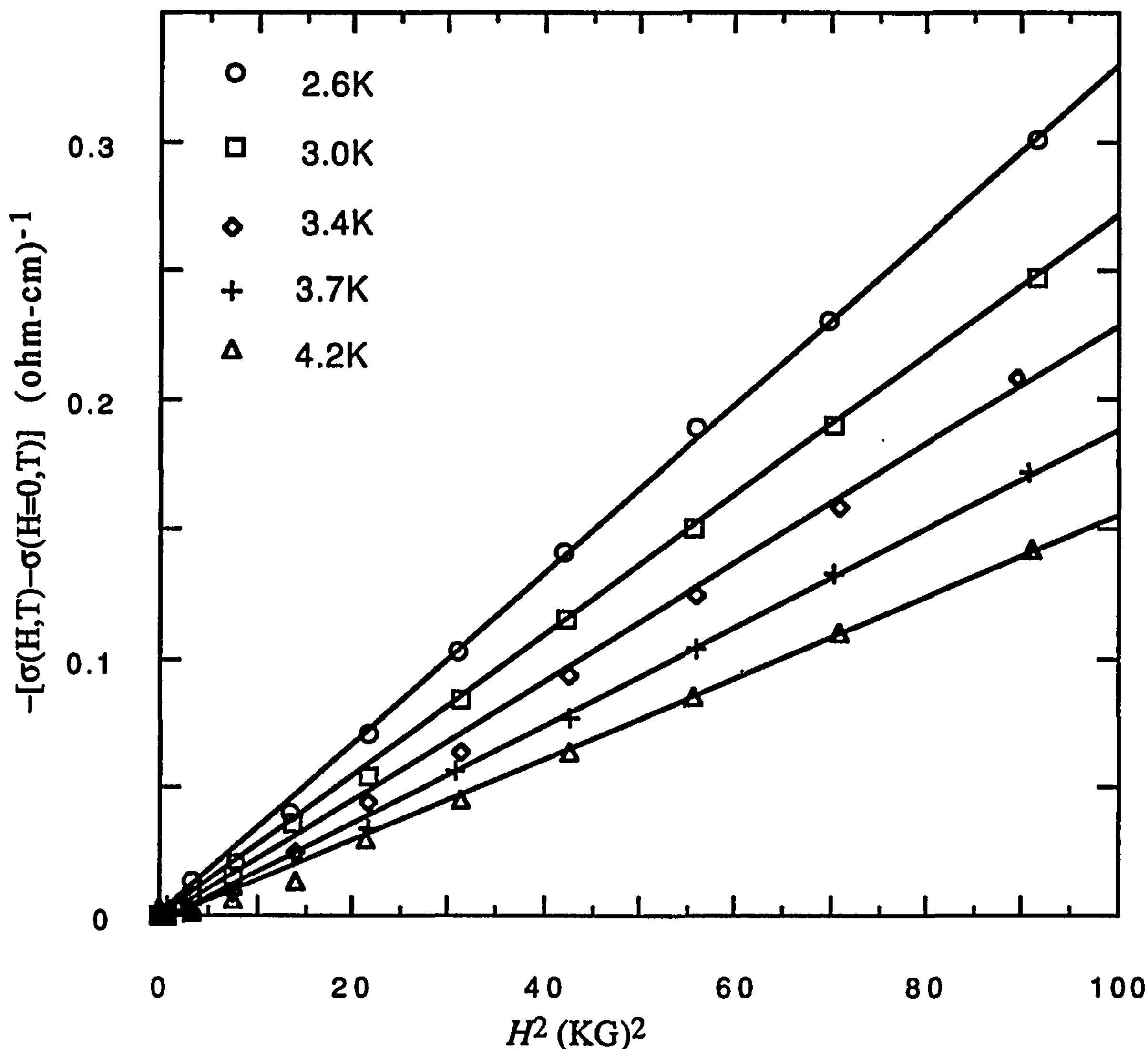

Fig. 4.40. The negative of $\Delta\sigma(H,T)$ plotted as function of the square of magnetic field at a few fixed temperatures. The concentration for this sample is $n = 4.95 \times 10^{18}$ cm^{-3}. More data for the same sample is shown in Fig. 4.27. The straight lines are guides to the eye.

We fitted the data to the expression

$$\Delta\sigma(H,T) = -C(T)H^2 \tag{4.4.12}$$

for small magnetic fields where the H^2 dependence is observed and plotted the values of $C(T)$ versus temperature on a double logarithmic scale in Fig. 4.41. $C(T)$ exhibits a power law dependence on temperature and varies roughly as $C(T) \propto T^{-3/2}$.

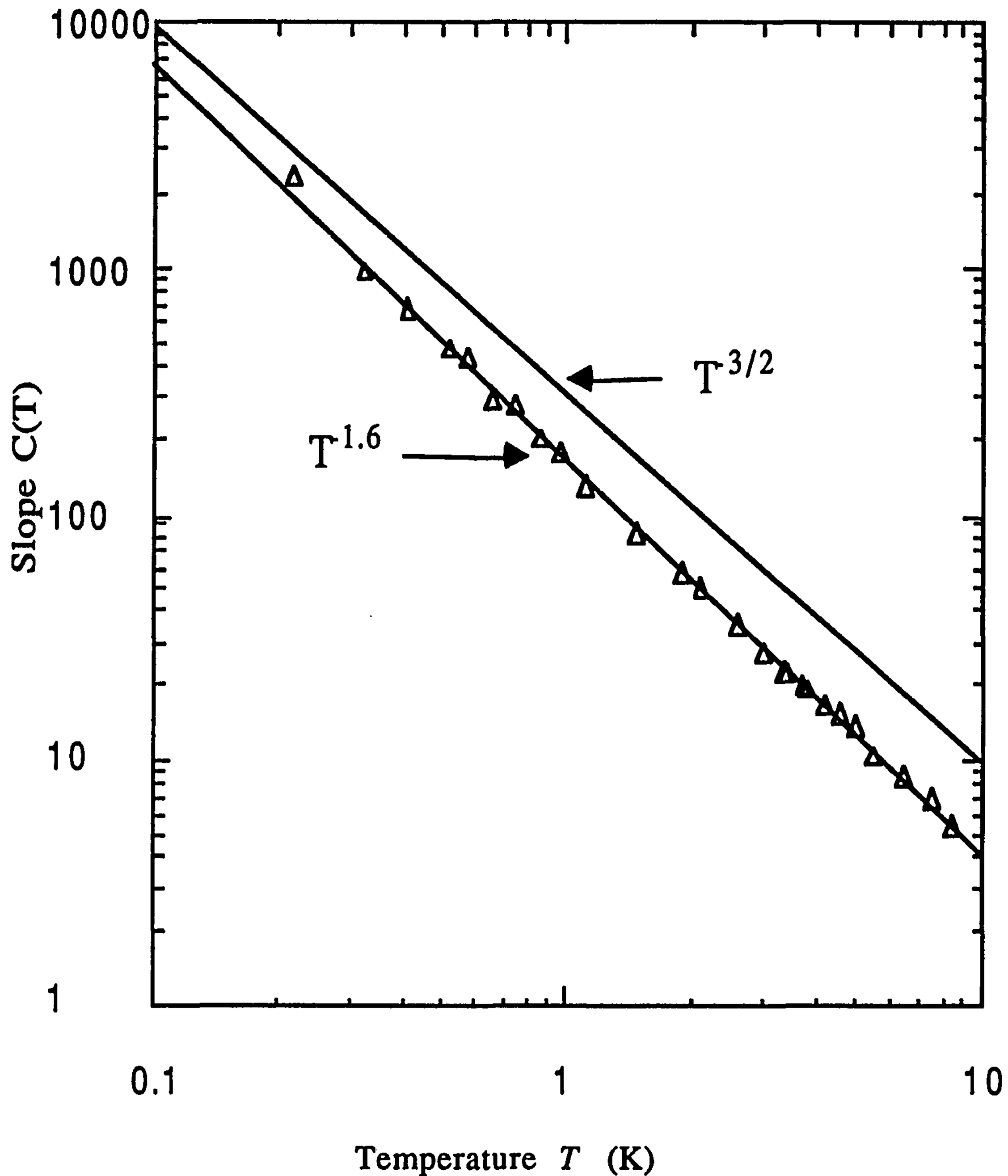

Fig. 4.41 The slope $C(T)$ of the H^2 dependence of the magnetoconductivity plotted as function of temperature on a double logarithmic scale for a Si:B sample with $n = 4.95 \times 10^{18}$ cm^3.

The low field magnetoresistances of four more Si:B samples were measured within a narrower temperature range (0.22K to 1.4K) and some of the data are plotted in Figs. 4.42 through 4.45.

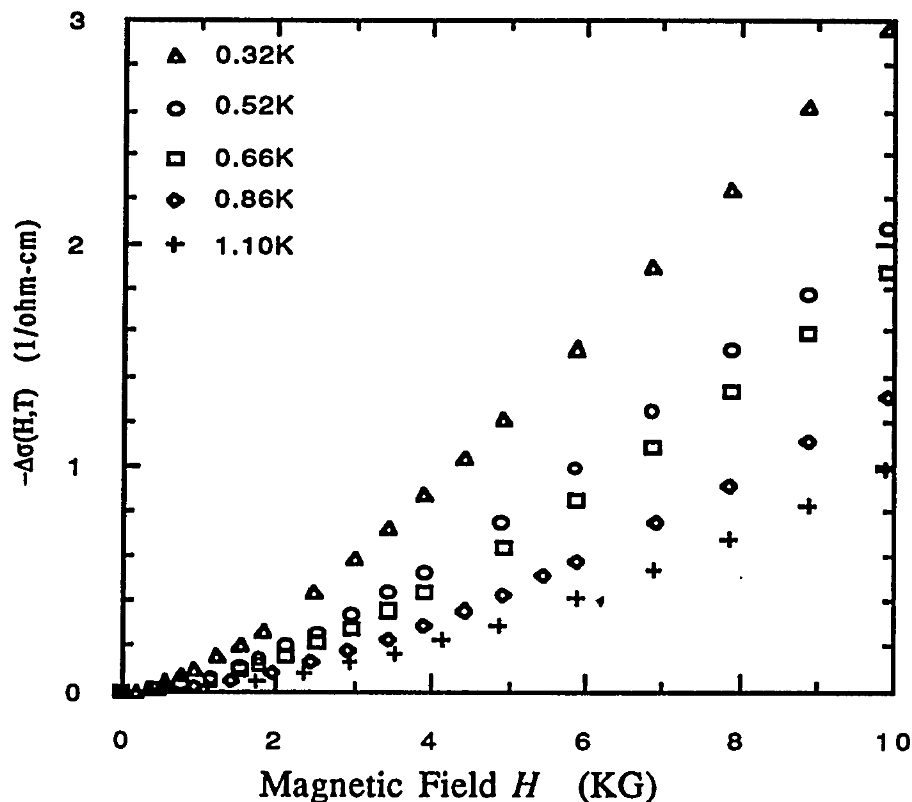

Fig. 4.42 (a) The negative of $\Delta\sigma(H,T)$ plotted versus magnetic field for a Si:B sample with $n = 5.22\text{x}10^{18}\ \text{cm}^{-3}$.

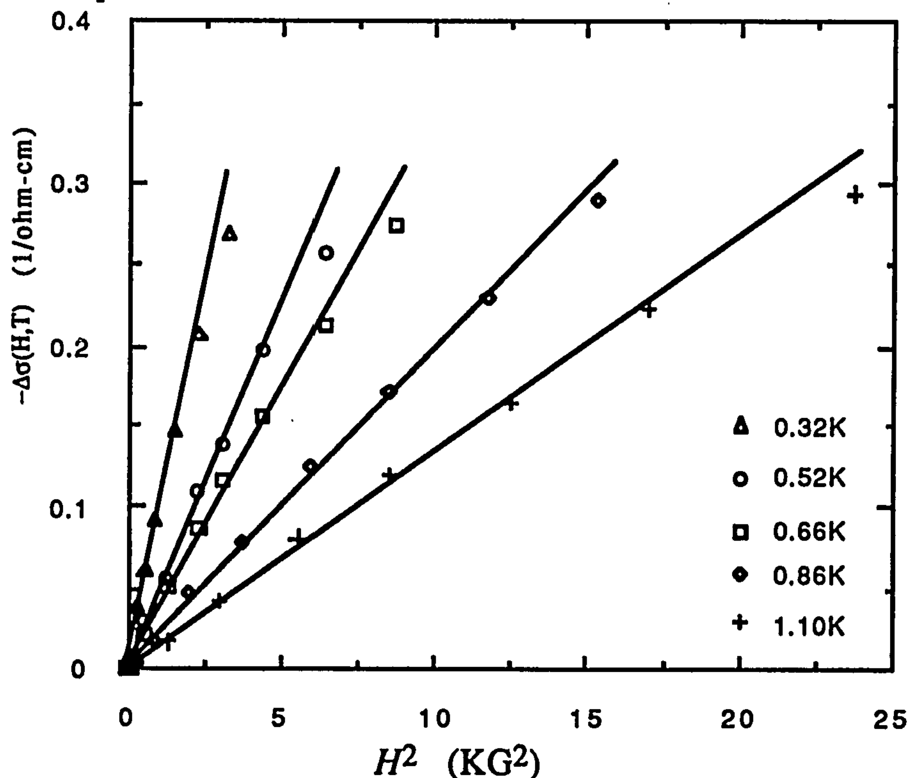

Fig. 4.42(b) The negative of $\Delta\sigma(H,T)$ plotted versus the square of magnetic field for a Si:B sample with $n = 5.22\text{x}10^{18}\ \text{cm}^{-3}$. The straight lines are guides to the eye.

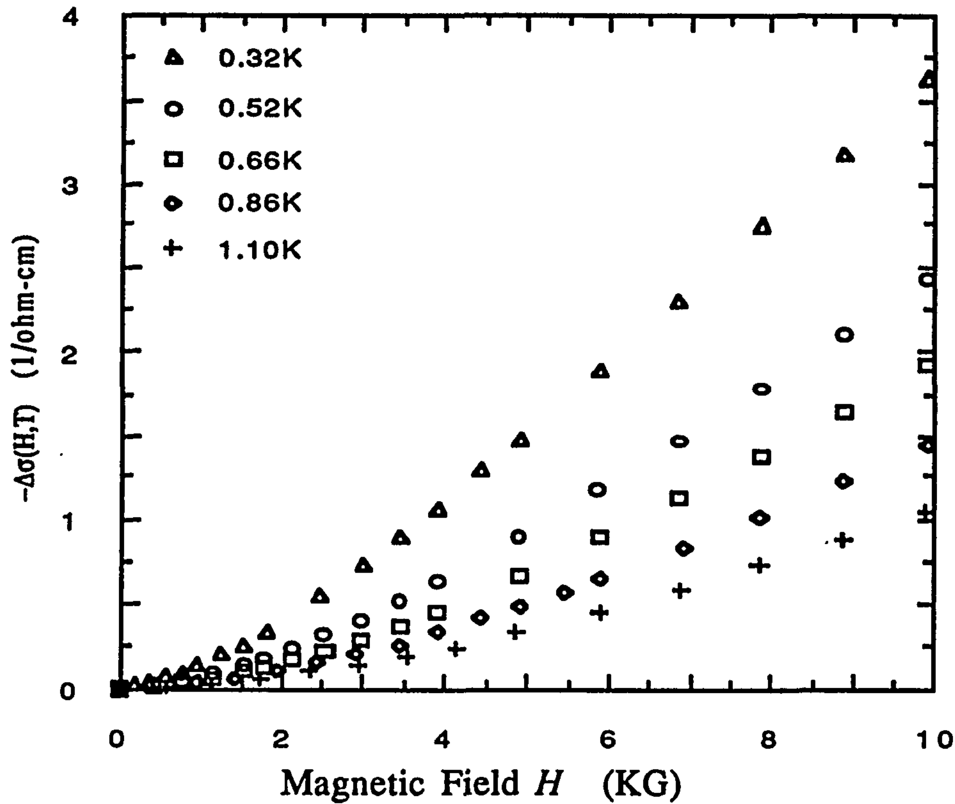

Fig. 4.43(a) The negative of $\Delta\sigma(H,T)$ plotted versus magnetic field for a Si:B sample with n = 4.72x10^{18} cm^{-3}.

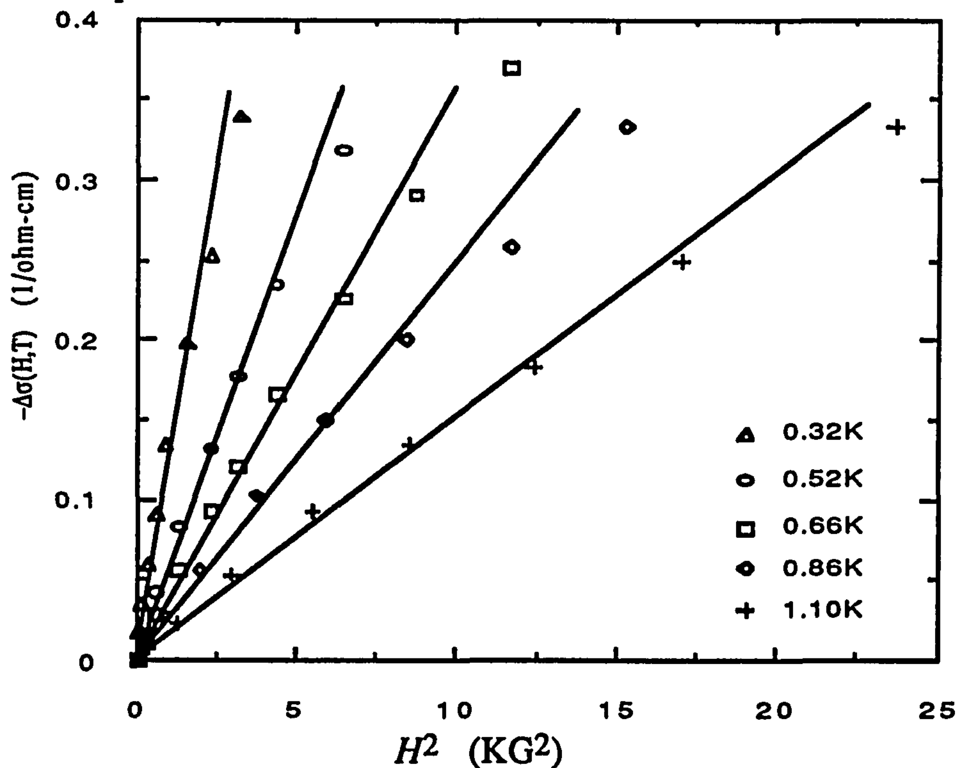

Fig. 4.43(b) The negative of $\Delta\sigma(H,T)$ plotted versus the square of magnetic field for a Si:B sample with n = 4.72x10^{18} cm^{-3}. The straight lines are guides to the eye.

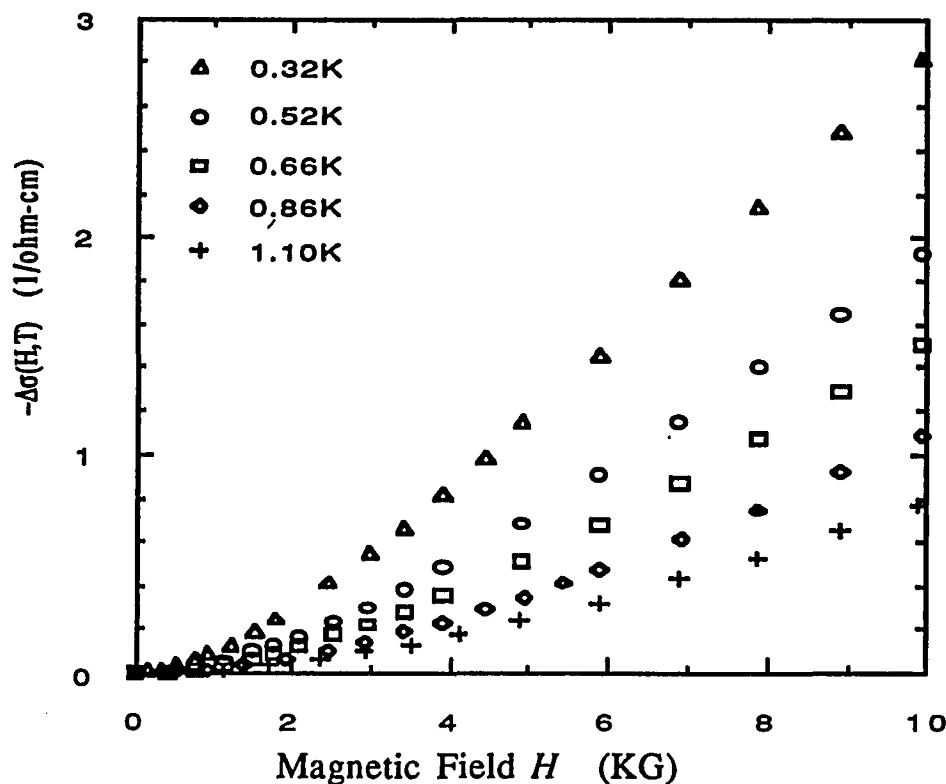

Fig. 4.44(a) The negative of $\Delta\sigma(H,T)$ plotted versus magnetic field for a Si:B sample with n = 4.20x10^{18} cm^{-3}.

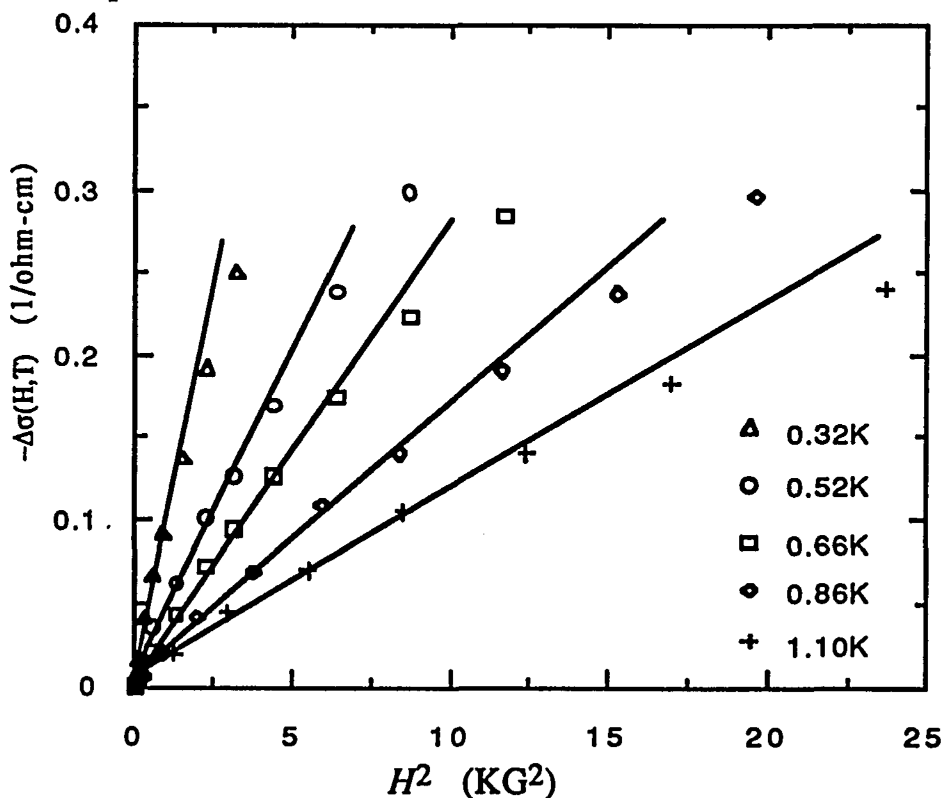

Fig. 4.44(b) The negative of $\Delta\sigma(H,T)$ plotted versus the square of magnetic field for a Si:B sample with n = 4.20x10^{18} cm^{-3}. The straight lines are guides to the eye.

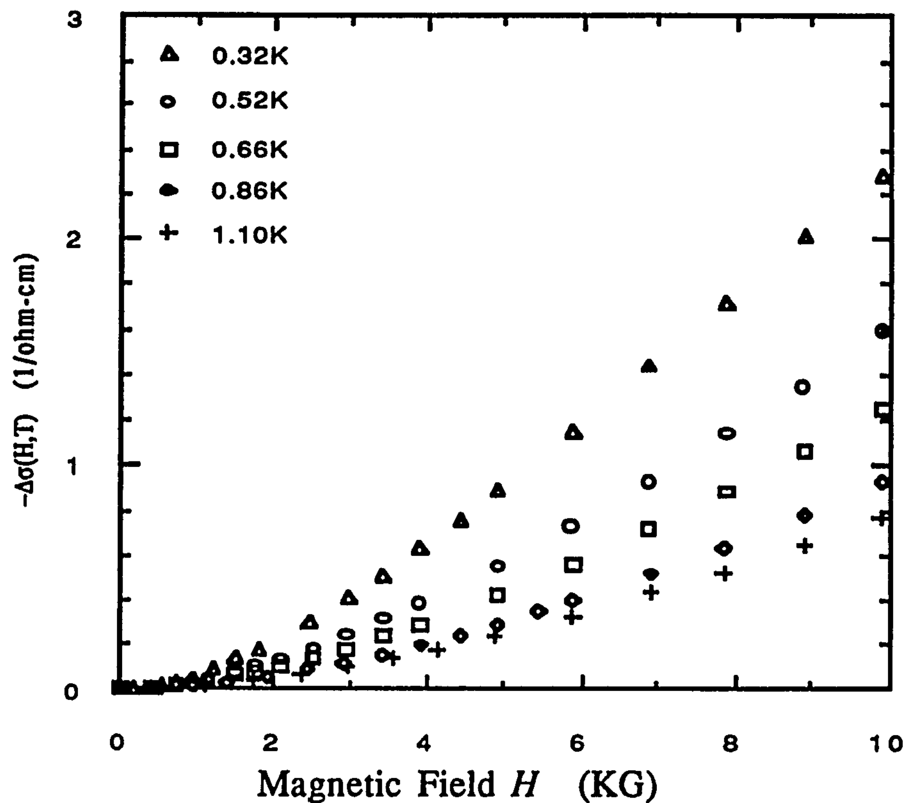

Fig. 4.45(a) The negative of $\Delta\sigma(H,T)$ plotted versus magnetic field for a Si:B sample with n = 4.11x10^{18} cm^{-3}.

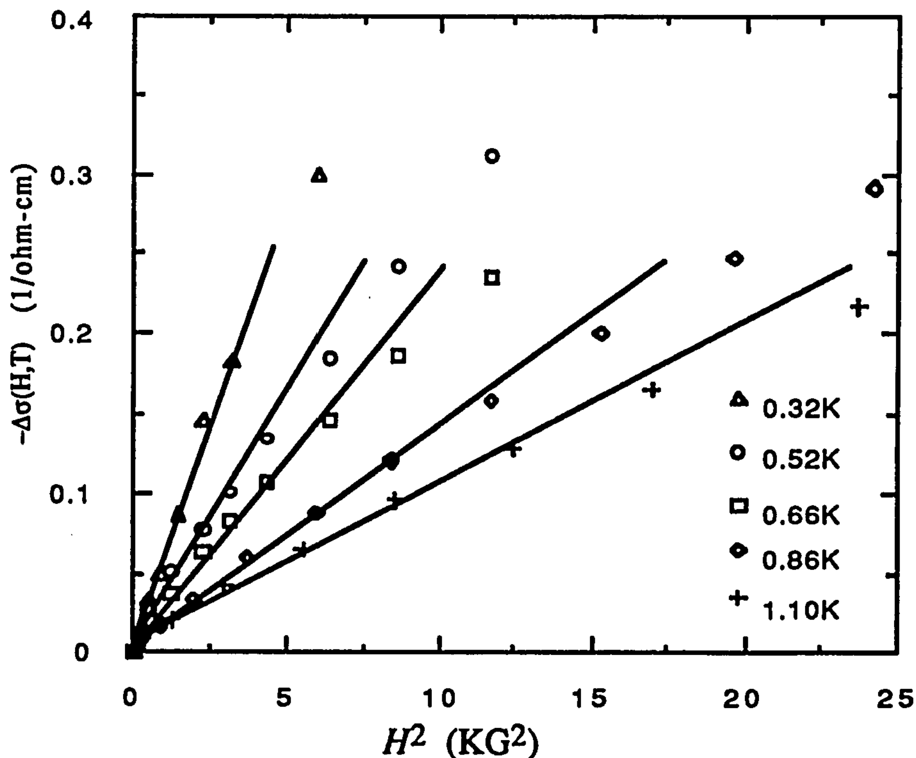

Fig. 4.45(b) The negative of $\Delta\sigma(H,T)$ plotted versus the square of magnetic field for a Si:B sample with n = 4.11x10^{18} cm^{-3}. The straight lines are guides to the eye.

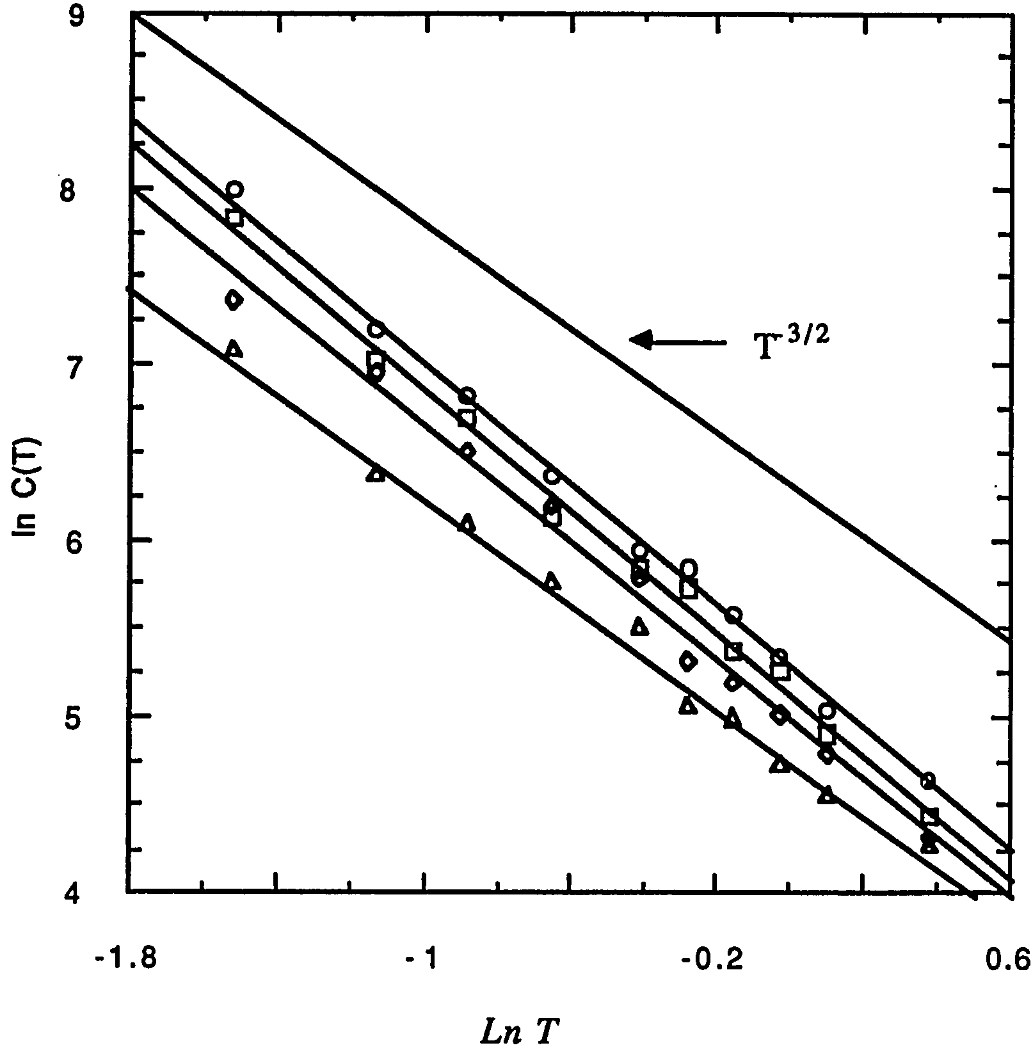

Fig. 4.46 The slope $C(T)$ of the H^2 dependence of the magnetoconductivity plotted as function of temperature for four Si:B samples. In units of 10^{18} cm^{-3}, their boron concentrations are: □ 5.22; ○ 4.72; ◇ 4.20; △ 4.20.

The contribution due to weak localization is obtained by subtracting the component due to interactions from $C(T)$. The interaction component at low fields is

$$\Delta\sigma_I(H,T) = -2.6\text{x}10^{-2}\,\alpha\gamma\tilde{F}_\sigma T^{-3/2} H^2 \qquad (4.4.13)$$

where the value of $\alpha\gamma\tilde{F}_\sigma$ is estimated from the high field data. The inelastic scattering time τ_{in} at each temperature was then calculated.

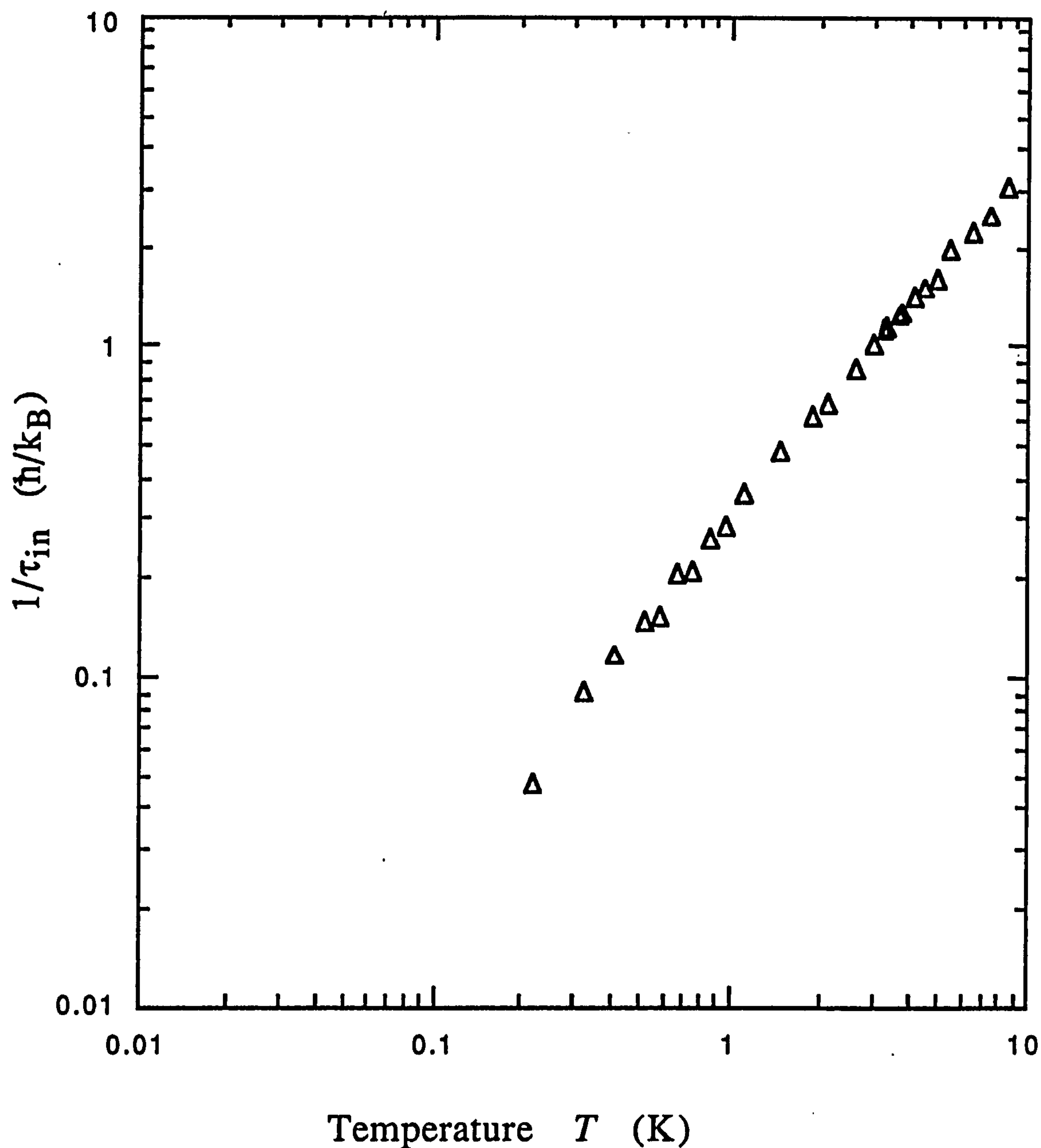

Fig. 4.47 The hole inelastic scattering rate $1/\tau_{in}$ in unit of $\hbar/k_B$ plotted against temperatures for a Si:B sample with $n =$ 4.95x10^{18} cm^3.

The values of τ_{in} so deduced are plotted against temperature in Fig.4.47. Our results show that the inelastic scattering time is roughly inversely proportional to temperature, that is $\tau_{in} \propto T^{-1}$.

Different predictions exist for the temperature dependence of τ_{in} In the case of electron-electron inelastic scattering, a power law is expected, that is $\tau_{in} \propto T^{-p}$ with $p = 2$ for a clean metal and p=3/2 in the case of a disordered metal[45]. More recently p=1 has been predicted for samples very near the transition[46]. It would seem therefore that our result agrees with this recent theory. Although this sample is almost the most metallic one among the samples we studied, it only has a concentration $n = 1.22n_c$. In a very recent study on Si:P[31], $p < 1$ was observed for samples near the transition, which they attributed to spin-scattering by localized moments. Our results indicate that the hole inelastic scattering rate $\hbar/\tau_{in} \propto k_B T$ for Si:B, rather than the form expected for both a clean and a dirty metal at low temperatures.

It should be noted that the value p ≈ 1 deduced here from the field dependence of σ is different from the p = 3/2 deduced from fitting the temperature dependence(see eq. 4.2.3 in section 4.2.a). Similar conclusions can be drawn by examining the data for Si:P, where the field dependence yields p ≤ 1. This discrepancy indicates that the behavior of σ near the transition is not well understood, and warrants further study.

4.5 Insulating Samples

We have also done some preliminary measurements on several insulating Si:B samples in the temperature range between 1.6 K and 4.2 K and in magnetic fields up to 4 Tesla, which we will briefly describe below.

4.5.a The Temperature Dependence of the Resistivity

The logarithm of the resistivity of four insulating Si:B samples is plotted in Fig. 4.48 as a function of $T^{-1/2}$. As shown in the plot, the resistivity for the two more insulating samples can be well described by

$$\rho = \rho_0 \exp[(T_0'/T)^{1/2}] \tag{4.5.1}$$

where ρ_0 and T_0' are constants. This may be associated with the Coulomb gap predicted by Efros and Shklovskii[47]. However, for the two less insulating samples, we can not clearly distinguish between Mott[48] hopping,

$$\rho = \rho_0 \exp[(T_0/T)^{1/4}] \tag{4.5.2}$$

and eq.(4.5.1). If we fit the data for all samples to eq. (4.5.1), the parameters T_0' listed in table 4.9 are obtained. Note that the value of T_0' for sample I-Si:B-1 was deduced within a temperature range only between 4.2K and 3.2K, and is therefore only approximate.

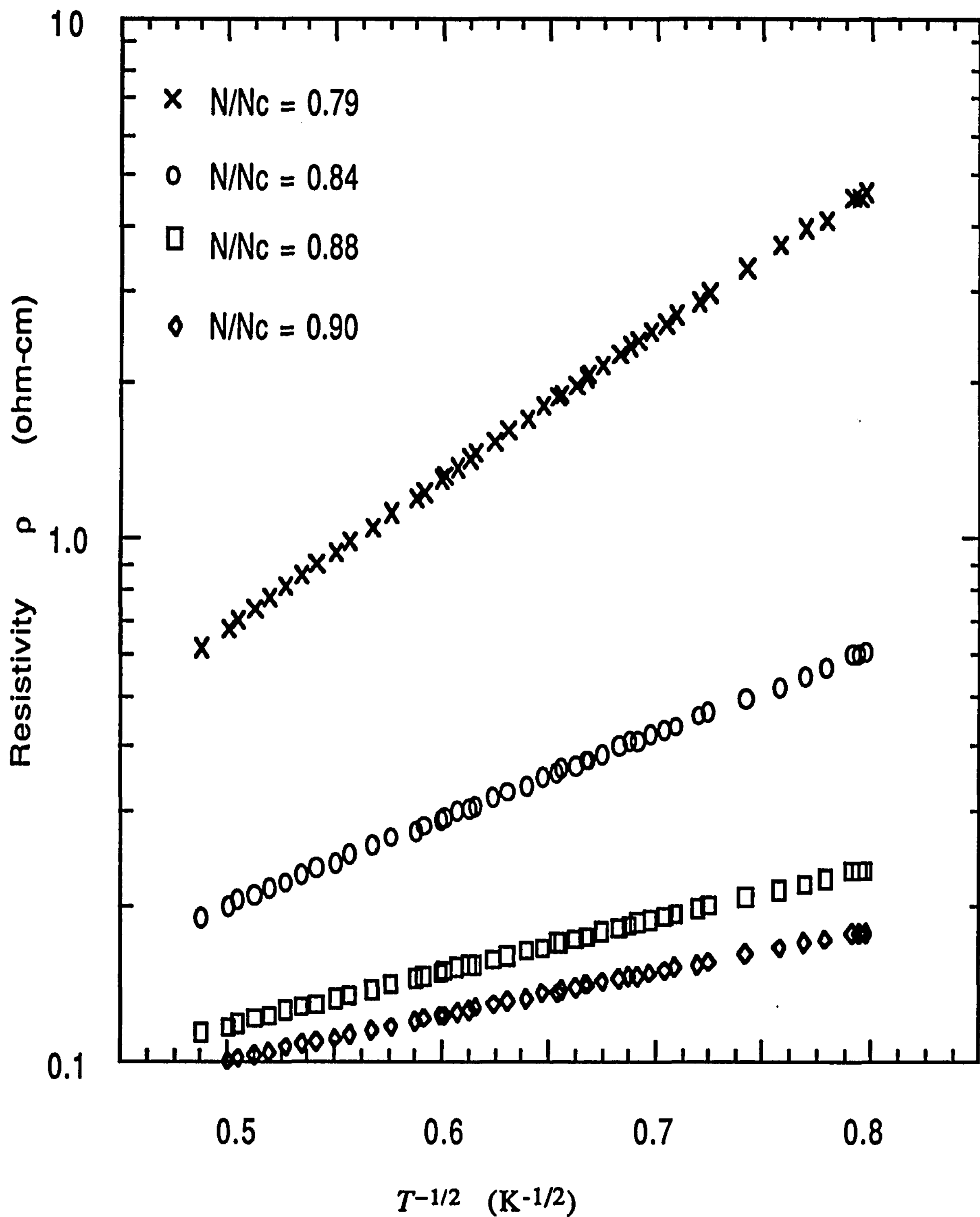

Fig. 4.48 The logarithm of the resistivities of four insulating Si:B samples plotted as a function of $T^{-1/2}$.

name	n (10^{18} cm^{-3})	n/n_c	T_0' (K)
I-Si:B-1	3.16	0.78	118
I-Si:B-2	3.21	0.79	43
I-Si:B-3	3.40	0.84	14
I-Si:B-4	3.59	0.88	5.5
I-Si:B-5	3.67	0.90	3.7

Table 4.9 Sample designation, absolute and relative boron concentrations, and parameter T_0'.

4.5.b The Magnetoresistance

The magnetoresistance of several Si:B samples taken at temperatures of 4.0 K and 1.6 K is plotted in Figs. 4.49 and 4.50 respectively. The resistivity of a single Si:B sample taken in several magnetic fields is plotted in Fig. 4.51. The most interesting feature is that the magnetoresistance is positive within the ranges of temperature and magnetic field of our measurements.

While it is well understood that spin-orbit scattering on the metallic side causes weak anti-localization which leads to a positive magnetoresistance, the role of spin-orbit scattering for the magnetoresistance on the insulating side is not clear. Pichard et al.[49] claim that the magnetoresistance in the hopping regime should be

positive in the presence of strong spin-orbit scattering, as it is on the metallic side. However, competing theories gives the opposite result. Meir et al.[50] showed that no matter what the strength of spin-orbit scattering, the magnetoresistance should always be negative in the hopping regime as long as the sample size is bigger than the localization length. Medina and Kardar[51] also predicted a positive magnetoresistance for strongly localized electrons in the presence of spin-orbit scattering. Results for Au-doped InO films by Shapir and Ovadyahu[52] showed that in the presence of spin-orbit scattering the low field magnetoresistance has a positive component at small fields for just-insulating samples and becomes negative at all fields for samples which are deeper in the insulating phase. Shapir and Ovadyahu[52] attribute the positive magnetoresistance near the transition to the continued importance of back-scattering processes, and its absence for large disorder to the reduced importance of the back-scattering loops relative to forward-scattering processes. Experiments on insulating *p*-type GaAs[53] also exhibit positive magnetoresistance.

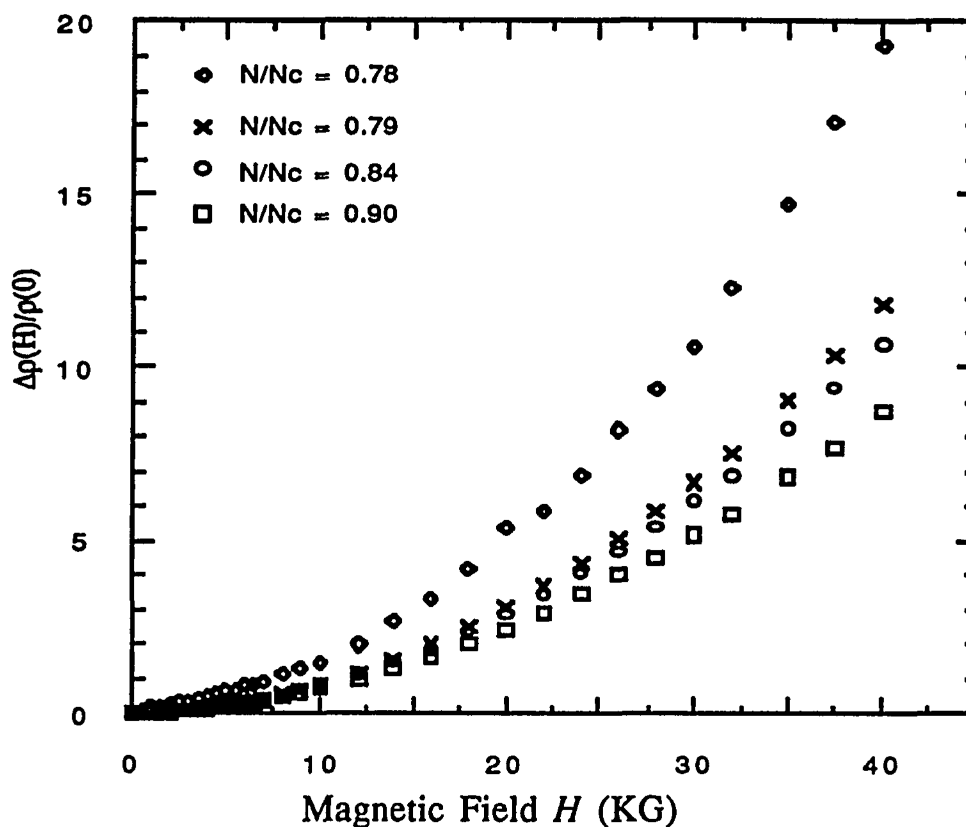

Fig. 4.49 The magnetoresistance of four insulating Si:B samples plotted versus magnetic fields at a fixed temperature of 4.0 K.

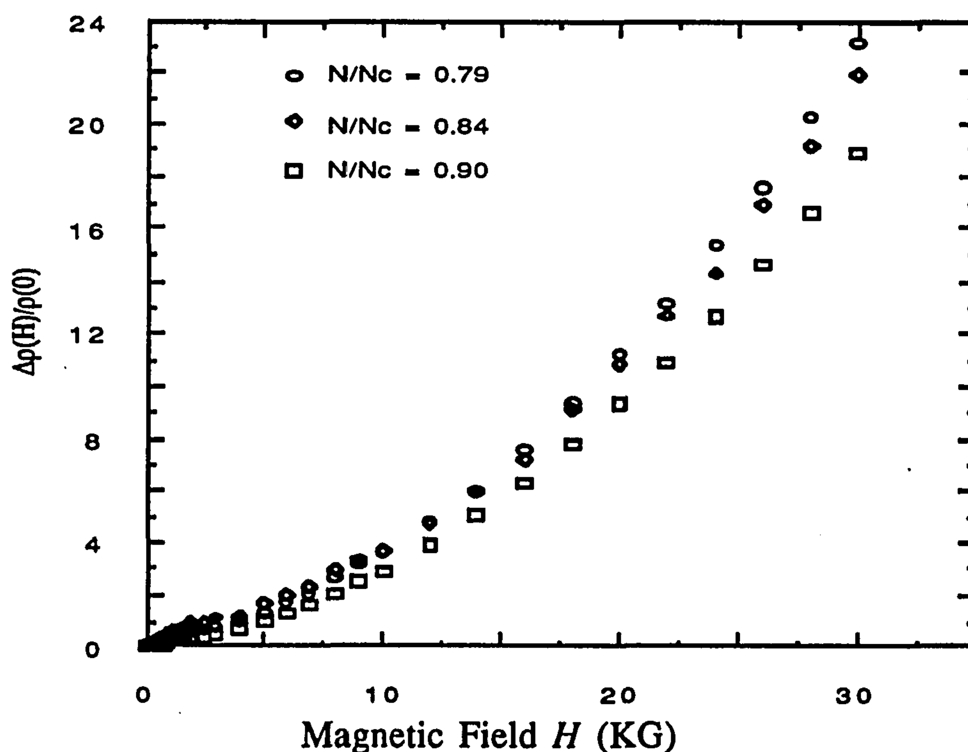

Fig. 4.50 The magnetoresistance of three insulating Si:B samples plotted versus magnetic field at a fixed temperature of 1.6 K.

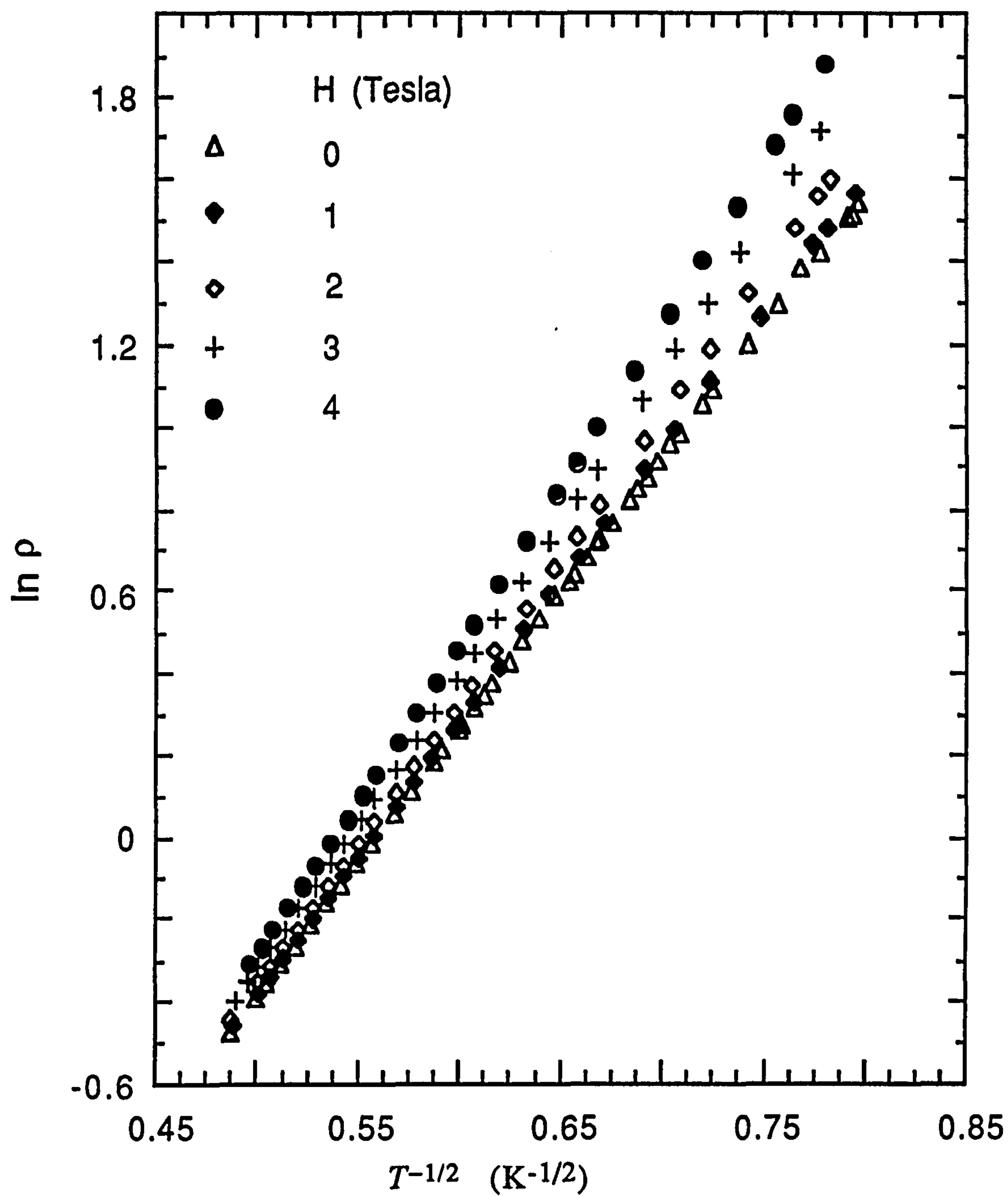

Fig. 4.51 The logarithm of resistivity of a single Si:B sample with n/n_c = 0.79 plotted as a function of $T^{-1/2}$ at various magnetic fields.

While the low field magnetoresistance of our Si:B samples and Au-doped InO films which are near the transition are both positive, there are major differences between them. The magnetoresistance of Au-doped InO films is negative at higher field while the magnetoresistance of insulating Si:B samples is always positive for all magnetic fields within our measurements, similar to metallic samples. While the positive magnetoresistance at high fields can be understood for metallic Si:B samples in terms of strong interaction effects, it is not clear at this point what causes the strongly positive high field magnetoresistance on the insulating side.

5. Summary and Suggestions for Future Work

5.1 Summary

In order to understand the mechanism of metal-insulator transitions, there have been extensive studies carried out on n-type doped semiconductors[1]. In contrast, there has been very little work done on p-type materials, and there is no systematic study of a metal-insulator transition which takes place in a p-type doped semiconductor. There are important differences for p-type doped semiconductors which make them interesting materials for study. For example, unlike in n-type materials, where spin-orbit effects are associated with heavy impurities, spin-orbit scattering is strong in p-type materials due to the structure of the valence bands[2]. A detailed investigation of the transport behavior of p-type material, and a comparison with its n-type counterpart can thus yield interesting information concerning the role of spin-orbit scattering, anisotropy and other factors associated with the nature of the bands.

We have studied the transport and magnetotransport properties of a series of p-type Si:B samples near the metal-insulator transition at temperatures down to 55 mK and in magnetic fields up to 9 Tesla. Through a detailed study of the temperature dependence of the conductivity of a set of carefully chosen Si:B samples, we have determined the critical conductivity exponent. We have also studied the critical conductivity exponent in a strong magnetic field. Through a systematic study of the temperature and magnetic field dependence of the conductivity and a comparison to n-type silicons,

we have revealed some of the similarities and differences between n- and p-type silicons. The following is a summary of our main findings.

Our study in zero magnetic field[3] shows the interesting result that the critical conductivity exponent for Si:B is $0.65^{+0.05}_{-0.14}$, which is close to the anomalous value of 1/2 found for other n-type uncompensated silicon systems, and different from the value near 1 found in most other materials[1]. This indicates that spin-orbit scattering does not determine the critical exponent as the theory predicts[4], at least in the case of silicon. Our result in magnetic fields[5] indicates that the critical exponent is shifted to a value near 1 by the application of a strong magnetic field. This is consistent with the prediction of the theory[4] and is the first observation of such a clear shift.

Our systemic study of the Si:B samples shows that the magnetoresistance of Si:B is always positive, which provides additional evidence for the strong spin-orbit scattering in Si:B. This is in contrast with the magnetoresistance of n-type silicon such as Si:P[6,7] which has a negative component due to weak localization. The absolute value of the magnetoconductivity of a Si:B sample is several times bigger than that of a Si:P[7] sample at the same temperature and magnetic field, even though they have similar values of n/n_c. The dramatic difference in the overall size of the magnetoresistance is probably associated with details of the band structure, and is also due to the fact that the contributions of localization and interactions

are of opposite sign in Si:P, while in Si:B the contributions are additive.

By studying the conductivity slope m in zero field, and m' in a strong field, as well as the dependence of the conductivity on magnetic field, we have deduced the interaction parameter F and its concentration dependence. Our study shows that the behaviors as well as the magnitude of the conductivity slope m in the relation $\sigma(T) = \sigma(0) + m\sqrt{T}$ as a function of reduced concentration n/n_c are very similar for n- and p-type silicon, despite the differences between the conduction and valence bands. In all the cases, m is negative for more metallic samples and changes sign as the concentration is reduced and the transition is approached. For Si:P[6] and Si:As[8], the sign reversal occurs at about $n/n_c = 1.04$, while for Si:B it occurs at about $n/n_c = 1.08$.

The slope of the conductivity in a magnetic field for the more metallic samples is negative for $g\mu_B H \ll k_B T$ and positive for $g\mu_B H \gg k_B T$. This can be explained qualitatively in terms of the Zeeman splitting[9]. The conductivity maxima occur at about $H/T = 2.5$ Tesla/Kelvin for Si:B, which is within 10 or 15% of the values of H/T where maxima are found to occur in Si:P[7]. However, these correspond to different values of $\frac{g\mu_B H}{k_B T}$ for the two systems since the their g-factors have different values. It is not clear at this point what causes this difference between the two systems. Since a theoretical treatment for p-type materials is not available, a detailed comparison with theory is impossible. Our results should serve as a comparison for the future relevant theories.

We have succeeded in measuring the magnetoresistance at very low magnetic fields from which we were able to deduce the slope of the initial H^2 dependence which contains information about the electron's inelastic scattering time[10]. With some assumptions, we have attempted a separation of the contribution to the low field magnetoresistance into the two effects, namely localization and interactions. We analyzed our detailed measurements of the magnetoresistance at low fields and deduced the inelastic scattering time and found that the inelastic scattering rate is roughly proportional to temperature, which is consistent with a recent theoretical prediction[11].

Our preliminary results show that the magnetoresistance of Si:B samples in the hopping regime is positive, which may imply that spin-orbit scattering is also important for insulating samples.

5.2 Suggestions for Future Work

5.2.a The Hall Coefficient

The behavior of the Hall coefficient as the transition is approached is an interesting subject. There are conflicting results for the Hall coefficient in different systems. In particular, the Hall coefficient for Ge:Sb[12] shows critical behavior, while the Hall coefficient for Si:As[13] does not. It has been suggested[14] that the critical behavior of the Hall coefficient found for Ge:Sb is due to strong spin-orbit scattering. By studying the Hall coefficient for Si:B,

we may be able to determine if spin-orbit scattering has the same effect on Si:B.

5.2.b The Dielectric Constant

Studies on Si:P[15] have shown that the dielectric constant exhibits critical behavior with an exponent which is twice that for the conductivity. Similar studies can be performed on Si:B. For dielectric constant measurements, direct electric contact to the sample, which is difficult for Si:B, is not required. Therefore the measurements of the dielectric constant for the Si:B samples should be easier compared with the measurements of the resistivity and the Hall coefficient.

5.2.c Stress Tuning of the Transition

Paalanen et al.[16] have done beautiful work on Si:P, where they studied the critical conductivity exponent by applying uniaxial stress to tune a sample through the transition. They also studied the critical behavior of the dielectric constant by stress-tuning an insulating sample[17]. Our experience shows that stress has a very large effect on p-type Si:B. One should note that by applying stress the degeneracy of the valence bands will be lifted and thus the spin-orbit scattering will presumably be reduced. By choosing a sample with the right concentration, it may be possible to tune a metallic sample all the way to the hopping regime, that is, to span the vicinity of the transition on both sides with a single sample. We can then

study the critical behaviors of the conductivity and possibly of the Hall coefficient, as well as that of the dielectric constant on a single sample. Further, we can study the properties of a sample under the combination of stress and magnetic field.

5.2.d Is Spin-Orbit Scattering Important in the Hopping Regime?

Our result shows that the magnetoresistance of Si:B samples in the hopping regime is positive. At the present time, we are not certain if this is due to the importance of spin-orbit scattering in the hopping regime. In order to investigate this, we can apply uniaxial stress on a insulating Si:B sample. Uniaxial stress lifts the degeneracy of the valence bands and thus reduces the spin-orbit scattering. If the low field magnetoresistance under stress becomes negative, this would indicate that the low field positive component in the absence of stress is due to spin-orbit scattering.

REFERENCES

Chapter 1

1 For a review, see G. A. Thomas, in "Localization and Interaction, D. M. Finlayson, ed. p. 29 (The Scottish Universities Summer School in Physics, St. Andrews,1986), p. 172, and references therein; Phil. Mag. B 52, 479 (1985).

2 N. F. Mott, Can. J. Phys. 34, 1356(1956); Phil. Mag. 6, 287 (1961); J. Hubbard, Prog. R. Soc. A(London) 276, 238 (1963); ibid. 277, 237(1964); ibid. 281, 401(1964).

3 P. W. Anderson, Phys. Rev. 102, 1008 (1958).

4 M. A. Paalanen, T. F. Rosenbaum, G. A. Thomas, and R. N. Bhatt, Phys. Rev. Lett., 48, 1284(1982).

5 T. F. Rosenbaum, K. Andres, G. A. Thomas, and P. A. Lee, Phys. Rev. Lett., 46, 568(1981); T. F. Rosenbaum, R. F. Milligan, M. A. Paalanen, G. A. Thomas, R. N. Bhatt and W. Lin, Phys. Rev. B 27, 7509(1983).

6 P. F. Newman and D. F. Holcomb, Phys. Rev. B 28, 628 (1983); W. N. Shafarman, D. W. Koon, and T. G. Castner, Phys. Rev. B 40, 1216(1989).

7 A. P. Long and M. Pepper, J. Phys. C, 17, L 425 (1984); Solid State Electron. 28, 61 (1985).

8 P. F. Newman and D. F. Holcomb, Phys. Rev. Lett., 51, 2144(1983).

9 G. A. Thomas, A. Kawabata, Y. Ootuka, S. Katsumoto, S. Kobayashi and W. Sasaki, Phys. Rev. B 26, 2113(1982).

10 Y. Ootuka, H. Matsuoka and S. Kobayashi, in *Anderson Localization*, edited by T. Ando and H. Fukuyama (Springer-Verlag, Berlin, 1988), p. 40.

11 M. J. Hirsch, U. Thomanschefsky, and D. F. Holcomb, Phys. Rev. B 37 8257(1988).

12 E. Abrahams, P. W. Anderson, D. C. Licciardello, and T. V. Ramakrishnan, Phys. Rev. Lett. 42, 693(1979).

13 C. Castellani, C. Di Castro, P. A. Lee and M. Ma, Phys. Rev. B 30, 527(1984); C. Castellani, G. Kotliar and P. A. Lee, Phys. Rev. Lett., 59, 323(1987).

14 S. Hikami, Progr. Theor. Phys. 64, 1466 (1980).

15 S. B. Field and T. F. Rosenbaum, Phys. Rev. Lett., 55, 522 (1985); D. W. Koon and T. G. Castner, Phys. Rev. Lett., 60, 1755 (1988); T. G. Castner, Phys. Rev. B 42, 5317(1990).

16 M. A. Paalanen, J. Graebner, R. N. Bhatt, and S. Sachdev, Phys. Rev. Lett., 61, 597(1988); A. Roy and M. P. Sarachik, Phys. Rev. B 37, 5531(1988); M. Milovanovic, S. Sachdev, and R. N. Bhatt, Phys. Rev. Lett., 63, 82(1989).

17 R. N. Bhatt and P. A. Lee, Solid State Commun., 48, 755(1983).

18 R. J. Elliott, Phys. Rev. 96,266(1954); A. Kawabata, J. Phys. Soc. Jan. 55, 3299(1986), and references therein; idib, 49, Suppl. A, 375 (1980).

19 Peihua Dai, Youzhu Zhang and M. P. Sarachik, Phys. Rev. Lett., 66, 1914 (1991).

20 Peihua Dai, Youzhu Zhang and M. P. Sarachik, Phys. Rev. Lett., 67, 136 (1991).

Chapter 2

1 N. F. Mott, Can. J. Phys. 34, 1356 (1956); Phil. Mag. 6, 287 (1961).

2 P. P. Edwards and M. J. Sienko, Phys. Rev. B 17, 2575 (1978).

3 J. Hubbard, Prog. R. Soc. A(London) 276, 238 (1963); ibid. 277, 237 (1964); ibid. 281, 401 (1964).

4 B. L. Altshuler and A. G. Aronov, Sov. Phys. JETP 50, 968 (1979); B. L. Alshuler and A. G. Aronov, JETP Lett. 30, 514 (1979).

5 N. F. Mott, Phil. Mag. 26, 1015 (1972); Phil. Mag. B 44, 265 (1981).

6 A. F. Ioffe and A. R. Regel, Proc. Semicond. 4, 237 (1960).

7 M. A. Paalanen, T. F. Rosenbaum, G. A. Thomas, and R. N. Bhatt, Phys. Rev. Lett., 48, 1284(1982).

8 N. F. Mott, in "Localization and Interaction, D. M. Finlayson, ed. p. 29 (The Scottish Universities Summer School in Physics, St. Andrews,1986).

9 P. W. Anderson, Phys. Rev. 102, 1008 (1958).

10 B. I. Shklovskii and A. L. Efros, Electronic properties of Deped Semiconductors, Vol. 45 of Springer Series in Solid State Sciences(Springer, Berlin, 1984).

11 N. F. Mott, Metal-Insulator Transitions (Taylor and Francis, London, 1974); N. F. Mott and E. A. Davis, Electronic Processes in Non-Crystalline Materials (Oxford University Press, Oxford, 1979).

12 D. J. Thouless, Phys Reports C 13, 93(1974); Phys. Rev. Lett., 39, 1167 (1977).

13 E. Abrahams, P. W. Anderson, D. C. Licciardello, and T. V. Ramakrishnan, Phys. Rev. Lett. 42, 693 (1979).

14 See, for example, P. A. Lee and T. V. Ramakrishnan, Review of Modern Physics 57, 287 (1985).

15 A. M. Finkelshtein, Zh. Eksp. Teor. Fiz. 86, 367 (1984) [Sov. Phys. JETP 59, 212 (1984)].

16 C. Castellani, C. Di Castro, P. A. Lee and M. Ma, Phys. Rev. B 30, 527(1984); C. Castellani, G. Kotliar and P. A. Lee, Phys. Rev. Lett., 59, 323 (1987).

17 T. F. Rosenbaum, K. Andres, G. A. Thomas, and R. N. Bhatt, Phys. Rev. Lett., 45, 1723 (1980).

18 For a review, see G. A. Thomas, in "Localization and Interaction, D. M. Finlayson, ed. p. 29 (The Scottish Universities Summer School

in Physics, St. Andrews,1986), p. 172, and references therein; Phil. Mag. B 52, 479 (1985).

19 M. Rohde and M. Micklitz, Phys. Rev. B 36, 7572 (1987).

20 G. Hertel, D. Bishop, E. G. Spencer, J. M. Rowell, and R. C. Dynes, Phys. Rev. Lett., 50, 743 (1983).

21 M. Yamaguchi, N. Nishida, T. Furubayashi, K. Morigaki, H. Ishimoto, and Ono, Physica B, 118, 694 (1983).

22 W. L. McMillan and J. Mochel, Phys. Rev. Lett., 46, 556(1981).

23 S. Yoshizumin, D. Mael, T. H. Geballe, and R. L. Greene, in *Localization and Metal-Insulator Transition*, edited by H. Fritzsche and D. Adler, (plenum, New York, 1985), p.77.

24 G. A. Thomas, A. Kawabata, Y. Ootuka, S. Katsumoto, S. Kobayashi and W. Sasaki, Phys. Rev. B 26, 2113 (1982).

25 M. J. Hirsch, U. Thomanschefsky, and D. F. Holcomb, Phys. Rev. B 37 8257 (1988).

26 Y. Ootuka, H. Matsuoka and S. Kobayashi, in *Anderson Localization*, edited by T. Ando and H. Fukuyama (Springer-Verlag, Berlin, 1988), p. 40.

27 P. F. Newman and D. F. Holcomb, Phys. Rev. B 28, 628 (1983).

28 W. N. Shafarman, D. W. Koon, and T. G. Castner, Phys. Rev. B 40, 1216 (1989).

29 P. F. Newman and D. F. Holcomb, Phys. Rev. Lett., 51, 2144 (1983).

30 A. P. Long and M. Pepper, J. Phys. C, 17, L 425 (1984); Solid State Electron. 28, 61 (1985).

31 G. Bergmann, Phys. Reports, 107, 1 (1984).

32 A.Kawabata, Solid State Commun. 38, 823 (1981).

33 N. F. Mott and M. Kaveh, Adv. in Phys., 34, 329 (1985).

34 A. Schmid, Z. Physik 271,. 251 (1974).

35 D. Belitz and K. I. Wysokinski, Phys. Rev. B 36, 9333 (1987).

36 A. Kawabata, Solid State Commun. 34, 431 (1980).

37 B L. Altshuler and A. G. Aronov, Electron-Electron Interactions in Disordered systems (ed. by A. L. Efros and M. Pollak), North-Holland, Amsterdam (1985), p. 1; B. L. Altshuler and A. G. Aronov, and D. E. Khmelnitskii, Sov. Phys. JETP 54, 411 (1981).

38 B. L. Altshuler and A. G. Aronov, Solid State Commun., 46, 429 (1983).

39 P. A. Lee and T. V. Ramakrishnan, Phys. Rev. B 26, 4009 (1982).

40 B. L. Altshuler and A. G. Aronov and P. A. Lee, Phys. Rev. Lett., 44, 1288 (1980).

Chapter 3

1. F. A. Trumbore, Bell Syst. Tech. J. 39, 205 (1960).

2 R. J. Capik, Bell Laboratories Internal Memo (unpublished, 1974).

3 L. J. van der Pauw, Phillips Pes. Rep., 13, 1 (1958).

4 W. R. Thurber, R. L. Mattis, Y. M. Liu, and J. J. Filiben, J. Electrochem. Soc. 127, 2291 (1980).

Chapter 4

1 W. R. Thurber, R. L. Mattis, Y. M. Liu, and J. J. Filiben, J. Electrochem. Soc. 127, 2291 (1980).

2 B. L. Altshuler and A. G. Aronov, Sov. Phys. JETP 50, 968(1979); B. L. Altshuler and A. G. Aronov, JETP Lett. 30, 514 (1979).

3 B. L. Altshuler and A. G. Aronov, Solid State Commun., 46, 429 (1983).

4 A. Kawabata, Solid State Commun. 38, 823 (1981).

5 N. F. Mott and M. Kaveh, Adv. in Phys., 34, 329 (1985).

6 A. Schmid, Z. Physik 271,. 251 (1974).

7 G. A. Thomas, A. Kawabata, Y. Ootuka, S. Katsumoto, S. Kobayashi and W. Sasaki, Phys. Rev. B 26, 2113 (1982).

8 R. N. Bhatt and P. A. Lee, Solid State Commun., 48, 755 (1983).

9 C. Castellani, C. Di Castro, P. A. Lee and M. Ma, Phys. Rev. B 30, 527 (1984).

10 T. F. Rosenbaum, R. F. Milligan, M. A. Paalance, G. A. Thomas, R. N. Bhatt and W. Lin, Phys. Rev. B 27, 7509 (1983).

11 G. A. Thomas, M. A. Paalance, and T. F. Rosenbaum, Phys. Rev. B 27, 3897 (1983).

12 W. N. Shafarman, D. W. Koon, and T. G. Castner, Phys. Rev. B 40, 1216 (1989).

13 G. A. Thomas, in "Localization and Interaction, D. M. Finlayson, ed. p. 29 (The Scottish Universities Summer School in Physics, St. Andrews,1986), p. 172, and references therein; Phil. Mag. B 52, 479 (1985).

14 C. Castellani, C. Di Castro, P. A. Lee and M. Ma, Phys. Rev. B 30, 527 (1984); C. Castellani, G. Kotliar and P. A. Lee, Phys. Rev. Lett., 59, 323 (1987).

15 P. F. Newman and D. F. Holcomb, Phys. Rev. B 28, 628 (1983).

16 A. P. Long and M. Pepper, J. Phys. C, 17, L 425 (1984); Solid State Electron. 28, 61 (1985).

17 P. F. Newman and D. F. Holcomb, Phys. Rev. Lett., 51, 2144 (1983).

18 G. A. Thomas, Y. Ootuka, S. Katsumoto, S. Kobayashi and W. Sasaki, Phys. Rev. B 25, 4288 (1982).

19 M. J. Hirsch, U. Thomanschefsky, and D. F. Holcomb, Phys. Rev. B 37, 8257 (1988).

20 Y. Ootuka, H. Matsuoka and S. Kobayashi, in *Anderson Localization*, edited by T. Ando and H. Fukuyama (Springer-Verlag, Berlin, 1988), p. 40.

21 R. J. Elliott, Phys. Rev. 96, 266 (1954).

22 A. Kawabata, J. Phys. Soc. Jan. 55, 3299(1986), and references therein; idib, 49, Suppl. A, 375 (1980).

23 G. Feher, J. C. Hansel and E. A. Gere, Phys. Rev. Lett. 5, 309 (1960).

24 J. M. Cherlow, R. L. Aggarwal, and B. Lax. Phys. Rev. B 7, 4547 (1973).

25 H. Roth, W. D. Straub, W. Bernard, and J. E. Mulhern, Jr., Phys. Rev. Lett. 11, 328 (1963).

26 K. Sugiyama, J. Phys. Soc. Jpn. 19, 1745 (1964).

27 D. R. Lomidze and S. A. Obukhov, Sov. Phys. Solid State 21, 1810 (1979).

28 M. Stohr, P. Janiszewski, and J. A. Chroboczek, Proceedings of the International Conc. on Physics of Shallow Impurities, 1990 (Institute of Physics).

29 M. C. Maliepaard, M. Pepper, R. Newbury, and G. Hill, Phys. Rev. Lett. 61, 369 (1988).

30 Y. Ootuka, H. Matsuoka, and S. Kobayashi, in *Disordered semiconductors*, edited by M. Kastner, G. Thomas, and S. Ovshinsky, Plenum Publishing Corporation, p. 91 (1987).

31 M. Paalanen and R. N. Bhatt, unpublished.

32 H. v. Lohneysen, Festkorperprobleme: Advances in Solid State Physics (Vieweg, Braunschweig, 1990), 30, 95 (1990); H. v. Lohneysen and M. Welsch, Preprint.

33 P. A. Lee and T. V. Ramakrishnan, Phys. Rev. B 26, 4009 (1982).

34 P. A. Lee and T. V. Ramakrishnan, Review of Modern Physics 57, 287 (1985).

35 G. Bergmann, Solid State Commun., 49, 775(1984); Phys. Rep. 107, 1 (1984).

36 S. Hikami, A. I. Larkin, and Y. Nagaoka, Prog. Theor. Phys. 63, 707 (1980).

37 G. Bergmann, Phys. Rev. 28, 2914 (1983).

38 B. L. Altshuler and A. G. Aronov, and D. E. Khmelnitskii, Sov. Phys. JETP 54, 411 (1981).

39 A. Kawabata, J. Phys. Soc. Jan. 55, 3299 (1986).

40 For examples, see J. B. Bieri, A. Fert, G. Creuzet and A. Schuhl, J. Phys. F, 16, 2099 (1986).

41 T. F. Rosenbaum, R. F. Milligan, G. A. Thomas, P. A. Lee, T. V. Ramakrishnan, and R. N. Bhatt, Phys. Rev. Lett., 47, 1758 (1981).

42 R. Raimondi, C. Castellani, and C. Di Castro, Phys. Rev. B 42, 4724 (1990).

43 D. Abraham and R. Rosenbaum, Phys. Rev. B 26, 1413 (1983).

44 B L. Altshuler and A. G. Aronov, Electron-Electron Interactions in Disordered systems (ed. by A. L. Efros and M. Pollak), North-Holland, Amsterdam (1985), p. 1.

45 A. Schmid, Z. Physik 271,. 251 (1974).

46 D. Belitz and K. I. Wysokinski, Phys. Rev. B 36, 9333 (1987).

47 B. L. Efros and B. I. Shklovskii, J. Phys. C 8, L49 (1975).

48 N. F. Mott, J. Non-Cryst. Solids 1, 1 (1968).

49 J. L. Pichard, M. Sanquer, K. Slevin, and P. Debray, Phys. Rev. Lett., 65, 1812 (1990).

50 Y. Meir, N. S. Wingreen, O. Entin-Wohlman, And B. I. Altshuler, Phys. Rev. Lett., 66, 1517 (1991).

51 E. Medina and M. Kardar, Phys. Rev. Lett., 66, 3187 (1991).

52 Y. Shapir and Z. Ovadyahu, Phys. Rev. B 40, 12441 (1989).

53 F. Tremblay, M. Pepper, R. Newbury, D. A. Ritchie, D. C. Peacock, J. E. F. Frost, G. A. C. Jones and G. Hill, Phys. Rev. B 41, 8572 (1990).

Chapter 5

1 G. A. Thomas, in "Localization and Interaction, D. M. Finlayson, ed. p. 29 (The Scottish Universities Summer School in Physics, St. Andrews,1986), p. 172, and references therein; Phil. Mag. B 52, 479 (1985).

2 R. J. Elliott, Phys. Rev. 96,266(1954); A. Kawabata, J. Phys. Soc. Jan. 55, 3299(1986), and references therein; idib, 49, Suppl. A, 375 (1980).

3 Peihua Dai, Youzhu Zhang and M. P. Sarachik, Phys. Rev. Lett., 66, 1914 (1991).

4 13 C. Castellani, C. Di Castro, P. A. Lee and M. Ma, Phys. Rev. B 30, 527(1984); C. Castellani, G. Kotliar and P. A. Lee, Phys. Rev. Lett., 59, 323 (1987).

5 Peihua Dai, Youzhu Zhang and M. P. Sarachik, Phys. Rev. Lett., 67, 136 (1991).

6 T. F. Rosenbaum, R. F. Milligan, M. A. Paalanen, G. A. Thomas, R. N. Bhatt and W. Lin, Phys. Rev. B 27, 7509 (1983).

7 M. A. Paalanen and R. N. Bhatt, unpublished.

8 W. N. Shafarman, D. W. Koon, and T. G. Castner, Phys. Rev. B 40, 1216 (1989).

9 P. A. Lee and T. V. Ramakrishnan, Phys. Rev. B 26, 4009 (1982); Review of Modern Physics 57, 287 (1985).

10 A. Kawabata, Solid State Commun. 38, 823 (1981); B. L. Altshuler and A. G. Aronov, and D. E. Khmelnitskii, Sov. Phys. JETP 54, 411 (1981).

11 46 D. Belitz and K. I. Wysokinski, Phys. Rev. B 36, 9333 (1987).

12 S. B. Field and T. F. Rosenbaum, Phys. Rev. Lett., 55, 522 (1985).

13 D. W. Koon and T. G. Castner, Phys. Rev. Lett., 60, 1755 (1988).

14 T. G. Castner, Phys. Rev. B 42, 5317 (1990).

15 H. F. Hess, K. DeConde, T. F. Rosenbaum, and G. A. Thomas, Phys. Rev. B 25, 5578 (1982).

16 M. A. Paalanen, T. F. Rosenbaum, G. A. Thomas, and R. N. Bhatt, Phys. Rev. Lett., 48, 1284 (1982).

17 M. A. Paalanen, T. F. Rosenbaum, G. A. Thomas, and R. N. Bhatt, Phys. Rev. Lett., 51, 1896 (1983).